Fall 2019

Physical and Biological Consequences of Giant Kelp (Macrocystis Pyrifera) Removals Within a Central California Kelp Forest

Steven Ryan Cunningham
California State University, Monterey Bay, scunningham@csumb.edu

PHYSICAL AND BIOLOGICAL CONSEQUENCES OF GIANT KELP (*MACROCYSTIS PYRIFERA*) REMOVALS WITHIN A CENTRAL CALIFORNIA KELP FOREST

A Thesis

Presented to the

Faculty of the

School of Natural Sciences

California State University Monterey Bay

In Partial Fulfillment

of the Requirements for the Degree

Master of Science

in

Marine Science

By

Steven Ryan Cunningham

Fall: 2019

CALIFORNIA STATE UNIVERSITY MONTEREY BAY

The Undersigned Faculty Committee Approves the

Thesis of Steven Ryan Cunningham:

PHYSICAL AND BIOLOGICAL CONSEQUENCES OF GIANT KELP (*MACROCYSTIS PYRIFERA*) REMOVALS WITHIN A CENTRAL CALIFORNIA KELP FOREST

_____
Michael Graham, Chair
Moss Landing Marine Labs

_____
Tom Connolly
Moss Landing Marine Labs

_____
Colleen Durkin
Moss Landing Marine Labs

Approved by the Dean of Graduate Studies

_____
Kris Roney, Dean
Associate VP for Academic Programs and Dean of Undergraduate and Graduate Studies

12/12/2019
_____
Approval Date

Approval Date

“Trying to understand the way nature works involves a most terrible test of human reasoning ability. It involves subtle trickery, beautiful tightropes of logic on which one has to walk in order not to make a mistake in predicting what will happen.”

Richard P. Feynman

ABSTRACT

Physical and Biological Consequences of Giant Kelp (*Macrocystis Pyrifera*) Removals Within a Central California Kelp Forest

by
Steven Ryan Cunningham
Master of Science in Marine Science
California State University Monterey Bay, 2019

The giant kelp (*Macrocystis pyrifera*) is a well-studied foundation species that builds complex biogenic habitat and contributes fixed carbon to the base of food webs. Kelp forest systems are some of the most productive ecosystems in the world and can sustain high levels of species richness and abundance. It has long been debated whether these systems are rich due to the (1) complex habitat structure of the giant kelp or (2) the kelp's high growth rates that provide an abundance of food for primary consumers. Giant kelp modifies its environment by creating shade with its surface canopy, slowing currents by surface drag, and adding habitat stratified through the water column. It has been debated if giant kelp or phytoplankton are more important to the stability of the food webs within kelp forest systems. Many studies have attempted to validate the importance of giant kelp to the associated community by kelp removal experiments, which are unable to separate physical from biological effects of kelp. I expand upon these studies here by creating artificial *Macrocystis* plots and measuring variables that are typically overlooked in kelp removal experiments such as, currents, POC/ PON, particle size distribution, temperature, turbidity, fluorescence, and phytoplankton concentration and carbon contribution. Three kelp beds were analyzed in Stillwater Cove, CA between June – October 2016. A randomized block design was used to test the differences in the measured variables among depth and treatments; control kelp, artificial kelp, and removed kelp. Each circular treatment plot was 10m in diameter and variables were measured weekly within blocks before (n=180) and after treatment (n = 216). There was no difference in POC/PON between control and kelp cleared treatments, indicating that a 10m plot is insufficient at reducing the ambient POC/PON. There was also no indication that the increased light in kelp cleared treatments increased phytoplankton concentrations to subsidize the missing kelp POC input, and the phytoplankton standing crop contributed very little (< 3%) to the standing POC pool. Particulates and POC/ PON were well mixed throughout kelp beds and clearings, with no benthic accumulation observed. Currents increased in speed within kelp removed plots, the velocity was still too slow for turbulent shearing. A subsequent dye tracking experiment with an acoustic doppler velocimeter showed that high-frequency motions associated with turbulence had higher energy levels within kelp beds compared to outside, and vertical velocities had higher variance within beds than outside. Furthermore, benthic dye release experiments showed that dye flowed further up in the water column inside kelp beds than outside and that dye detection duration was dependent on the presence of giant kelp and increased wave orbital velocities. These results indicate that waves have a higher impact on vertical mixing within kelp beds than currents within Stillwater Cove. Mixing in kelp beds blends particulates evenly through the water column and removal plots have no impact on total POC/PON but may change particle distribution.

TABLE OF CONTENTS

PAGE

LIST OF FIGURES

PAGE

√

LIST OF TABLES

PAGE

ACKNOWLEDGEMENTS

This work was made possible by funding from the David and Lucille Packard Foundation, MLML Scholar Award, MLML Wave Award, the Undergraduate Research Opportunities Center at CSU Monterey Bay.

First, I would like to thank my thesis committee members Mike Graham, Tom Connolly, and Colleen Durkin for their advice and council while navigating through the program. Their combined skills and knowledge forged me into a well-rounded scientist able to view the environment through various angles.

I would also like to thank my enablers, the people who make it possible to do what we do at Moss Landing Marine Labs; Diana Steller the dive safety officer, John Douglas and Brian Ackerman at the boats facility, and the MLML shop crew. These people bent over backwards to make sure the students can go about their work efficiently and without hesitation.

I made some amazing friends at MLM, my lab mates and cohort especially bonded over late nights in the lab and intense fieldwork days and nights. A special thanks to Lindsay Cooper, Cody Dawson, Stephan Bitterwolf, for being my ride or die crew who were always there every step of the way. Thanks also to my interns Jay Low, Philip Ericsson, and John Freutel who helped with various stages of this work.

Finally, thanks to my family who have watched my progression through college and have always been supportive. Every time I fell, they would help pick me back up.

INTRODUCTION

The ecosystem concept dates to the early twentieth century, chiefly with the perspectives of Clements (1939) and Tansley (1935) (reviewed by Sheail 1987), which spawned an entire field of scientific exploration into ecosystem ecology. Clements (1939) proposed to study an ecosystem by a reductionist approach, looking at more individual-based interactions to find ecological patterns. Later, these interaction patterns would be incorporated into what are now called food webs or box-flow charts (reviewed by Raffaelli 2006). Tansley (1935) subsequently proposes that an ecosystem should couple biological and physical dynamics to form a single 'ecological system'. Tansley's (1935) ecosystem concept was embraced (Sheail 1987), with the term ecosystem ultimately being defined as "a unit comprising a community of organisms and their physical and chemical environment, at any scale, in which there are continuous fluxes of matter and energy" (Willis 1997). Currently, in the field of ecosystem ecology, there is a push for predictive ecosystem models, which have come to the interest of policy makers (Sheail 1987, Mann 1988, Fulton et al. 2003, Moorcroft 2006). These models would need to incorporate all biological processes and physical dynamics of the system, as described by Tansley's (1935), however, the diversity of organisms in a community makes this task difficult (Pimm 1982, Sheail 1987).

Dayton (1972) realized that a more simplistic approach to predicting ecosystem responses to disturbances was by studying the species upon which the community are dependent. Rather than parceling out every individual species interaction in an ecosystem, Dayton (1972) suggested that the primary objective in studies designed to predict community responses should be to identify the foundation species: "those which have a disproportionately important influence on the structure of the community." Foundations species are very similar to Paine's (1969, and later Power's 1996), concept of a keystone species: "one whose effect is large, and disproportionately large relative to its abundance." The difference between them is that a keystone species effect is linked to consumption of lower trophic level species via top-down control (Hairston et al. 1960, Power 1996), whereas a foundation species is a form of bottom-up control through energy and habitat provision (White 1978, Power 1996). Once the foundation species has been identified,

rigorous experimentation can help better understand the physical and biological processes acting upon the community (Dayton 1972).

Giant kelp (*Macrocystis pyrifera)* is a well-studied foundation species (Foster and Schiel 1985, Graham et al. 2007, Schiel and Foster 2015). *Macrocystis* is a brown alga (Laminariales, Phaeophyceae) that grows on rocky substrate down to 55m deep (reviewed by Graham et al. 2007, Schiel and Foster 2015) along temperate rocky coastlines roughly between 57° and 27° N also 57° and 6° S (Foster and Schiel 1985, Steneck et al. 2003, Graham et al. 2007) and reaches the water's surface creating a thick surface canopy. When aggregated, this 3-dimensional structure has a striking resemblance to a boreal forest, and thus has been called a kelp forest (Foster and Schiel 1985).

Kelp forests are some of the most productive and dynamic ecosystems in the world (Lieth and Whittaker 1975, Dayton 1985, Graham et al. 2007, Krumhansl et al. 2016). This is because kelps have high biomass turnover and can achieve net primary production (NPP) rates of 2.3kg dry weight m^{-2} $year^{-1}$ making kelp forests the most productive ecosystem (in terms of $g/m^2/yr$) in the biome (Whittaker and Likens 1973, Gerard 1976, Reed et al. 2008, reviewed by Reed and Brzezinski 2009, Krumhansl et al. 2016). It is believed that the combination of energy and habitat provision promotes high species abundance and diversity (Foster and Schiel 1985, Graham et al. 2007, Graham et al. 2008). Within a single kelp bed in central California, Pearse and Lowry (1974) observed 369 species of algae and invertebrate inhabitants, while Quast (1971) identified over 50 species of fish can be found in habitats associated to kelp forests. In southern California and Baja, 130 species of algae and nearly 800 species of animals reside within kelp forests (North 1971). However, it is uncertain what proportion of the community is associated with giant kelp as a food source or as a source of habitat and shelter (Graham et al. 2007, 2008).

Ecologists have attempted to understand the importance of giant kelp to its associated community through rigorous study and experimentation. It is known that the giant kelp affects the environment simultaneously by two factors: (1) the physical structure that provides shelter (Watanabe 1984, Carr 1989, 1994), shading (Edwards

1998, Clark et al. 2004), and dampening of water flow (Jackson 1997, Gaylord et al. 2007, Rosman et al. 2007, 2010); and (2) energy provision to food webs in the form of fixed carbon and nitrogen (Foster and Schiel 1985, Graham 2004).

The most conspicuous linkage between *Macrocystis* and its associated community assemblage is the biogenic habitat itself. The thallus of the giant kelp acts as a stratified complex habitat that can be used as refuge by several species (Foster and Schiel 1985, Graham et al. 2007, Schiel and Foster 2015). The holdfasts of subtidal *M. pyrifera* thalli are conical 3-dimensonal structures made from dichotomously branched haptera that act to anchor the entire thallus to the substrate (Fig. 1). The haptera and interstitial spaces between them are colonized by a diverse assemblage of algae, invertebrates, and fishes (reviewed by Schiel and Foster 2015). Isotopic studies have identified particulate organic matter (POM) as the base of the food web within complex algal-structured communities (Fredriksen 2003, Grall et al. 2006, Page 2008, Overstrom-Coleman 2009, Schaal et al. 2012, Miller and Page 2012, Miller et al. 2013, Yorke et al. 2013). It is still unclear, however, if these organisms reside in kelp thalli due to the complex structure of the algal habitat, the POM provided by the host alga itself, or both. Mid-water fronds and canopies also host many species of fish, mobile and sessile invertebrates (Carr 1989, 1994, 2011, De Martini and Roberts 1990, Levin 1993, Graham 2004). Watanabe (1984) found that three species of gastropods, although they are herbivores, utilize *Macrocystis* as a refuge from predation rather than a food source. Other studies have also shown that giant kelp blades act as habitat for encrusting bryozoans (Dixon et al. 1981); the giant kelp's ability to extend through the water column enables the bryozoans to inhabit areas of increased water flow, which gives them better access to drifting food particles (Duggins et al. 1990). Some have speculated that POM availability to consumers is dependent on flow mitigation by *M. pyrifera* (Jackson 1983, Rosman et al. 2007).

Hydrodynamic forces within and around kelp beds are also influenced by the presence of giant kelp (Jackson 1983, Graham 2003, Gaylord et al. 2007, Rosman et al. 2007). Drag by *Macrocystis* through the water column results in only 20-70% of flow from prevailing currents extending into the center of a kelp forest (Gaylord et al. 2007); kelp beds have been shown to reduce the current velocity by nearly a factor of 4 (Jackson

1997, Gaylord et al. 2007, Rosman et al. 2007). Kelp beds, therefore, act similarly to airplane wings, causing flow to increase around the periphery by 200% (Gaylord et al. 2007). The dominant flow in California is alongshore (Rosman et al. 2010), however, the across shore current is thought to be responsible for much of the nutrient transport into and out of a kelp bed (Jackson 1998). To better understand the relationship between kelp density and flow impediment, a 1/25 scale kelp forest model was created in two density configurations with and without kelp surface canopies (Rosman et al. 2010). Rosman et al.'s (2010) model concluded that, in a dense forest where frond bundles equaled 0.3m diameter and individuals were spaced 3.75m apart, flow diminished within 14m into the forest. The biological implications for such water flow retardation rests on the ability of particulates to fall through the water column rather than be exported. Falling particulates is critical for the feeding of suspension feeders and successful recruitment of a variety of organisms that rely on spore settlement including *Macrocystis* itself (Gaylord et al. 2002, Graham 2003). A decrease in turbulent mixing is expected to lead to smaller within-bed fluxes of neutrally buoyant particles like phytoplankton and other POM (Denny and Shibata 1989, Rosman et al. 2010). Nevertheless, few studies have attempted to understand flow dynamics through kelp beds on smaller spatial scales, and the effect of kelp stipe density on flow or transport of particles. While past studies have focused on currents through and around kelp beds, little is known about how waves are impacted through kelp beds.

Another physical effect of the *Macrocystis* canopy on the environment is that it diminishes irradiance through the water column beneath it (reviewed by Schiel and Foster 2015). Giant kelp dominates the coasts by outcompeting other autotrophs; shading provided by its sprawling canopy reduces surface irradiance to 0.5-1% at the sea floor (Neushul 1971, Reed and Foster 1984, Clark et al. 2004). This dampening of light is sufficient to dramatically reduce understory growth and recruitment of understory algae (Dayton et al. 1984, Reed and Foster 1984, Clark et al. 2004). Dayton et al. (1984) concluded that the resilience of kelp patches from autotroph invasion was driven by competition for light. The effects of canopy shading on phytoplankton is not well documented, although Foster and Schiel (1985) noted that after storms thin macroalgal abundances, diatoms were observed to form thick mats on the benthos indicating that

benthic diatoms may be opportunistic in the absence of kelp shading. Therefore, patchiness of kelp might reflect phytoplankton-derived particulate organic carbon (POC) throughout a kelp bed emphasizing the importance of isolating phytoplankton from kelp-derived POC.

Macrocystis is one of the most important contributors of energy to the kelp forest community food web in California (Graham 2004, Page et al. 2008, Miller and Page 2012). As defined by Foster and Schiel (2015), primary consumers feed directly on attached algae, detritivores feed on detached drift or liter material, and planktivores feed on material produced in or imported into a kelp forest. The most conspicuous primary grazer in kelp forests is the sea urchin (Foster and Schiel 1985, Estes and Duggins 1995, Graham et al. 2007), which has a penchant for feeding on the haptera of *Macrocystis* (Tegner and Dayton 1981, Estes and Duggins 1995). Such grazing can lead to the dislodgment of the entire kelp thalli and create urchin barrens (Dean et al. 1984, Foster and Schiel 1985, Harrold and Reed 1985, Estes and Duggins 1995, Graham et al. 2007). As mentioned before, the loss of giant kelp is strongly associated with significant reduction in biodiversity (Graham 2004). It is because of this biodiversity loss that many ecologists have studied top-down control of sea urchin populations in kelp systems (Cowen 1983, Tegner 1983, Estes and Duggins 1995, Hamilton et al. 2011). Schiel and Foster (2015, Table 8.1) described other primary consumers found in California kelp beds, including numerous echinoderms, mollusks, and arthropods.

Marine ecologists have suggested that most kelp-derived productivity enters the food web, not by direct grazing, but by production of particulate organic matter (POM) (Gerard 1976, Duggins and Eckman 1997, Graham 2004) via kelp tissue sloughing or senescence and its consumption by filter feeders (Mann 1972, Dayton et al. 1984, Kaehler et al. 2006, Rodriguez et al. 2013). Kelp-derived POM can be quantified by measuring POC through the water column, although this method works best in higher latitudes where phytoplankton contributions to POM are low (Duggins 1994). Teasing apart the contribution of kelp-derived detritus to kelp food webs from other sources of POM has proven difficult due to an inability to quantify phytoplankton-derived POM (Page et al. 2008, Yorke et al. 2013).

A variety of methods have been used in attempt to isolate kelp POM from others, most notably is the use of stable isotope analysis (Fredriksen 2003, Page et al. 2008, Overstrom-Coleman 2009, Miller and Page 2012, Miller et al. 2013, Yorke et al. 2013). The stable isotopes $\delta^{13}C$ and $\delta^{15}N$ have been used as a tracer of kelp-versus phytoplankton-derived POM within food webs studies (reviewed by Schiel and Foster 2015). Defining $\delta^{13}C$ and $\delta^{15}N$ signals for kelp and phytoplankton is contentious (Fredriksen 2003, Page 2008, Yorke et al. 2013). Environmental samples within a kelp bed are assumed to be a 2-source mix of kelp and phytoplankton particulates (Fredriksen 2003, Miller et al. 2013) and therefore, ecologists have relied on obtaining phytoplankton samples far offshore for planktonic $\delta^{13}C$ and $\delta^{15}N$ signal. This approach assumes negligible contribution of kelp particulates within the offshore sample, no change in phytoplankton community composition from offshore to inshore, and similar environmental metabolic interactions between offshore and nearshore phytoplankton. Phytoplankton carbon and nitrogen fractionation are variable due to environmental conditions, location in the water column, and metabolic rates (Tortell et al. 2000, Laws et al. 2002, Needoba et al. 2003, Altabet 2006). Therefore, using isotopic values from offshore phytoplankton to set the phytoplankton $\delta^{13}C$ and $\delta^{15}N$ signature in a two-source mixing model may bias results in food web analysis. A possible solution to this problem is to image phytoplankton in water samples and estimate the organic carbon by each cell volume.

Some of the most convincing studies that solidify the giant kelp as a foundation species have been removal experiments. Kelp removals are common practice to assess the effect of disturbances, such as deforestation by urchins or storms (Byrnes et al. 2011) or competition for light and space (Kimura 1980, Reed and Foster 1984, Edwards 1998, Clark et al. 2004). In southern California, Graham (2004) studied the effects of deforestation of giant kelp beds on community composition, and he concluded that 36% of the common kelp forest species were reduced in deforested areas, 25% of which were kelp forest-obligates, and an overall reduction in 90% of all species. From these studies it is certain that giant kelp has a substantial effect on the kelp forest community (Graham 2004, Byrnes et al. 2011). Currently, international ecological groups, such as the Kelp Ecosystem Ecology Network (KEEN), still conduct such kelp removal experiments. In

these experiments, the response variables are almost always other macro-organisms with aims to identify associations between other species and giant kelp. The inability to isolate trophic from structural effects has, however, resulted in ambiguity of interaction-pathways (Graham et al. 2004, 2007, 2008).

In other marine ecosystems, foundation species have been studied by the creation of artificial habitats, effectively isolating structural effects. Artificial coral reefs have been widely used around the world for coastal erosion mitigation (Hegde 2010), fishery restoration (Bohnsack 1989, Santos and Monteiro 1997, Rilov and Benayahu 1998, Charbonnel 2002), and tourism (Polak and Shashar 2013). Nagelkerken and Faunce (2007) constructed artificial mangroves on Curacao Island and, after 28 days of implementation, reef fish colonized the artificial mangroves from natural coral reefs, indicating that reef fish were dependent on the structure of mangroves for inshore recruitment. Bell (1985) used artificial seagrass beds to assess the community reliance on the seagrass *Zostera capricorni*. Bell's (1985) study showed differences in community structure, which Bell (1985) claimed was only attributed to the time constraints of the study and did not address seagrass grazing. These studies largely aimed to assess community habitat associations and ignored trophic linkages and structural effects that drive habitat associations. No one has attempted to manufacture an artificial kelp forest to assess trophic or habitat associations.

This study used large scale artificial kelp plots to investigate physical impacts within kelp forests. These plots were compared to unmanipulated kelp forests and kelp removal areas to test the artificial kelp design and separate the physical from biological effects of giant kelp. While most kelp forest ecology studies focus on species associations and interactions, I focused on the physical and biological effects of kelp that might influence species associations. Specifically, I asked the following questions: 1) Do kelp removals impact local levels of POC or PON? 2) Do kelp removals impact phytoplankton densities through the water column? 3) Does the loss of kelp change how particle sizes are distributed though the water column? 4) Are there changes in ocean currents within kelp clearings? 5) Does kelp affect the propagation of wind generated waves? By better understanding how the giant kelp's biological and physical effects impact the

environment, ecologists will be able to better understand the mechanisms behind species associations within kelp forest ecosystems. Through the use of small patches within kelp beds, future studies will have a more robust understanding of the mechanisms responsible for organism response to kelp removals.

MATERIALS AND METHODS

Study site

Stillwater Cove (SWC), California (36°33'40.02"N, 121°56'50.31"W) is a small embayment with one southerly ocean boundary (Fig. 2). The western headland, Pescadero Point, provides shelter from northerly swells while the southern headland, Point Lobos, protects SWC from southerly wave action making SWC accessible to study the entire year (Donnellan 2004). The substrate is mostly composed of sandstone and plateaus of granodiorite with depth ranging up to 15 m. *Macrocystis pyrifera* is the dominant canopy-forming alga, while the understory is composed mainly of *Pterygophora californica, Desmarestia ligulata,* and *Stephanocystis osmundacea* (Reed and Foster 1984, Clark et al. 2004, Overstrom-Coleman 2009).

Experimental design

The study site was broken into three blocks, with each block equating to one entire kelp bed (Fig. 2). Blocks ranged from 60 – 70 m in length, with the distance between blocks between 200 - 400 m (Fig. 2). Within each block there were three treatment plots: one removal of *Macrocystis*; one removal of *Macrocystis* with the addition of artificial kelp; and one control where no kelp was removed or added (Fig. 3). Each plot was a 10-m diameter circle at a depth of ~7 m. Plot distances within blocks

ranged from 15 - 40 m apart within blocks, to keep plots at similar depths, a uniform distance was not possible due to the seafloor topography. In clearing plots, *Macrocystis* was cleared by cutting all stipes at the holdfast below the primary dichotomy. The stipes were then pulled out of the bed by boat and released. Every week the surface canopy was trimmed within the clearings to avoid encroachment of surrounding kelp stipes into the study plot.

Construction of artificial kelp

To fully understand the effects of giant kelp on its associated system, physical and biological factors need to be disentangled. To isolate the physical components of giant kelp, artificial kelp was constructed and designed to mimic naturally occurring *M. pyrifera.* The artificial kelp needed similar buoyancy, surface area, and blade density to best mimic effects on shading and flow dampening. Blade density and holdfast size were modeled after North's (1971) reported average of total *M. pyrifera* blade area/ stipe length, average stipe width, average blade internode length, and holdfast average height and width (North 1971, Tables 30 and 64, Fig. 9). The average buoyant force of a single *M. pyrifera* frond was reported to be 2.49N (Utter and Denny 1996).

Stipes were made from 0.95cm diameter polypropylene line and blades were cut uniformly from plastic tarp by hydraulic press. Blades were cut to be 64 cm long and had a tapered width being 7 cm at its widest point (Appendix A, Fig A1). Each blade had a surface area of 448 cm^2. The blades were arranged up the stipe to match North's (1971) area/ stipe length. The stipes were 9 m in length with 40 blades on each stipe to make a frond. Blades were fastened to the polypropylene stipe by zip ties. Starting from the holdfast, blade internode distance for the first 10 blades was 30 cm, the next twenty blades had an internode distance of 10 cm, and the last 10 had an internode distance of 5 cm (Appendix A, Fig. A1).

Natural stipe density and the number of thalli per/plot were estimated by running a subtidal swath transect through two kelp beds in SWC (Appendix A Fig. A2). A histogram of the stipes per-individual shows the probability of stipe size classes in SWC (Appendix A Fig. A3). To match this distribution, the artificial plots consisted of 3 thalli

with 3 fronds, 5 thalli with 8 fronds, 2 thalli with 16 fronds, and 1 thallus with 28 fronds. This range fell within a 75% chance of occurrence found in SWC within the depth range < 7.6 m between June-September 2015 (Appendix A Fig. A4). The 75% cut off was made due to the expense and labor of constructing larger thalli, while maintaining a realistic distribution in a small plot.

Once construction was complete, the artificial frond buoyancy was estimated to be 2.9N, slightly more buoyant than Utter's (1996) value of 2.49N. The conical holdfast dimensions were based off North's (1971) average observation (diameter 1 = 45 cm, diameter 2 = 15 cm, height = 30 cm). The polypropylene stipe lines were pulled through the periphery of a 45 cm diameter plastic dish 5 cm deep. The dish was then filled with cement and allowed to harden (Appendix A Fig. A6). Plastic mesh was then wrapped into a conical shape and filled with more polypropylene line as holdfast haptera. The cone was wrapped around the base of the stipe lines and zip tied to keep in place. Each artificial kelp thalus was secured to the seafloor by two eye bolts 9.5mm diameter and 15cm in length. These bolts were placed in holes drilled into the bedrock by a pneumatic drill and fastened by lag shields and Z-Spar epoxy (Appendix A Fig. A4).

Sample collection

To test variability in water currents through the treatment plots, a SonTek® Acoustic Doppler Profiler (ADP) was deployed during sampling. The ADP was hung by cables 1 m below the water surface from a small craft anchored within the plots. In conjunction with the ADP, a portable underway data acquisition system (UDAS) was used to sample seawater characteristics (Fig. 4). This flow-through system, powered by two electric diaphragm pumps, integrated a suite of standard hydrographic instrumentation, including Seabird's SBE 38 Digital Oceanographic Thermometer and SBE 45 Thermosalinograph, SCUFA Fluorometer, and a Wet Labs C-Star 10 cm Transmissometer sensing temperature, salinity, turbidity, and chlorophyll fluorescence, respectively. The UDAS was equipped with 4 intake vinyl hoses, 2.54 cm in diameter, that reached to 4 depths of the water column: 0m; 2.5m; 5m; and 7.5m, top to bottom respectively. Water was pumped through a course plastic mesh filter (2mm pore size) then through a network of vinyl tubing that passed through each sensor. The UDAS had

an outflow that expelled water out the other side of the vessel. 1L of water was pumped from each depth through the sensors and expelled into opaque plastic bottles. The bottles were kept in a large covered plastic bin on deck floating in seawater to keep cool. Samples were then taken to the lab and processed within 4 hours of collection.

While sampling, the research vessel was anchored in the center of each plot. The intake hoses were deployed by hand over the gunnel and were switched on individually by a 4-way connector. Each hose had a 0.9kg weight attached to the descending end to ensure no hose coiling or drifting. All UDAS sensors were set to sample at a rate of 0.5 cps, while the ADP averaged flow vectors every minute for each depth bin of 0.7m. The UDAS pumping system had a turnover rate of 30s, therefore, each sample depth was pumped for 60 seconds to flush the system, then the water sample was collected. Water collection time was recorded and UDAS data were averaged for 30 seconds during the sample collection. To assess spatial and temporal variations within kelp beds, all sites were sampled once a week from 6/13/2016 – 7/14/2016 pre- manipulations for a total of 5 samples/plot/depth (n = 180). After treatment manipulations were established, two weeks were allocated for the plots to flush and stabilize from their localized disturbance. After the two weeks, sampling commenced once a week in each plot from 8/25/2016 – 10/13/2016 for a total of 6 samples/plot/depth (n = 216).

Response of POC and PON to giant kelp removal

To investigate the sources and distribution of POC and PON, 400 mL of collected water samples taken from each sampling interval at each depth were vacuum filtered onto a pre-combusted Whatman 2.5cm glass fiber filter (GF/F) (Parsons et al. 1984). The filters were then dried at 60° C and placed into a small sealed desiccator until processed for POC/PON content (Parsons et al. 1984). POC and PON (μg/mL) were quantified using an Exeter Analytical Inc. CE-440 Elemental Analyzer. Due to tidal fluctuations, it became clear that during occasional low tides, 5 m depth became the bottom and therefore hose length 7.5 m and 5 m were considered the same depth. The data were adjusted to new depths: surface (0m), mid (2.5m), and sea bottom (~6 m determined by ADP signal).

To assess if there was a pattern of organic carbon and nitrogen concentration through the water column within kelp beds, a blocked one-way ANOVA was used to test if there was a difference in POC and PON concentration (µg/mL) among depth in all plots before treatment. After the treatments were applied to plots, POC and PON (µg/mL) differences were tested among fixed depths and randomized treatments, and treatment*depth by a two-way blocked ANOVA. A post-hoc Tukey HSD test was used on significant factors to discriminate significant levels within factors. POC and PON data were observed to be left-skewed and were log transformed for analysis. To test if POC and PON differences by treatments were due to a spatial phenomenon, a before-after approach was used. The difference in current speed from each study location, before and after treatment application was tested. The assumption of equal variance was tested by Leven's test of variances, then paired means were compared by either Student's or Welch's t-test.

Diatom-derived POC and abundance in response to giant kelp removal

Seawater POC was measured, however, the source of the POC was ambiguous. To address the prevailing notion that phytoplankton contributed a large percentage to the POC pool within kelp beds, phytoplankton and other particulate concentration and size were compared among treatment, depth, and depth*treatment. Diatoms vary spatially and temporally in Monterey Bay (Werner 1977) and make up >80% abundance of phytoplankton larger than 10µm diameter within 20m depth (Garrison 1979), therefore diatoms were used as an indicator of phytoplankton response to kelp removal.

A 50mL subsample of the original 2L water sample collected from the UDAS was placed in a falcon tube and centrifuged at 1500 rounds/minute for 20 min, as described in USGS Laboratory Analysis (1987). After centrifuging, 45mL of the supernatant was removed by aspiration and 0.05mL of glutaraldehyde was added as a fixing agent (Graham and Mitchell 1999). Particles were quantified by Sedgewick Rafter slide and a light microscope at 100x magnification. Twenty random fields of view were imaged per-slide, then using ImageJ particle analysis software calibrated with 45.0µm Fluoresbrite YG-Microspheres, each particle was enumerated and 2-dimensional surface area was

calculated. To separate diatoms, all images were reviewed and every particle that was a diatom was categorized as such. This method yields a detectability cell density > 150 cells/L. Previous studies in Monterey recorded average phytoplankton > 10µm diameter at ~ $2.75x10^5$ cells/L, max = $1.3x10^6$, min = $4.28x10^4$ (Knauer and H. Martin 1973). Therefore, the lowest counts missed in this study would represent < 0.3% of the minimum density reported by Knauer and H. Martin (1973).

To investigate if diatoms were photo-opportunists in kelp removal areas, diatom densities (n/L) were compared across treatment, depth, and treatment*depth. Many of the samples contained zero counts yielding a left skewed non-parametric dataset. To address this issue, the diatom data were assessed using a two-step analysis. First, by assigning a binary presence or absence value and running logistic regressions against all variables, then second, by running a blocked two-way ANOVA on the log-abundance data only, as described by Fletcher et al. 2005). numbered, and surface area was calculated (Grishagin 2015) (Appendix B)

To estimate diatom-derived POC, Menden-Deuer's (2000) formula was used (equation 1), where the amount of organic carbon is proportional to the cell volume.

$$1) \quad \text{pgC cell}^{-1} = 0.288 \times \text{cell volume}^{0.811}$$

To use Menden-Deuer's equation, the diatom volume (µL) was estimated by equivalent spherical diameter (ESD) (Stemmann and Boss 2012). From a 2-dimensional image, diatom surface area was transformed to ESD by equation 2.

$$2)\quad \mathrm{ESD} = 2\sqrt{\frac{A}{\pi}}$$

The equivalent spherical volume (ESV) could then be derived from the ESD (equation 3).

$$3)\quad \mathrm{ESV} = \frac{4}{3}\pi\left(\frac{ESD}{2}\right)^3$$

Organic carbon by diatoms (µg/L) was calculated and the abundance data were log-transformed and tested among treatments, depth, and depth* treatment using a blocked two-way ANOVA. Diatom derived carbon was also regressed against total POC to assess the strength of the relationship.

Particle distribution and predictors of POC

To test if non-diatom particulates differed among treatments and depth, particle concentration (n/L) and individual particle surface areas were calculated using the ImageJ analysis from the same images as the diatom analysis (Appendix B). Total particulates were not a good indicator due to the range of sizes, therefore, the particle sizes needed to be assessed as well. In order to test the difference in particulate sizes among treatments and depth, particle size distribution (PSD) slopes were calculated by binning the particle size data and fitting a curve to the histogram as described by Stemmann and Boss (2012). PSD curves were calculated by Python script (Appendix C).

Particle concentration (n/L) and the PSD slope were compared among treatments, depth, and depth* treatment by a blocked two-way ANOVA. To assess which variables measured from the UDAS were best at predicting POC and PON within kelp beds, turbidity (NTU), fluorescence (µg/L), and beam attenuation (1/m) were regressed against POC and PON. In order to test if diatoms were accountable for the fluorescence signal, diatom concentration and non-diatom particulates were regressed against fluorescence. Finally, diatom and non-diatom particulate concentrations were regressed against POC and PON the strengths between the two sources of POC and PON.

Effect of giant kelp removal on temperature and salinity

Oceanographic conditions, salinity (PSU) and temperature (C), were analyzed

from each depth zone among treatments to assess if kelp shade had a cooling effect within plots and if there existed any halocline or thermocline within the study area. Salinity and temperature were compared among water depth, treatment, and depth* treatment by a blocked two-way analysis of variance (ANOVA) tests. Tukey's honest significant difference (HSD) test was used to define the significance within factors.

Effect of giant kelp removal on currents

The ADP produced 1-minute averages of north, east, and vertical velocity components (cm/s). Using the Pythagorean theorem ($a^2+b^2 = c^2$), water speed was calculated. The ADP data quality was validated by first discriminating the seafloor by strong acoustic amplitude spikes (SonTek 2000). To test the effect of giant kelp removal on currents (cm/s), the ADP was deployed at every plot during water collections and averaged a run time of 7 minutes.

Variation in vertical and horizontal currents between treatments and depth were assessed by a two-way blocked ANOVA on post-treatment ADP data. All significant factors were followed by post-hoc Tukey HSD tests to define differences between each level of depth and treatment. To test if current speed differences by treatments were due to a spatial phenomenon, a before-after approach was used. The difference in current speed from each study location, before and after treatment application, was tested. The assumption of equal variance was tested by Leven's test of variances, then paired means were compared by either Student's or Welch's t-test.

Kelp stipe impact on wave orbital velocities and vertical mixing

To test the hypothesis that the thallus of *Macrocystis* caused vertical mixing from the bottom up, within kelp beds, a series of fluorescein dye releasing experiments were implemented in and out of the kelp beds, and among varying stipe bundles and velocities. Using a single microfluorometer array composed of 3 Turner Designs self-contained underwater fluorescence apparatuses (SCUFAs) attached to a vertical line through the water column in 1.5 m intervals from the bottom (Fig. 5). SCUFAs were calibrated to detect the dye (µg/mL) at a sampling rate of 0.5Cps. To capture water velocity, the

fluorometer array was coupled with a Nortek acoustic Doppler velocimeter (ADV) placed on the seafloor to measure water velocity components; *Y* (North), *X* (East), and *Z* (vertical) coordinates at a sampling rate of 2cps.

For each dye release experiment, the ADV, SCUFA array, and dye injection tube were positioned by SCUBA divers. Once in place, divers would exit the water onto a small R/V located at least 10m downstream from the experimental site. Three grams of fluorescein dye (Uranine powder 40%) were mixed with seawater in a 140cc syringe and pumped through vinyl tubing to the sea bottom 1m upstream from the array. An additional 420cc of seawater was pumped through the tubing allowing the dye to pass all the way through the tubing. Sensors recorded for 20 minutes after dye release, after which they were retrieved by line.

Fluorescence and water velocity fluctuate naturally causing ambiguity in detecting the dye from the environment. To correct for ambient fluorescence, the SCUFA array was cast into a kelp bed, void of dye, for 2 hours sampling at 0.5Cps, and the maximum deviation from the mean was recorded as a noise maximum. For each dye release trial, each SCUFA recorded the mean ambient fluorescence for one minute, and the noise maximum was added to create a dye detection threshold. To capture the maximum variation in water velocity, the velocity components *X* and *Y* were rotated to the principal axis (PA) (Emery and Thomson 1998). To reduce noise in the dataset and capture the largest velocities, the standard deviation of PA1 defined as *U* was used in all analyses.

The first experiment tested if there was a difference in vertical dye movement inside and outside of kelp beds and to assess if kelp slowed wave orbital speeds. Eight random sites were chosen along Carmel State Beach, California (Fig. 6). These sites were chosen due to a lack of subtidal pinnacles and coastal points obstructing waves entering the kelp beds. Each site was coupled with one sample in and one sample out of the bed. First, the instruments were placed in the kelp bed behind the first row of *Macrocystis* and the dye was released on the upstream side of the *Macrocystis* stipes. The sensors were then moved outside the bed upstream of the first dye release, and the next dye run started. To test for a difference in vertical dye detection, a Pearson Chi-squared

test was used for each SCUFA in and out of the kelp bed. To test for a difference in water velocity (*U)*, a T-test was used to compare the means for *U* and the standard deviation of vertical velocity in and out of kelp beds.

To aid in the assessment of kelp's impact on waves and turbulence, a velocity spectrum was created ($m^2*s^{-2}*cps^{-1}$) illustrating the wave frequency in cycles per second (cps) (Emery and Thomson 1998). Due to data loss from the ADV, data from only 4 of the 6 previous dye releasing experiments were analyzed. *U* data was transformed to a periodogram using a Fast Fourier Transform, then transformed to a power spectrum. The power spectra were smoothed using Welch's method and a Hanning window (Appendix D) and a 95% confidence interval was computed as described by Emery and Thomson (1998).

The second experiment tested the importance of the number of *M. pyrifera* stipes and the seawater velocity on vertical movement of dye released. To ensure a wide range of water velocities, 5 additional kelp sites were randomly selected within a sheltered area of Stillwater Cove, CA (Fig. 6). These 5 sites were added to the dataset collected from experiment one in Carmel bay. For each kelp site, the number of stipes was recorded that separated the dye injection tube from the SCUFA array. The effect of *M. pyrifera* stipes and horizontal water velocity *U* on vertical dye detection duration (s) was assessed using linear regression.

RESULTS

Sources and variation in POC and PON

In establishing a baseline of POC and PON distribution within kelp beds, POC and PON concentration (µg/L) from unmanipulated plots were compared among depth by a blocked one-way ANOVA. There was a significant difference in POC by depth (ANOVA: $F_{2,131} = 3.64$, $p < 0.001$, Table 1), where the mid water (2.5m) had lower concentrations of POC than the bottom and water, while there was no difference between the surface and bottom water (Tukey HSD, $p < 0.05$, Fig. 7). There was no significant difference in PON by depth (ANOVA: $F_{2,131} = 1.86$, $p = 0.158$, Table 1). After

treatments were applied, POC varied significantly by treatment (blocked two-way ANOVA POC: $F_{2,161} = 6.62$, $p < .01$), however, PON did not, (Table 2, Fig. 8 & 9), where POC was higher within artificial treatments compared to kelp and kelp cleared treatments (Tukey HSD, $p < 0.05$). Higher concentrations of POC and PON from the seafloor (~6m) seem to be the source of variation (Fig. 8 & 10). It is notable that, while not statistically significant, the mean POC and PON were also higher within the clearing treatments at the bottom depth compared to control kelp treatments. To test if results were spatially dependent, mean POC and PON were compared before and after treatment. There was no significant difference in mean POC and PON due to treatment, confirming the prior ANOVA results (Table 3).

Diatom contribution to POC in response to kelp removal

To test if diatoms are photo-opportunists, diatom concentration (n/L) was tested among treatment and depth. There was no significant difference in diatom presence among treatments (X^2: $R^2 = 0.005$, $p = 0.658$) or depths (X^2: $R^2 = 0.01$, $p = 0.43$) (Table 4a). However, there was a significant difference in diatom density among depths (blocked two-way ANOVA: $F_{2,67} = 10.619$, $p < 0.001$, Table 4b), where diatom abundance was highest on the sea floor (~6m) compared to midwater (2.5m) and surface water (0m) (Tukey HSD, $p < 0.05$, Fig. 11). To assess if total POC was dependent on diatom organic carbon, diatom-derived carbon (µg/L) was regressed against total POC (µg/L) when diatoms were present. There was no significant relationship between diatom-derived carbon and total organic carbon ($R^2 = 0.518$, $F_{1,63} = 3.39$, $p = 0.07$, Fig. 12).

To test if diatom-derived carbon varied among depth and treatment a blocked two-way ANOVA was used to test differences in diatom derived carbon among depth, treatments, and treatment* depth. There was no significant difference in diatom-derived carbon among treatments, depth, or depth* treatment (blocked two-way ANOVA: $F_{10,63} = 1.312$, $p = 0.248$, Table 5). It is worth noting, while not statistically significant, mean diatom-derived was lower in the clearing treatments at the surface and mid water depths compared to other treatments, however, this pattern changed at the bottom water depth where diatom-derived carbon was higher compared to the control treatment (Fig 13).

Overall, diatoms were found to contribute very little to the overall POC pool (max = 2.92%, mean = 0.53%, min = 0.015%).

Particle distribution and predictors of POC

To characterize particles among treatments and depth, particle concentration (n/L) and PSD slope were tested by a blocked two-way ANOVA. Particle concentration was log-transformed to normalize right-skewed data. There was no block effect and the block was removed from the analysis. There was a significant difference in PSD by depth (blocked two-way ANOVA: $F_{10,66} = 1.06$, $p = 0.044$, Table 6) where the mid water PSD slope was higher than the bottom or surface waters (Tukey HSD, $p < 0.05$) (Fig. 14). There was no significant difference in particle concentration, however, particle concentration by depth was found to be near significant (blocked two-way ANOVA: $F_{2,110} = 2.8$, $p = 0.061$, Table 6) where the bottom water had the highest concentration compared to mid and surface waters.

Using data from the UDAS, other measured variables were tested as predictors of POC and PON. Beam attenuation (1/m), fluorescence (ug/L), and turbidity (NTU) were regressed against POC and PON. There was a significant, but weak, relationship between POC and PON and fluorescence (Regression; POC: $R^2 = 0.052$, $F_{1,161} = 8.7$, $p = 0.003$; PON: $R^2 = 0.2$, $F_{1,161} = 40.23$, $p < 0.001$). However, there was no significant relationship between POC and PON by turbidity (Regression; POC: $R^2 = 0.002$, $F_{1,161} = 0.036$, $p = 0.54$, PON: $R^2 = 0.0002$, $F_{1,161} = 0.04$, $p = 0.83$) or beam attenuation (Regression; POC: $R^2 = 0.0005$, $F_{1,161} = 0.087$, $p = 0.76$, PON: $R^2 < 0.0001$, $F_{1,161} = 0.0006$, $p = 0.98$) (Fig. 16, Table 7). Fluorescence was the best predictor of POC and PON from the UDAS, therefore fluorescence was regressed against diatoms and particles to see which variable was driving the fluorescence-POC/PON signal. Fluorescence had a significant relationship to non-diatom particulate concentration (n/L) (Regression; $R^2 = 0.076$, $F_{1,119} = 9.74$, $p = 0.0023$), while there was no significant relationship between fluorescence and diatom concentration (cell/L) (Regression; $R^2 = 0.002$, $F_{1,65} = 0.12$, $p = 0.72$) (Fig. 17).

($\pm$ 1.7The two sources of POC and PON, were assumed diatoms and everything else (non-diatom particulates), therefore diatom cell concentration and non-diatom

particulates concentration were tested by regression. There was a significant relationship between total non-diatom concentration and POC & PON ($R^2 = 0.53$, $F_{1,120} = 141.8$, $p < 0.001$; $R^2 = 0.52$, $F_{1,120} = 131.93$, $p < 0.001$), respectively (Fig. 18). There was no significant relationship between diatom concentration and POC & PON ($R^2 = 0.04$, $F_{1,66} = 3.27$, $p = 0.074$; $R^2 = 0.032$, $F_{1,66} = 2.19$, $p = 0.14$) respectively (Fig. 19).

Effect of giant kelp removal on temperature and salinity

Salinity and temperature were analyzed to assess if kelp shade also has a cooling effect within plots and if a halocline or thermocline existed within the study area. There was a significant difference in temperature by depth (two-way ANOVA; $F_{2,18} = 10.02$, $p = 0.001$) (Table 8). Temperature was significantly different at all depths, warmest water resided at the surface and cooled with increasing depth (Tukey HSD, $p < 0.05$, Fig. 20). However, there was no treatment effect on temperature, nor an interacting effect of temperature* depth. There was no difference in salinity among treatment, depth, or treatment* depth (Table 9).

Effect of giant kelp removal on currents

The ADP data quality was validated by first discriminating the seafloor by signal amplitude inflection point (SonTek 2003) (Fig. 21). Upon discriminating the seafloor within plots, it was evident that the two bottom zones (5m and 7.5m) were overlapping due to tidal fluctuation. To fix this issue, the depth zones were re-described as surface (0m), mid (2.5m), and bottom (depth of signal amplitude inflection point). Once the seafloor was identified, the signal was then assessed for errors in the velocity data by the acoustic signal being reflected off kelp within plots, velocities were plotted against signal amplitude, SE, and signal to noise ratio, SE is defined $SE = \frac{SD_{velocity}}{\sqrt{(number\ of\ pings)}}$. The velocity in the SE calculation includes the Doppler noise (SNR) is defined as $\sigma = \frac{number\ of\ pings}{F\Delta z\sqrt{N}}$ where F is the acoustic frequency, Δz is the sampling cell range in meters, and N is the number of samples (pings). As the SNR decreases below 3dB the SE increases rapidly (SonTek 2003). While kelp did increase the signal amplitude and signal

to noise ratio, the SE was virtually unchanged indicating the velocity data was unaffected by the kelp (Fig. 21).

The mean current speed differed among treatments (Table 10; 2-way blocked ANOVA $F_{2,161} = 10.05$, $p < 0.0001$). The current speed within kelp cleared plots was significantly faster than plots with artificial and natural kelp (Tukey HSD; $p < 0.05$, Fig. 22), where kelp cleared plots contained the fastest currents ($\overline{x} = 3.99$ cm/s), while control plots contained the slowest currents ($\overline{x} = 2.2$ cm/s). There was no significant difference in vertical speeds between treatments, depth, or depth*treatment (Table 11). To test if the differences in currents by treatment were spatially dependent instead of treatment dependent a before/ after approach was used. The current speeds were compared for each study plot before and after treatment. In all clearing and one artificial treatment, currents were significantly faster compared to their same location before treatment (t-test, $p < 0.001$) (Fig. 23, Table 12).

Kelp stipes impact on wave orbital velocities and vertical mixing

To test the hypothesis that the presence of giant kelp facilitated vertical flow, dye was pumped to the benthos and detected by a micro-fluorometer array inside and outside of kelp beds along Carmel State Beach, CA. A Pearson's Chi-square test showed that there was no difference in dye detection between bottom and mid water within and outside of kelp beds (Fig. 24). However, there was a significant difference in dye detection at the uppermost sensor (Pearson; $X^2 = 9.479$, $p = 0.002$), where dye was detected 100% of the time within kelp beds, compared to being detected only 16.7% of the time outside of the kelp bed.

To test the impact of *Macrocystis* on wave orbital velocities and turbulence , the ADV was deployed in and out of 5 different kelp beds off Carmel State Beach CA. Comparing the means of the standard deviation of the principle axis velocity (U) as a proxy for wave orbital velocity showed that there was no difference in wave orbital velocity among inside and outside of kelp beds (Student's t; $t = -0.395$, $p = 0.695$), where $\overline{U}$ was 13.9 cm/s, $U_{max} = 20.4$ cm/s, and $U_{min} = 3.4$ cm/s. There was also no difference in the SD of the velocity component Z (Student's t; $t = -0.38$, $p = 0.7$). To investigate

directionality of vertical water speed, the mean and SD of *Z* was plotted (Fig. 25). The plot shows little difference in the vertical direction of water flow ($\overline{Z}$). The plot also shows that the SD of *Z* had higher variance within kelp beds compared to outside, indicating more extreme values.

To test for differences in kinetic energy, which is proportional to velocity squared (m^2*s^{-2}) by frequency (cps) inside and outside of beds, power spectra of velocity along the principal axis were analyzed. The frequency accounting for the most energy were long waves at ~$10^{-1.5}$ cps or a wave period (*T)* of 31.6s (Fig. 26). Wave energy was similar or higher outside of kelp beds in the lower frequencies (< $10^{-0.5}$ cps, *T* > 3.16s), however there was a difference at the higher frequency range (>$10^{-0.5}$ cps). At these higher frequencies, there was a shift and higher energy was observed inside the beds. Plotting the calculated 95% confidence interval (Fig. 26) shows that 2 out of the 4 spectra showed that energy within the >$10^{-0.5}$ cps range was significantly higher. However, all 4 spectra have the same pattern of kelp beds having higher energy in the shorter frequencies (>$10^{-0.5}$ cps). It also appears that there may be a detection limit indicated by all plots leveling off at ~10^{-5} ($m^2*s^{-2}*cps^{-1}$), therefore, even if there was a difference in kinetic energy at high frequencies it would be undetectable.

To test if the size of the *Macrocystis* stipe bundle was related to the efficiency of diverting horizontal (x y) orbital velocity to vertical (z), stipes were enumerated during dye releasing experiments and an additional 4 sheltered sites were added to increase variability in orbital velocities (Fig. 6). Dye detection duration (s) was used as the response variable to determine the degree of water movement. A two-way ANOVA revealed that at the sea bottom (SCUFA 1) and upper water (SCUFA 3), dye duration was related to the interaction of stipe number and water velocity (Bottom water: $F_{1,9} = 6.17$, $p = 0.047$, Upper water: $F_{1,9} = 6.15$, $p = 0.047$), while the midwater (SCUFA 2) showed no relationships between dye duration and stipe number, *U*, or *U** stipe number (Table 13). Plotting dye duration against the interaction term (*U** stipes) showed that at the seafloor dye residence time decreases with increasing stipes and water speed ($R^2 = 0.45$, $F_{1,9} = 6.7$, $p = 0.031$), while dye duration in the upper water increases with increasing stipes and water speed ($R^2 = 0.69$, $F_{1,9} = 18.32$, $p = 0.0027$) (Fig. 27). The middle water however,

showed no relationship between dye duration and stipe number ($R^2 = 0.32$, $F_{1,9} = 3.80$, $p = .087$). To assess if the dye was being moved by turbulence caused by *U**stipes Reynolds number was calculated using stipe bundle diameter and *U*. Reynolds number is defined as $R = \frac{\rho V D}{\mu}$ where ρ is the fluid density, V is the fluid velocity, D is the diameter of the object the fluid passes and μ is the dynamic viscosity of the fluid. As R increases from 300 → $3x10^5$ the flow transitions from laminar to turbulent (Fig. 28). Assuming the stipes are a single cylinder, R was calculated for each dye release (Table 14). R ranged from $1.74x10^3$ to $2.08x10^4$ and dye duration and R were positively correlated. It appeared that $R > 2.5x10^3$ consistently moved dye to the upper water column while $R < 2.5x10^3$ failed to move dye upward 4.5m from the bottom.

DISCUSSION

Kelp forests are some of the most productive and dynamic ecosystems in the world (Lieth and Whittaker 1975, Dayton 1985, Graham et al. 2007). The giant kelp acts as the foundation species responsible for providing energy in the form of fixed carbon and a physical habitat (Graham et al. 2007). Many studies have focused on species associations and interactions within kelp forests by performing kelp removals. However, kelp removals affect the ecosystem by removing trophic energy and physical habitat leaving species linkages ambiguous. This study disconnected the energy provision from habitat by constructing artificial kelp habitat. Instead of measuring community response, other parameters were analyzed that could be influential to kelp forest communities, POC, PON, phytoplankton, particle size distribution, turbidity, currents, and temperature. Artificial kelp sites were compared to natural and kelp cleared plots. This study shows that POC, PON, particle size distribution, and phytoplankton are not significantly affected by kelp removal plots within the kelp forests. What was affected by kelp removal was seawater currents. Currents significantly increased in speed within kelp removal plots, determined from the one-minute averages from the ADP. Furthermore, this study investigated the effects of waves interacting with giant kelp and found observed elevated turbulence within kelp beds, this is likely due to vortex shedding when waves interact with kelp. Wave energy breaks into turbulence upon impact with kelp

stipes. This process is capable of resuspending particulates into the water column. These findings help illustrate that small-scale kelp removals are have more physical impacts to the kelp forest system than biological, reinforcing that past and future kelp removal experiment community results are likely more physically affected than biologically.

The artificial kelp was overall a success in replicating a complex natural environment, but there was still room for improvement. In terms of physical structure, the artificial kelp did dampen sea currents (Figs. 22 & 23) but was less successful at shading compared to natural kelp (Appendix A Fig. A9). The artificial kelp plots likely had more irradiance because the artificial kelp didn't sprawl across the water surface the same as natural kelp; it was more easily moved by wind and was observed to bunch up to the downwind side of the plot. Still the artificial kelp was observed to be a suitable habitat hosting numerous organisms including fish, crab, gastropods, and epibionts (Appendix A Fig. 7,8). The artificial kelp plots also showed similar current speed as the control kelp plots, meaning the surface area drag was similar. The biggest problem of encountered was fouling. Diatoms and other epiphytes colonized the artificial kelp which confounded POC / PON. The goal was to keep the kelp structure and remove the kelp POC input. While it is unlikely that epiphytes would have had as much growth as giant kelp, it likely cased POC ambiguity within artificial plots. This artificial kelp design is appropriate for short duration studies (< 2 months), after which fouling could be intense enough to weigh down artificial stipes and distort natural buoyancy. A design improvement would be figuring out how to reduce fouling, and using a material that was non-fibrous, such as the rope used. The fibrous material enabled epiphytes to root into the stipe material.

The kelp beds within this study showed that POC (< 2 mm) ranged from 158.57 - 7359.63 $\mu g*L^{-1}$ ($\bar{x}$ = 531.52, SD = 801.78). These values are higher than the previously reported average of ~300 $\mu g*L^{-1}$ by Overtrom-Coleman (2009) during the same season, however, Overtrom-Coleman (2009) collected smaller particulates (< 1 mm) and only sampled one depth zone (10 cm above the seafloor). The current study's average POC was also similar to another study at Mohawk Reef, California from 2007-2011, where the average POC through the water column within kelp beds was ~574 $\mu g*L^{-1}$ (Yorke et al. 2013). All these values are substantially higher than POC reported offshore. Hill and

Wheeler (2002) measured POC in the northern California current and reported the average POC at 3 m depth to be 151.2 $\mu g*L^{-1}$. Clearly there is more primary production nearshore, which has been attributed to nutrient inputs such as upwelling and rivers (Hill and Wheeler 2002). That primary production acts as the base of the nearshore food chain. Understanding the production sources and utilization of primary production into trophic food webs is vital to understand coastal ecosystems.

Since the first study quantifying POC within kelp beds by Gerard (1976), studies have aimed to illustrate how particulates are able to fall to the seafloor within kelp beds for other organisms to feed upon (Gaylord et al. 2002, Graham 2003, Rosman et al. 2010). With such high turnover of kelp biomass, it would be reasonable to assume that kelp detritus would exceed grazers' demands and accumulate on the seafloor. This study has shown that there is no accumulation of POC or PON (< 2 mm) on the seafloor within kelp beds. While mean POC was significantly higher on the seafloor compared to the mid water, there was no difference between the surface water and seafloor (Fig. 7). This congregation of POC in the upper and bottom water may be due to boundary layer effects. The kelp canopy and the sea floor exert the most drag on water flow within kelp beds (Rosman 2010, Denny 2014). These boundary layers may cause particulates to get trapped within the mixing layer. If there is a more turbulent layer over a thermocline, a neutral particle is expected to re-enter the mixed layer numerous times when it encounters the wake of the lower layer (Lande and Wood 1986). Upon leaving the layer, particles may sink faster through the midwater and again get trapped within the bottom layer. After application of treatments, higher mean POC concentrations were found at the bottom of artificial and kelp cleared treatments compared to control plots, but only the artificial treatment was significantly higher (Fig. 9). One block seemed to be driving the variance (Fig. 10) and was observed to have higher rugosity than that of other plots. Since the intake hoses were lowered without viewing the landing location, it is possible that the hose intake landed in a crevasse full of trapped detritus. Future benthic POC studies should have an increased number of blocks to account for extremely high benthic POC variability.

While the sea floor did show higher POC and PON in kelp removal plots compared to the control, the removal of kelp had no significant effect on POC, PON, PSD, or concentration of particulates (Fig. 8, 9, 14). This lack of pattern can be due to 3 possible reasons: 1) giant kelp doesn't contribute very much to the particulate signal; 2) the plot size (10 m diameter) was too small to change the POC signal; or 3) the currents moved particulates to an adjacent area downstream. The first point has been argued by Yorke et al. (2013) who quantified POC and PON production rates from kelp blades to only contribute 1% of total POC. However, Yorke et al. (2013) only counted particulates that were suitable for filter feeders (< 250μm). Such particle selection likely underestimates giant kelp's contribution to the POC pool because all larger particulates eventually break down into smaller particulates (Rodriguez 2013). Rodriguez (2013) observed that kelp biomass was primarily lost by senescence of fronds. If fronds can stay within the system and be broken down along the substrate, then a large portion of kelp detritus has been ignored by Yorke et al. (2013). A recent study by Miller et al. (2015) shed some light on the second issue (small plot size) where a much larger size clearing (40m x 40m) was used. In their study, Miller et al. (2015) concluded that the invertebrates' diets didn't change in the absence of *Macrocystis,* meaning the invertebrates still had free access to kelp particulates even though kelp had been removed. Miller et al (2015) concluded that the adjacent kelp biomass was enough to add POC to the clearing, hypothesizing that POC signals would vary over larger scales than previously thought. What remains unknown, is how large a kelp clearing need be to significantly lower the POC signal within the plot, or how far away from a kelp bed does a plot need to be to be rid of the POC signal. Overstrom-Coleman (2009) showed that the kelp POC signal for a kelp bed can be detected up to 500m away from the source, but more information is needed about the source as far as kelp bed size and density. Furthermore, does that lower POC signal exist but has been carried to another part of the bed? Currents moving particulates into cleared plots would take about 8-9 minutes to move water through the cleared plot with the average current speed ~2 $cm*s^{-1}$

Macrocystis has been identified as the competitive dominant for light in giant kelp forests (Reed and Foster 1984, Clark et al. 2004). While previous investigations focused on sub-canopy kelps and understory algae, none have quantified the shading impact on

phytoplankton. This study showed that diatom concentration was higher in the bottom water, but there was no significant difference by treatment, meaning that diatoms didn't appear to increase in areas with increased light availability (Fig. 11). Foster and Shiel (1985) had noted that benthic diatoms formed thick matts where kelp was absent. While this study does agree that the highest concentration of diatoms was found on the benthos, no diatom bloom was observed in kelp cleared plots. After kelp was removed, two weeks were allocated for system flushing and stabilization; within this time, it is possible that diatoms increased and an increase in grazer activity reduced the numbers. Another possibility why this study didn't show a boom of benthic diatoms is that the pumping system was not strong enough to rip them off the substrate. Benthic diatoms can attach themselves with their multistrand tethers that arise along the raphe openings and extend from the cell forming a holdfast-like attachment with the substratum (Higgins et al 2003). A better alternative to water pumping for benthic diatoms density estimations would be settlement plates. Settlement plates could be bolted or weighted down and retrieved periodically for accurate counts. Pelagic diatoms float in the water column and are moved by currents. The water pumps were good for collecting pelagic diatoms, however at the rate that water moved through the plots, diatoms generated within the 10 m diameter plot would be carried away within minutes. If there was a positive relationship on diatoms from lack of shade, it didn't appear to persist within the plots, but the signal could have been carried away. To capture such an event, water collection swaths would need to be conducted downstream from the plot area.

Ecologists have attempted to separate the POC contributions by kelp and phytoplankton within kelp forest ecosystems. Some have quantified the POC contribution by kelp (Gerard 1976, Reed et al. 2008, Overstrum-Coleman 2009, Yorke et al. 2013), while others looked to consumers (Duggins et al. 1989, 1994, 1997, Miller et al. 2011, 2013, 2015). This study has shown that diatoms contribute ~ 2.9% to the total POC pool within kelp beds. Using only twenty images made diatom detection problematic. In some samples, diatoms weren't located within 20 images, and thus, created zeros in the dataset. Future studies should look at images until a certain number of diatoms are reached. Venrick (1978) recommended that in a sample, cells should be counted to 100 yielding a precision of ±20% within a 95% confidence interval. In some cases, this may not be

possible where diatom density is extremely low and larger quantities of water are logistically difficult to obtain. None the less, by only analyzing samples where diatoms were present, it was clear that diatom-derived carbon was quite low. Even with low precision (±50%) diatoms would still contribute less than 10% of the total standing POC pool. Even though the standing crop of diatoms was low compared to reports of giant kelp (Reed et al. 2008), if we take into account the growth rate of diatoms, assuming a cell doubling/day and integrating through the water column diatoms net primary production (NPP) could be estimated between 0.06 - 0.76g C/m^2/day during this study, where Reed et al. (2008) reported 1.83g - 3.5g C/m^2/day for giant kelp. If we assume a two-source model, then diatoms would contribute 20% total NPP. While this time period was a non-diatom bloom period one could assume that during periods where kelp is reduced by the winter storms and phytoplankton begin to bloom, the scales would be tipped into phytoplankton becoming the primary producer for at least a short while.

Fluorescence had a weak but significant relationship with POC and PON. This indicated that primary productivity contributed to the POC and PON pool. While there was no relationship of diatoms and POC/ PON we can assume that most of the fluorescence was caused by kelp and other macro algae. The weak fluorescence relationship likely existed because fluorescence measures light excitation of chlorophyll pigments (Maxwell. and Johnson 2000). The structure of chlorophyll degrades after cell death, and the process is accelerated by light intensity. Pigments nearly completely degrade (99.4%) within one day at only 37% average surface irradiance (60 Ein m^{-2} *d^{-l}) (Nelson 1993), whereas the organic carbon from algae can take weeks to be degraded by the microbial community (Biddanda 1988). The even weaker relationship between POC/ PON and turbidity was harder to explain. The SCUFA turbidity (NTU) failed in predicting POC/ PON. Seawater clarity on such fine scales may not change enough to effect NTU. The data showed that the seawater turbidity median was 6 NTU while the 75% quartile was at 9 NTU. The SCUFA used light beam attenuation through a volume of water with particulates, the microscope images are of a thin spread of particulates which reduces particle overlap. The SCUFA was a crude device for the level of particulates in most samples.

The average currents within the kelp beds were relatively slow (~ 2 cm*s^{-1}), close to the detectability threshold of the ADP (SonTek 2003). Slow currents are common within kelp beds, Jackson (1997) reported between 2-3 cm*s^{-1} in Point Loma. From the signal-to-noise ratio and standard error of the ADP velocity readings, there was no reason to believe that kelp stipes distorted the velocity signal in any way. There could have been issues determining between the sea floor and thick understory of *Pterygophora*, but this would have only shortened the depth of the ADP beam inflection point and the velocity data within the understory was discarded. While the accuracy of such slow speeds was low (SE ± 1.5 cm*s^{-1}), it is certain that the currents in control plots were relatively slower than the kelp cleared areas. In kelp cleared areas, the average currents were found to be twice as fast as currents within control and artificial kelp plots (Fig. 18, 19). One artificial plot showed increased current speed toward the end of the experiment (Fig. 19). There were two observations that could explain this anomaly, 1) urchins holding artificial stipes down 2) self-entanglement. Urchins are known to feed on drift kelp (Harrold and Reed 1985). As kelp encounters an urchin, the urchin will grab the kelp with its tube feet and hold it until it's ready to feed. Within the study sites a few artificial fronts were observed to be completely pulled down by several urchins. If enough fronds were pulled down the drag would have been significantly reduced. Self-entanglement was also observed within artificial plots which could have changed the total surface area and reduce drag. To eliminate these issues a few maintenance dives were conducted. In future artificial kelp studies urchins should be relocated away from plots and maintenance dives should be done weekly for untangling and epiphyte removal.

The result that currents speed up within kelp removal plots appears to be novel. One possible mechanism is wind. Rosman (2010) showed that most of the drag by giant kelp was within its sprawling canopy. This canopy would cause drag within the water and create a barrier to wind stress. Wind forcing is known to be a prevailing force that drives coastal currents (Ekman 1902, Sverdrup 1947). A scaling analysis of the simplified momentum equation $u\frac{\partial u}{\partial x} = \frac{1}{\rho}\frac{\partial \tau}{\partial z}$ was used to estimate wind forcing upon the plot where, u is horizontal water velocity, ρ is the density of seawater, τ is the wind stress (N*m^{-2}) , x = distance (10m), and z is the depth of the water to be moved (6m). Using a seven-year

average wind stress during the summer months in Monterey Bay (~ 0.05 $N*m^{-2}$) (Pennington and Chavez 1999) water acceleration was calculated to be 0.83 $cm*s^{-1}$ within kelp cleared plots. While this can't explain the 2 $cm*s^{-1}$ difference between control and kelp removed plots, the wind stress of the exact study area is unknown and is applying some force on the cleared area.

Another explanation of why currents accelerated in kelp cleared areas are other forces that influence ocean currents. Water density gradients determined by temperature and salinity can also drive costal currents (Huang 2009) and Rosman (2007) claimed that density driven flows are important within kelp forests in Santa Cruz, CA. While there was no indication of a vertical density gradient with no difference in salinity by depth within the study plots, there was a difference in temperature by depth (Fig. 20, Table 8), however without a larger sampling area it would be difficult to detect a horizontal density gradient that would account for a density forced flow. There was no difference in the current speed by depth, however, there was a depth dependent directionality of the currents. The average current vector within plots, the surface water tends to move to the Southwest (offshore), while the bottom water moves Northwest (shoreward) (Fig. 29). These results are similar to a long-term oceanographic study at Stillwater Cove by Carroll (2009). Carroll found that the bottom boundary layer moved Northeast entering the mouth of the cove during the summer (Jun. – Oct. 2006). Carroll (2009) concluded that the Northwest flow became stronger in shallower waters, however, measurements were only taken to a depth of 9 m. In doing so, Carroll failed to capture the water mass exodus from the cove. The Carmel Marine Canyon offshoots within 2.5 km from the study site (Fig. 30). Carroll (2009) attributed the currents in Stillwater Cove to internal waves from the Carmel Canyon along with seasonal wind-driven upwelling. Cold dense water from the canyon likely moves shoreward (Northeast) and the surface water is advected out to sea (Southwest) by wind forcing.

The most likely explanation for increased current speed within kelp cleared plots, is that the work against the moving body of water was removed and the water returned to its previous speed that it would have been before entering the kelp bed. Bernoulli's principle (1738) states that for an inviscid flow, an increase in the speed of the fluid

occurs simultaneously with a decrease in pressure or a decrease in the fluid's potential energy. However, the theory of conservation of energy states that energy is never lost but transformed (Mendl 1988). When moving water encounters kelp, pressure against the kelp is increased and transforms some of the flow energy into turbulence, a chaotic distribution of flow speeds and directions. The fate of turbulence is dissipation and on extremely small scales, energy is released by creating heat. Turbulent water decreases in mean speed, then eddies are dissipated at a rate ϵ. ϵ can be derived by $\epsilon \sim u^3/\ell$ where ℓ represents the size of the largest eddies or the width of the flow and u is the fluid velocity (Tennekes and Lumley 1972). Therefore, smaller eddies created by kelp stipes would dissipate quickly and join the ambient flow. This has been demonstrated on larger scale models involving clearings in a terrestrial forest. Frank and Ruck (2008) concluded that with increasing clearing width between two forests, the air speed within the clearing increases. The forest model does illustrate the conservation of energy and diversion of flow on large scales, however, unlike a kelp forest an arboreal forest has airflow above the canopy that streams into the clearing low pressure zone downstream of the forest. More rigorous studies are needed to outline the complexity of turbulence and flow within kelp forests and kelp cleared zones. I have illustrated a conceptual model showing how seawater velocity may move through a kelp cleared area (Fig. 31).

Waves, like currents, were also impacted by the *Macrocystis* thallus. While there was no significant change in velocity component *Z* inside kelp beds compared to outside (Fig. 25), vertical velocity is highly subject signal interference with the dominant velocity components *X* and *Y*. If the ADV is slightly tilted, horizontal velocity can be mistaken as vertical. As wave move to shallower water, the orbits become more elliptical (Denny 2014). Eventually the ellipse becomes elongated along the horizontal axis, and the motion feels back and forth, this is what is typically referred to as surge. Therefore, wave energy in the horizontal (x-y) plane increases as the water column becomes shallower (shoreward) while the energy in the vertical (z) plane decreases with depth (Denny 2014). When horizontal orbits are encountering kelp structure, some energy is being displaced vertically along the downstream side of the kelp stipes. This has also been observed in subtidal vegetation where the wake created by submerged vegetation changed the sediment deposition patterns downstream of the vegetation (Hu et al. 2018). This

phenomenon is common with other grounded vertical calendrical objects like pylons. The turbulence on the downstream side of the object can lift surrounding sediment and move it downstream, engineers call this scouring (Kobayashi 1992).

The wave power spectrum (Fig. 26) between 4 paired samples of velocity fluctuations inside and outside of kelp beds were observed to show differences in higher frequency waves (>$10^{-0.5}$ Cps). Waves in Monterey bay during the summer have an average period of 6-8 s ($10^{-0.8}$ – $10^{-0.9}$ Cps) with the highest deviation being $10^{-0.6}$ Cps (NOAA station 46042; Appendix E). Higher frequencies are likely smaller eddies and turbulent shedding from the larger waves entering shallow waters. However, the amount of energy inside the kelp bed was higher within these higher frequencies, showing that there was more turbulence within kelp beds. Panel A and C has the highest difference in high frequency wave energy and had the highest Reynolds number, $3.3x10^3$ and $1.96x10^3$ respectively. Panel D had a slightly lower Reynolds number $1.90x10^3$ compared to panel C however there was no significant difference in higher frequencies. This could be due to the instruments detectability limit or spacing by kelp stipes, as the Reynolds numbers are calculated assuming a single column. Rosman et al. (2007, Fig. 10) showed a similar spectra comparing much longer period internal waves inside and outside of a kelp bed in Santa Cruz, CA. The figure showed higher energy in longer periods (T = 1 day) outside of the kelp bed compared to inside the bed, however, these trends converge on higher frequencies (10^{-2} cpd). In this study, the instrument was able to sample much higher frequencies (10^0 cps), where higher energies were within the kelp bed.

The benthic dye releasing experiment showed that dye moved from the sea bottom to the surface only within kelp beds (Fig. 24). The combination of sheltered sites with wave exposed sites showed that the dye duration was significantly related to U (m/s)* stipe number (Fig. 27, Table 13). Dye duration had a negative relationship with increasing U (m/s)* stipe number within the bottom water, while having a positive relationship at the surface water. This means that the dye was washed away faster at the bottom with increasing U (m/s)* stipe number at the same time more dye was detected in the surface water. These results are again backed by the calculation on Re, where dye duration had a positive trend with Re. One unanswered question is how much the

substrate impacts the waves. The study area had a very defined kelp forest border, which was determined by the presence or absence of rocky substrate, while outside of the bed was dominated by sandy bottom. Did these rocks also have an impact on waves? During this study, three kelp beds were tested for vertical dye transfer, then the beds were removed and tested again. Before the manipulation, the dye moved from the bottom to the surface, while after the kelp removal the dye only made it to the mid water as in the rest of the out of bed trials. Unfortunately, this test was only completed once for one day each. This led to the inability to sperate the effect of wave orbit speed, as there was no variation to analyze. I would recommend a well replicated BACI design (Underwood 1994) where each bed is tested in the same day as manipulation, where each bed is tested on separate days to keep each paired test in the same wave environments.

Vertical variations within kelp beds could explain how particulates are able to be so evenly distributed though the water column. While it's known that currents slow through kelp beds, and the prevailing ecological paradigm is for particulates to settle, this study has shown that waves likely play a larger role than currents in particulate dispersal, also shown by Rosman et al. (2007) by internal-waves and Lagrangian transport due to surface waves (Stokes drift). Currents within beds are slow, and at such slow speeds would be incapable of causing vertical turbulent shedding when stationary objects are encountered (Denny 1988). Rosman et al. (2010) also came to this conclusion using a 1/25-scale kelp model claiming that the kelp canopy drag slows the current down to the point that turbulence generated by the kelp wake make little difference though a dense kelp bed. Waves on the other hand, move much faster, typically as a wave moves shoreward through a kelp bed, the water depth decreases closer to shore. As the depth decreases, the orbit becomes more and more elliptical causing more and more energy in the horizontal plane (Denny 2014). What is unknown, is if this increasing *X*-*Y* axis energy can maintain through a kelp bed, and at what density kelp would need to be to dissipate the increasing surge.

This study sheds more light on other giant kelp clearing experiments findings. In the case of studies where giant kelp was removed for shading effects (Reed and Foster 1984, Shiel 1985, Clark et al. 2004), the response variable was sub canopy or understory

macroalgae. We now know that currents were also impacted by the removal of the giant kelp structure. Higher flow could affect the uptake rates of nitrogen needed for algae growth (Denny and Roberson 2002). This would likely be the case where nitrogen was limited and flow within the kelp bed was relatively slow. In cases of kelp removal studies and organism impact (Graham 2004, Byrnes et al. 2011, Miller et al. 2015), this study has shown that kelp removals within a bed does not affect the POC available to consumers and therefore, the physical structure is responsible for organism variation. This finding was recently realized by Miller et al. (2015) in a much larger clearing (40 x 40 m). Miller et al. (2015) found invertebrates to decrease in abundance and diets remained unchanged by *Macrocystis* removal. Miller et al. (2015) discussed that slower flow within kelp beds could reduce consumption and larval supply via decreased flux (Nowell and Jumars 1984, Butman et al. 1988), but leaned toward the theory that particles fall to consumers in slower flows (Labarbera 1984). What Miller et al. (2015) didn't consider, was the ability for currents to speed up when kelp is removed and particulates to be mixed within kelp bed instead of falling. This could help explain why in their removal plot, invertebrates diet remained unchanged (free access to POC) and decreased in cover (lower settlement rates). Settlement in different flow regimes have been poorly studied, but it is believed that propagules have a settlement response to different flow regimes (Abelson and Denny 1997). It stands to reason that the settlement rates would vary in different hydrodynamic environments.

CONCLUSIONS

It appears that small scale *Macrocystis* removal experiments within kelp beds are investigations into the absence of the physical structure. Particulates, POC, and PON are well mixed through kelp beds likely due to turbulence caused by wave orbitals shearing off *Macrocystis* stipes. It is still unknown if wave orbital velocities are diminished in larger beds, such as Point Loma, California. Currents are too slow to cause turbulent mixing within kelp beds. Currents are slowed through the bed, however, within removal plots currents can speed back up, the exact mechanism remains unknown. When kelp is removed within a bed, there is no change to POC concentration, however, there was some indication that POC may increase within the bottom waters within clearing. The POC

signal is likely a range scale dependent on the size of the surrounding bed. This study found that diatoms contribute less than 3% of total POC within kelp beds, and that diatoms concentration is higher on the benthos. Diatoms have not shown themselves to be long term photo-opportunists in the absence on *Macrocystis* shade. This study concluded that kelp-derived POC is more abundant and available to consumers which may be more important on larger spatial scales. On smaller spatial scales within kelp beds, it appears that physical effects of the giant kelp have higher impacts.

LITERATURE CITED

Abelson, A., Denny, M. (2007). Settlement of marine organisms in flow. *Annual Review of Ecology and Systematics*, 28(1), 317-339

Altabet, M.A. (2006). Isotopic tracers of the marine nitrogen cycle: present and past. In:Volkman JK (ed) *Handbook of Environmental Chemistry*, Vol 2. Marine Organic Matter:biomarkers, isotopes and DNA: 251–293.

Atkinson, M.J. and Smith, S.V. (1983). C: N: P ratios of benthic marine plants 1. *Limnology and Oceanography*, *28*(3), pp.568-574.

Bane, J.M., Spitz, Y.H., Letelier, R.M. and Peterson, W.T. (2007). Jet stream intraseasonal oscillations drive dominant ecosystem variations in Oregon's summertime coastal upwelling system. *Proceedings of the National Academy of Sciences*, USA 104(33), 13262-13267.

Beckley, L., Branch, G. A. (1992). Quantitative scuba-diving survey of the sublittoral macrobenthos at subantarctic Marion Island. *Polar Biology,* 11, 553-563.

Bell, J.D., Steffe, A.S., Westoby, M. (1985). Artificial seagrass: How useful is it for field experiments on fish and macroinvertebrates? *Journal of Experimental Marine Biology and Ecology,* 90, 171–7.

Bodkin J.L. (1988). Effects of kelp forest removal on associated fish assemblages in central California. *Journal of Experimental Marine Biology and Ecology,* 117, 227–38.

Bohnsack, J.A. (1989). Are high densities of fishes at artificial reefs the result of habitat limitation or behavioral preference? *Bulletin of Marine Science,* 44(2), 631-645.

Butman, C., Grassle, J., Webb, C. (1988). Substrate choices made by marine larvae settling in still water and in a flume flow. *Nature,* 333, 771-773.

Byrnes, J.E., Reed, D.C., Cardinale, B.J., Cavanaugh, K.C., Holbrook, S.J. and Schmitt, R.J., (2011). Climate-driven increases in storm frequency simplify kelp forest food webs. *Global Change Biology,* 17, 2513-2524.

Carroll, D. (2009). Carmel Bay: Oceanographic dynamics and nutrient transport in a small embayment of the central California coast. *Master's Thesis, California State University, Monterey Bay.*

Carr, M.H. (1989). Habitat selection and recruitment of an assemblage of temperate zone reef fishes. *Journal of Experimental Marine Biology and Ecology,* 146, 113–37.

Carr, M.H. (1994). Effects of macroalgal dynamics on recruitment of a temperate reef fish. *Ecology,* 75, 1320-1333.

Carr, M.H., Reed, D.C. (2011). Conceptual issues relevant to marine harvest refuges: examples from temperate reef fishes. *Canadian Journal of Fisheries and Aquatic Sciences,* 50, 2019-2028.

Chamberlain, Y.M. (1965). Marine algae of Gough Island. *Bulletin of the British Museum (Natural History) Botany,* 3, 173-232.

Charbonnel, E. (2002). Effects of increased habitat complexity on fish assemblages associated with large artificial reef units (French Mediterranean coast). *ICES Journal of Marine Science,* 59(suppl), S208–13.

Clements, F.E., Shelford, V.E. (1939). Bio-ecology. New York: J. Wiley and Sons. Cook SA 1962 Genetic system, variation, and adaptation in Eschscholzia californica. *Evolution,* 16, 278-299.

Clark R.P. Edwards M. S., Foster. M. S. (2004). Effects of shade from multiple kelp canopies on an understory algal assemblage. *Marine Ecology Progress Series,* 267, 107-119.

Collins, T.J. (2007). ImageJ for microscopy. *Biotechniques,* 43(1 Suppl), 25-30.

Cowen, R.K. (1983). The effects of sheephead (*Semicossyphus pulcher*) predation on red sea urchin (*Strongylocentrotus franciscanus*) populations: an experimental analysis. *Oecologia*, 58, 249–55.

Dayton, P.K. (1972). Toward an understanding of community resilience and the potential effects of enrichments to the benthos at McMurdo Sound, Antarctica. In *Proceedings of the Colloquium on Conservation Problems in Antarctica* (pp. 81-96). Lawrence, Kansas, USA, Allen Press.

Dayton, P.K., Currie, V., Gerrodette, T., Keller, B.D., Rosenthal, R., Tresca, D.V. (1984). Patch dynamics and stability of some California kelp communities. *Ecological Monographs,* 54, 253–289.

Dean, T.A., Schroeter, S.C., Dixon, J.D. (1984). Effects of grazing by two species of sea urchins(*Strongylocentrotus franciscanus* and *Lytechinus anamesus*) on recruitment and survival of two species of kelp (*Macrocystis pyrifera* and *Pterygophora californica*). *Marine Biology,* 78, 301-313.

Denny, M.W., Shibata, M.F. (1989). Consequences of surf-zone turbulence for settlement and
external fertilization. *American Naturalist,* 134, 859-889.

Denny, M., Roberson, L. (2002). Blade motion and nutrient flux to the kelp, Eisenia arborea. *The Biological Bulletin,* 203(1), 1-13.

Denny, M. (2014). *Biology and the mechanics of the wave-swept environment* (Vol. 917). Princeton University Press.

De Martini, E.E., Roberts, D.A. (1990). Effects of giant kelp (*Macrocystis*) on the density and abundance of fishes in a cobble-bottom kelp forest. *Bulletin of Marine Science,* 46, 287 300.

Dixon, J., Schroeter, S.C., Kastendiek, J. (1981). Effects of the encrusting bryozoan, *Membranipora membranacea,* on the loss of blades and fronds by the giant kelp, *Macrocystis pyrifera* (*Laminariales*). *Journal of Phycology,* 17, 341-345.

Donnellan, M. (2004). Spatial and temporal patterns of kelp canopies in central California. Master's Thesis, San Jose State University, California.

Duggins, D.O., Simenstad, C.A., Estes, J.A. (1989). Magnification of secondary production by kelp detritus in coastal marine ecosystems. *Science* 245, 170–173.

Duggins, D.O., Eckman, J.E., Sewell, A.T. (1990). Ecology of understory kelp environments. II. Effects of kelps on recruitment of benthic invertebrates. *Journal of Experimental Marine Biology and Ecology* 143, 27–45.

Duggins, D.O., Eckman, J.E. (1994). The role of kelp detritus in the growth of benthic suspension feeders in an understory kelp forest. *Journal of Experimental Marine Biology and Ecology,* 176, 53–68.

Duggins, D.O., Eckman, J.E. (1997). Is kelp detritus a good food for suspension feeders? Effects of kelp species, age and secondary metabolites. *Marine Biology,* 128, 489–95.

Ekman, V. (1902). On the influence of the earth's rotation on the wind driven current in the Ocean. *Nyt Mag Naturv*, 40, 37-63.

Edwards, M.S. (1998). Effects of long-term kelp canopy exclusion on the abundance of the annual alga *Desmarestia ligulata* (Light F). *Journal of Experimental Marine Biology and Ecology* 228, 309–26.

Elton, C.S. (1927). Animal ecology. *University of Chicago Press.*

Emery, W.J., Thomson, R.E. (1998). Data analysis methods in physical oceanography. *Oceanographic Literature Review*, *1*(45).

Estes, J.A., Duggins, D.O. (1995). Sea otters and kelp forests in Alaska: generality and variation in a community ecological paradigm. *Ecological Monographs,* 65, 75-100.

Fletcher, D., MacKenzie, D., Villouta, E. (2005). Modelling skewed data with many zeros: a simple approach combining ordinary and logistic regression. *Environmental and ecological statistics*, 12(1), 45-54.

Foster, M.S., Schiel, D.R. (1985). The ecology of giant kelp forests in California: a community profile. *US. Fish and Wildlife Service Biological Report,* 85(7.2).

Fredriksen, S. (2003). Food web studies in a Norwegian kelp forest based on stable isotope ($\delta^{13}C$ and $\delta^{15}N$) analysis. *Marine Ecology Progress Series,* 260, 71–81.

Fulton, E.A., Smith, A.D.M., Johnson, C.R. (2003). Effects of complexity on marine ecosystem models. *Marine Ecology Progress* Series 253, 1–16.

Gaylord, B., Reed, D.C., Raimondi, P.T., Washburn,L., McLean, S.R. (2002). A physically based model of macroalgal spore dispersal in the wave and current dominated nearshore. *Ecology,* 83, 1239-1251.

Gaylord, B., Rosman, J.H., Reed, D.C., Koseff, J.R., Fram, J., MacIntyre, S. (2007). Spatial patterns of flow and their modification within and around a giant kelp forest. *Limnology Oceanography,* 52, 1838–52.

Garrison, D.L. (1979). Monterey Bay phytoplankton I. Seasonal cycles of phytoplankton assemblages. *Journal of Plankton Research*, 1(3), pp.241-265

Geider, R.J., MacIntyre, H.L., Kana, T.M. (1997). Dynamic model of phytoplankton growth and acclimation: responses of the balanced growth rate and the chlorophyll a: carbon ratio to light, nutrient-limitation and temperature. *Marine Ecology Progress Series,* 148, 187-200.

Gerard, V.A. (1976). Some aspects of material dynamics and energy flow in a kelp forest in Monterey Bay, California. *Ph.D dissertation, University of California Santa Cruz.*

Ghelardi, R. J. (1971). Species structure of the animal community that lives in *Macrocystis pyrifera* holdfasts. *Nova Hedwigia,* 32, 381-419.

Graham, M.H., Mitchell, B.G. (1999). Obtaining absorption spectra from individual macroalgal spores using microphotometry. *In Sixteenth International Seaweed Symposium,* 231-239

Graham, M.H. (2003). Coupling propagule output to supply at the edge and interior of a giant kelp forest. *Ecology,* 84, 1250-1264

Graham, M.H. (2004). Effects of local deforestation on the diversity and structure of southern California giant kelp forest food webs. *Ecosystems,* 7, 341–357.

Graham, M.H., Vásquez, J.A., Buschmann, A.H. (2007). Global ecology of the giant kelp *Macrocystis*: from ecotypes to ecosystems. *Oceanography and Marine Biology An Annual Review,* 45, 39–88.

Graham, M.H., Halpern, B.S. and Carr, M.H. (2008). Diversity and dynamics of Californian subtidal kelp forests. *Food webs and the dynamics of marine reefs*, 103.

Grall, J., Le Loch, F.Guyonnet, B. Riera, P. (2006). Community structure and food web based on stable isotope analysis of North Eastern Atlantic maerl bed. *Journal of Experimental Marine Biology and Ecology* 338, 1-15.

Grishagin, I.V. (2015). Automatic cell counting with ImageJ. *Analytical biochemistry*, 473, 63-65.

Hairston, N. G., Smith, F. E., Slobodkin, L. B. (1960). Community structure, population control, and competition. *American Naturalist,* 94, 421-424.

Halpern, B.S., Cottenie, K., Broitman, B.R. (2006). Strong top-down control in southern California kelp forest ecosystems. *Science,* 312, 1230-1232.

Hamilton, S. (2011). Extensive geographic and ontogenetic variation characterizes the trophic ecology of a temperate reef fish on southern California (USA) rocky reefs. *MarineEcology Progress Series,* 429, 227–244.

Harrold, C. and Reed, D.C. (1985). Food availability, sea urchin grazing, and kelp forest community structure. *Ecology*, 66, 1160-1169.

Higgins, M.J., Molino, P., Mulvaney, P. and Wetherbee, R. (2003). The structure and nanomechanical properties of the adhesive mucilage that mediates diatom-substratum adhesion and motility 1. *Journal of Phycology*, 39(6), 1181-1193.

Hill, J.K., Wheeler, P.A. (2002). Organic carbon and nitrogen in the northern California current system: comparison of offshore, river plume, and coastally upwelled waters. *Progress in Oceanography*, 53(2-4), 369-387.

Hu, Z., Lei, J., Liu, C., Nepf, H. (2018). Wake structure and sediment deposition behind models of submerged vegetation with and without flexible leaves. *Advances in water resources*, *118*, 28-38.

Huang, H., Imran, J., Pirmez, C., Zhang, Q., Chen, G. (2009). The critical densimetric Froude number of subaqueous gravity currents can be non-unity or non-existent. *Journal of Sedimentary Research*, *79*(7), 479-485.

Hulbert, J. H. (1984). Pseudoreplication and the design of field experiments in ecology. *Ecological.Monographs,* 54, 187-211.

Jackson, G.A. (1998). Currents in the high drag environment of a coastal kelp stand off California. *Continental Shelf Research,* 17, 1913–1928.

Jackson, G.A., Winant, C.D. (1983). Effect of a kelp forest on coastal currents. *Continental Shelf Research,* 2, 75–80.

Jones, M. B., Azevedo, J. M. N., Neto, A. I., Costa, A. C., Martins, A. M. F. (1999). Island, ocean and deep-sea biology. *Proceedings of the 34th European Marine Biology Symposium,* 13-17.

Johnson, N. L. (1949). Systems of frequency curves generated by methods of translation. *Biometrika*, 36(1/2), 149-176.

Kaehler, S., Pakhomov, E., Kalin, R. (2006). Trophic importance of kelp-derived suspended particulate matter in a through-flow subAntarctic system. *Marine Ecology Progress Series,* 316, 17-22.

Kimura, R. S. (1980). The effects of harvesting *Macrocystis pyrifera* on understory algae in Carmel Bay, California. Masters Thesis, California State University, Fresno.

Kobayashi, T. (1992). 3d analysis of flow around a vertical cylinder on a scoured bed. *Coastal Engineering Proceedings*, *1*(23), 3482-3495.

Krumhansl, K.A., Okamoto, D.K., Rassweiler, A., Novak, M., Bolton, J.J., Cavanaugh, K.C., Connell, S.D., Johnson, C.R., Konar, B., Ling, S.D. and Micheli, F., 2016. Global patterns of kelp forest change over the past half-century. *Proceedings of the National Academy of Sciences*, 113(48), 13785-13790.

Labarbera, m. (1984). Feeding currents and particle capture mechanisms in suspension feedinganimals. *American Zoologist*, 24 (1), 71-84.

Lam, K., Li, J.Y., Chan, K.T. (2003). Flow pattern and velocity field distribution of cross-flow around four cylinders in a square configuration at a low Reynolds number. *Journal of Fluids and Structures,* 17, 665–79.

Lande, R., Wood, A.M. (1987). Suspension times of particles in the upper ocean. *Deep Sea Research Part A. Oceanographic Research Papers*, 34(1), 61-72.

Laws E.A., Popp B.N., Cassar N., Tanimoto J. (2002). ^{13}C discrimination patterns in oceanic phytoplankton: likely influence of CO_2 concentrating mechanisms, and implications for palaeoreconstructions. *Functional Plant Biology,* 29, 323–333.

Levin, P.S. (1993). Habitat structure, conspecific presence and spatial variation in the recruitment of a temperate reef fish. *Oecologia,* 94, 176–85.

Levins, R. (1974). Discussion paper: the qualitative analysis of partially specified systems. *Annals of the New York Academy of Sciences,* 231(1 Mathematical), 123–38.

Lund, J., Kipling, C., Cren, E.D. (1958). The inverted microscope method of estimating algal numbers and the statistical basis of estimations by counting. *Hydrobiologia,* 11, 143-170.

Mann, K.H., Breen, P.A. (1972). The relation between lobster abundance, sea urchins, and kelp beds. *Canadian Journal of Fisheries and Aquatic Sciences,* 29, 603–5.

Mann K.H. (1988) Towards predictive models for coastal marine ecosystems. In: Pomeroy L.R., Alberts J.J. (eds) Concepts of Ecosystem Ecology. Ecological Studies (Analysis and Synthesis), vol 67. *Springer, New York, NY.*

Mandl, F. (1988). Statistical Physics (2nd ed.*). Chichester New York Brisbane, Toronto Singapore: John Wiley & sons.*

Maxwell, K. and Johnson, G.N. (2000). Chlorophyll fluorescence—a practical guide. Journal of *experimental botany*, 51(345), 659-668.

Menden-Deuer, S., Lessard, E.J. (2000). Carbon to volume relationships for dinoflagellates, diatoms, and other protist plankton. *Limnology and Oceanography,* 45, 569-579.

Meneghini, J. R., Saltara, F., Siqueira, C.L.R., Ferrari, J.A. (2001). Numerical simulation of flow interference between two circular cylinders in tandem and side-by-side arrangements. *Journal of Fluids and Structures,* 15, 327–50.

Miller, R. J., Page, H. M. (2012). Kelp as a trophic resource for marine suspension feeders: a review of isotope-based evidence. *Marine Biology,* 159, 1391–402.

Moorcroft, P.R. (2006) How close are we to a predictive science of the biosphere? *Trends in Ecology & Evolution*, 21, 400-407.

Nagelkerken I, Faunce C. H. (2007). Colonisation of artificial mangroves by reef fishes in a marine seascape. *Estuarine, Coastal and Shelf Science,* 75:417–22.

Needoba, J. A., Waser, N. A., Harrison, P. J., Calvert, S. E. (2003). Nitrogen isotope fractionation in 12 species of marine phytoplankton during growth on nitrate. *MarineEcology Progress Series* 255, 81−91.

Nelson, J. R. (1993). Rates and possible mechanism of light-dependent degradation of pigments in detritus derived from phytoplankton. *Journal of Marine Research,* 51, 155–79.

Neushul, M. (1971). Submarine illumination in *Macrocystis* beds. *Nova Hedwigia Beihefte,* 32, 241-254.

Norberg, C. (2001). Flow around a circular cylinder: aspects of fluctuating lift. *Journal of Fluids and Structures,* 15, 459-469.

North, W. (1971). The biology of giant kelp beds *Macrocystis* in California. *Nova Hedwigia Beihefte,* 32, 1-600.

Nowell, A., Jumars, P. (1984). Flow Environments of Aquatic Benthos. *Annual Review of Ecology and Systematics*, 15(1), 303-328

Novak, J. M., Wootton, T., Doak, D. F., Emmerson, M., Estes, J. A., Tinker, T. M. (2011). Predicting community responses to perturbations in the face of imperfect knowledge and network complexity. *Ecology,* 92, 836-846.

Overstrom-Coleman, M. (2009). Spatiotemporal variability and ecological significance of Macrophyte-derived particulate organic matter (POM) within and surrounding a central California giant kelp forest. *Thesis, Moss Landing Marine Laboratories, California State University Monterey Bay.*

Page, H. M., Reed, D. C., Brzezinski, M. A., Melack, J. M., Dugan J. E. (2008). Assessing the importance of land and marine sources of organic matter to kelp forest food webs. *MarineEcology Progress Series,* 360, 47-62.

Parsons, T. R., Yoshiaki, M., Lalli, M. C. (1984). A Manual of Chemical and Biological Methods for Seawater Analysis. *Oxford: Pergamon*. Print.

Pearse, J. S., Lowry, L. F. (1974). An annotated species list of the benthic algae and invertebrates in the kelp forest community at Point Cabrillo, Pacific Grove, California. *Coastal Marine Laboratory,University of California Technical Report.*

Pennington, T. J., & Chavez, F. P. (2000). Seasonal fluctuations of temperature, salinity, nitrate, chlorophyll and primary production at station H3/M1 over 1989–1996 in Monterey Bay, California. *Deep Sea Research Part II: Topical Studies in Oceanography*, 47(5–6), 947–973.

Pimm, S. L. (1982). Food Webs. *London: Chapman and Hall.*

Polak, O., Shashar, N. (2013). Economic value of biological attributes of artificial coral reefs. *ICES Journal of Marine Science,* 70, 904–12.

Power, E. M., Tilman, D., Estes, J., Menge, B., Bond,W., Mills, S., Daily, G., Castilla, J., Lubchenco, J., Paine, R. (2006). Challenges in the Quest for Keystones. *BioScience* 46, 609-620.

Puccia, C. J., Levins, R. (1985). Qualitative modelling of complex systems: an introduction toloop analysis and time averaging. *Harvard university,* 8, 259.

Quast, J. C. (1971). Some physical aspects of the inshore environment, particularly as it affects kelp bed fishes. *Nova hedwigia Beihefte,* 32, 229-240.

Raffaelli, D. (2010). Ecosystem ecology: a new synthesis. *Cambridge University.*

Ramsing, N., Gundersen, J. (1994). Seawater and gases. Tabulated physical parameters of interestto people working with microsensors in marine systems. Version 1.0. Revised tables compiled at Max Planck Institute for Marine Microbiology. Bremen, Germany.

Redfield, A. C. (1934). On the proportions of organic derivatives in sea water and their relation to the composition of plankton. *James Johnstone memorial,* 176-192.

Reed, D. C., Foster, M. S. (1984). The effects of canopy shadings on algal recruitment and growth in a giant kelp forest. *Ecology,* 65(3), 937-948.

Reed, D. C., Rassweiler, A., Arkema, K. K. (2008). Biomass rather than growth rate determines variation in net primary production by giant kelp. *Ecology,* 89, 2493-2505.

Reed, D. C., Brzezinski, M. A. (2009). Kelp forests. in Laffoley, D., Grimsditch, G. The management of natural coastal carbon sinks. *International Union for Conservation of Nature.*

Reilly, T. E., Franke, L., Bennett, G. D. (1987). Techniques of Water-Resources Investigations of the United States Geological Survey.

Rilov, G., Benayahu, Y. (1998). Vertical artificial structures as an alternative habitat for coral reef fishes in disturbed environments. *Marine Environmental Research,* 45, 431–51.

Rosman, J. H., Koseff, J. R., Monismith, S. G., Grover, J. (2007). A field investigation into the effects of a kelp forest *Macrocystis pyrifera* on coastal hydrodynamics and transport. *Journal of Geophysical Research,* 112, C02016.

Rosman, J. H., Monismith, S. J., Denny, M. W., Koseff, J. R. (2010). Currents and turbulence within a kelp forest *Macrocystis pyrifera*: Insights from a dynamically scaled laboratory model. *Limnology. Oceanography,* 55, 1145-1158.

Santos, M. N., Monteiro, C. C. (1997). The Olhão artificial reef system (south Portugal): Fish assemblages and fishing yield. *Fisheries Research,* (1-2), 33–41.

Schaal, G., Riera, P., Leroux, C. (2012). Food web structure within kelp holdfasts (*Laminaria)*: a stable isotope study. *Marine Ecology,* 33, 370-376.

Sheail, J. (1987). Seventy-five years in ecology: *The British Ecological society.* Blackwell Scientific Publications, Oxford.

SonTek ADP® (2003). Acoustic Doppler Profiler Technical Documentation

Stemmann L., Boss E. (2012). Plankton and particle size and packaging: from determining optical properties to driving the biological pump. *Annual Review Marine Science,* 4: 263−290.

Steneck, R. S., Graham, M. H., Bourque, B. J., Corbett, D., Erlandson, J. M., Estes, J. A., Tegner, M. J. (2003). Kelp forest ecosystems: biodiversity, stability, resilience and future. *Environmental Conservation,* 29, 436–59.

Sverdrup, H. U. (1947). Wind-driven currents in a baroclinic ocean; with application to the equatorial currents of the eastern pacific. *Proceedings of the National Academy of Sciences*, *33*(11), 318.

Tansley, A. G. (1935). The use and abuse of vegetational concepts and terms. *Ecology,* 16, 284 307.

Tegner, M., Dayton, P. (1981). Population structure, recruitment and mortality of two sea urchins (Strongylocentrotus franciscanus and S. purpuratus) in a kelp forest. *MarineEcology Progress Series,* 5, 255-268.

Tegner, M. J., Levin, L. A. (1983). Spiny lobsters and sea urchins: Analysis of a predator-prey interaction. *Journal of Experimental Marine Biology,* 73:125–50.

Tennekes, H., Lumley, J. (1972). a first course in turbulence. *The Massachusetts Institute of Technology.*

Tortell, P., Rau, G., Morel, F. (2000). Inorganic carbon acquisition in coastal Pacific phytoplankton communities. *Limnology and Oceanography*, 45(7), 1485-1500.

Turner, J. (2002). Zooplankton fecal pellets, marine snow and sinking phytoplankton blooms. *Aquatic Microbial Ecology*, *27*(1), 57–102.

Underwood, A. J. (1994). On Beyond BACI: Sampling designs that might reliably detect environmental disturbances. *Ecological Applications*, *4*(1), 3–15.

Utter, B., Denny, M. (1996). Wave-induced forces on the giant kelp *Macrocystis pyrifera* (Agardh): field test of a computational model. *Journal of Experimental Biology,* 199, 2645–2654.

Venrick, E. L. (1978). The implications of subsampling. *Phytoplankton manual. UNESCO,* 75- 87.

Vinyard, W. C. (1979). Diatoms of North America. *Mad River Press*, *Eureka, California*.

Watanabe, J. M. (1984). The influence of recruitment, competition, and benthic predation on spatial distributions of three species of kelp forest gastropods *Trochidae: Tegula*. *Ecology*. 65(3), 920-936.

Werner, D. (1977). The biology of the diatoms. *University of California Press*.

White, T. R. C. (1978). The importance of relative shortage of food in animal ecology. *Oecologia*, 33, 71-86.

Whittaker, R. H., Likens, G. E. (1973). The primary productivity of the biosphere. *HumanEcology*, 1, 299-369.

Willis, A. J. (1997). The ecosystem: an evolving concept viewed historically. *Functional Ecology*, 11, 268-71.

Yorke, E. C., Miller, J. R., Page, M. H., Reed, C. D. (2013). Importance of kelp detritus as a component of suspended particulate organic matter in giant kelp *Macrocystis pyrifera*. *Marine Ecology Progress Series,* 493, 1131-125.

FIGURES

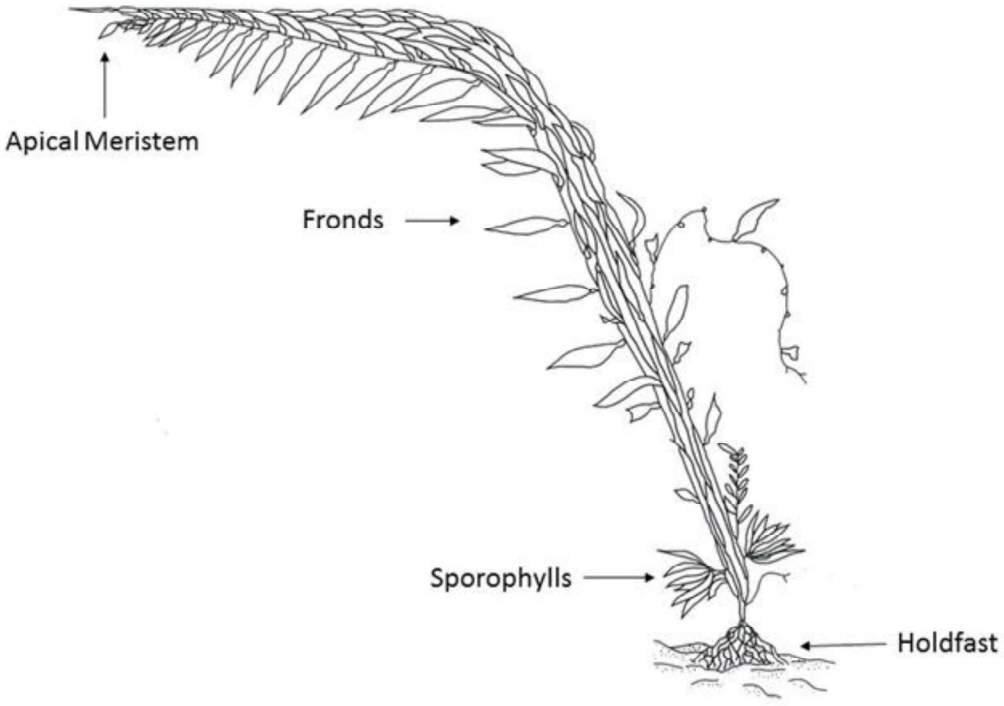

Figure 1: (*Macrocystis pyrifera*) thallus held to substrate by holdfast. Each individual frond consists of a stipe and attached blades. (Image adapted from North 1971)

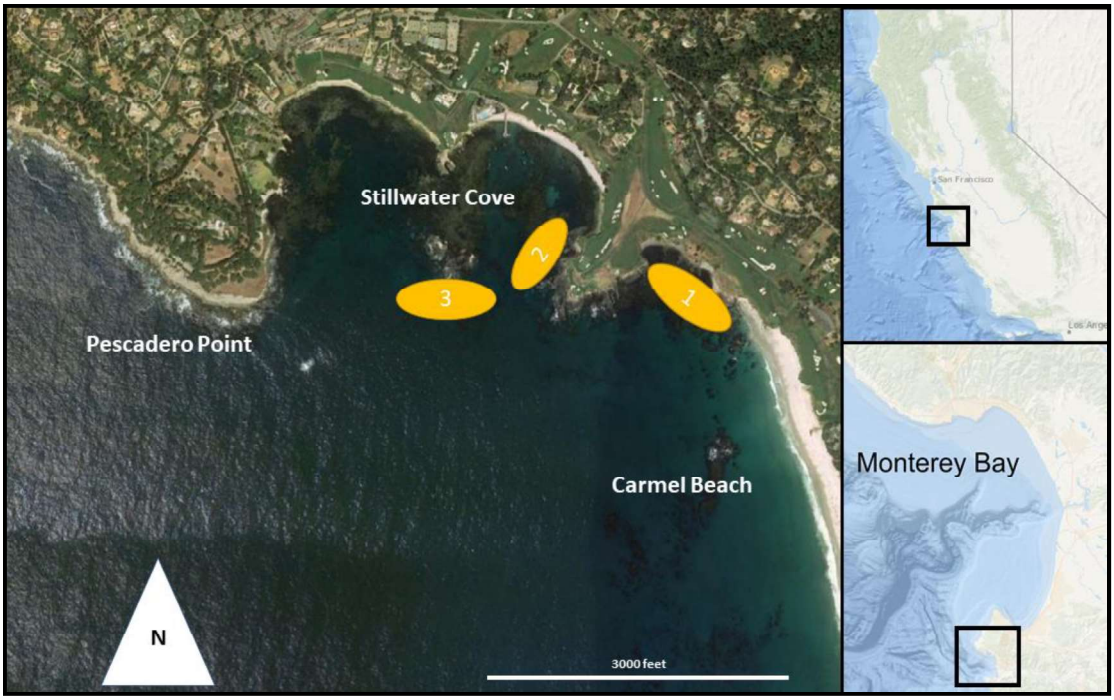

Figure 2: Blocked study sites located in Carmel, CA. Numbered ovals indicate approximate size and location of study kelp beds.

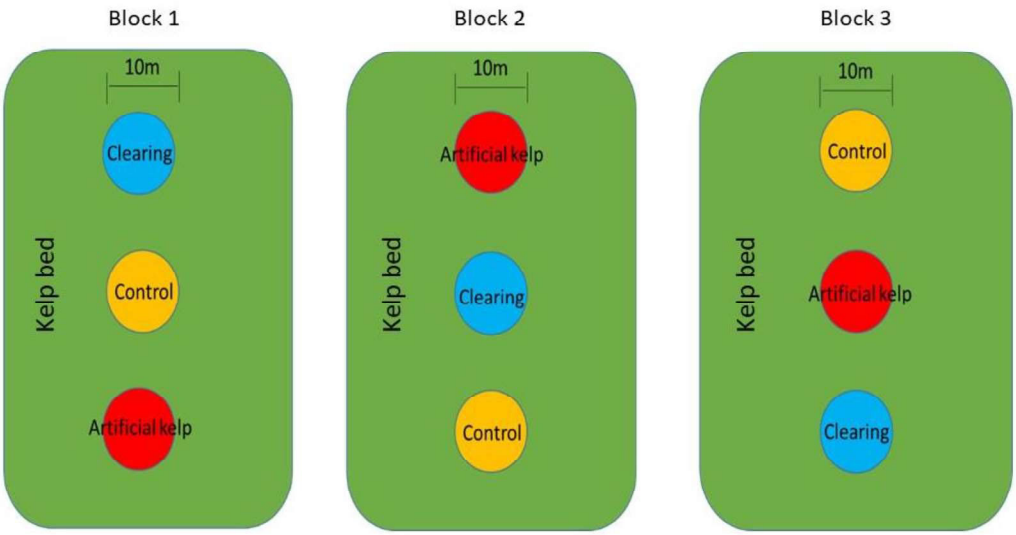

Figure 3: Randomized block design for the study. Each block represented a kelp bed; within each bed was one replicate of each treatment: a cleared plot where giant kelp was removed; an artificial plot where giant kelp was been removed and replaced with artificial kelp; and a control plot where natural kelp remained. Each plot was circular 10m in diameter.

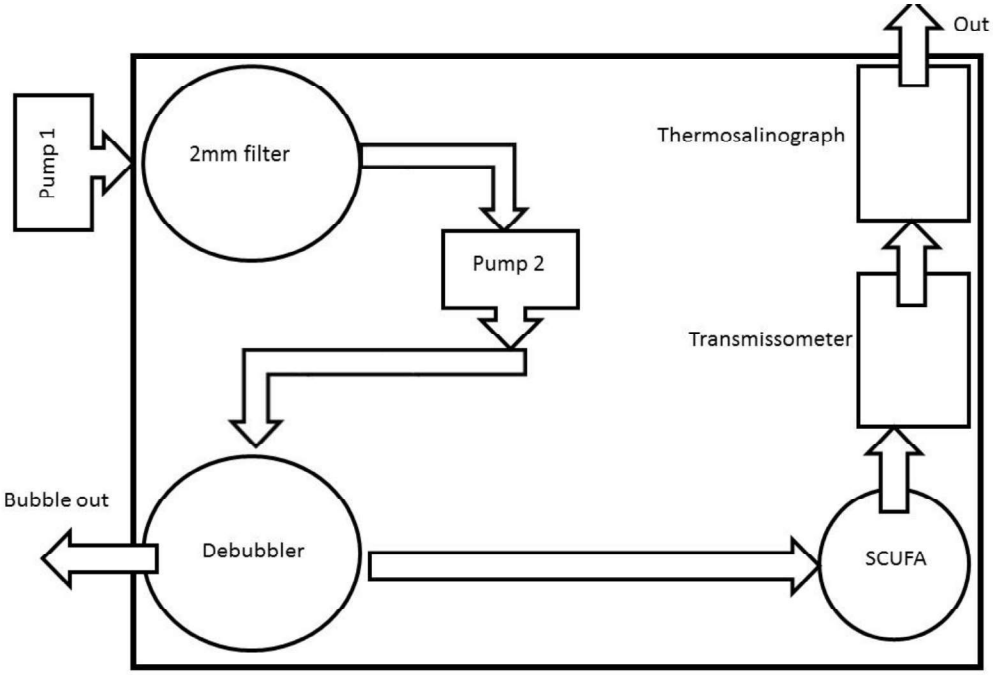

Figure 4: The UDAS (underway data acquisition system) is a flow-through system, powered by two electric diaphragm pumps with 12-foot lift capacity. The water was pumped through a suite of standard hydrographic instrumentation including: a Seabird SBE 38 Digital Oceanographic Thermometer and SBE 45 Thermosalinograph; SCUFA Fluorometer; Wet Labs C-Star 10 cm Transmissometer, sensing temperature, salinity, turbidity, and chlorophyll fluorescence, respectively. The debubbler allowed for air bubbles to leave the system before being transferred to sensors. These sensors gave a live data stream directly to a portable computer.

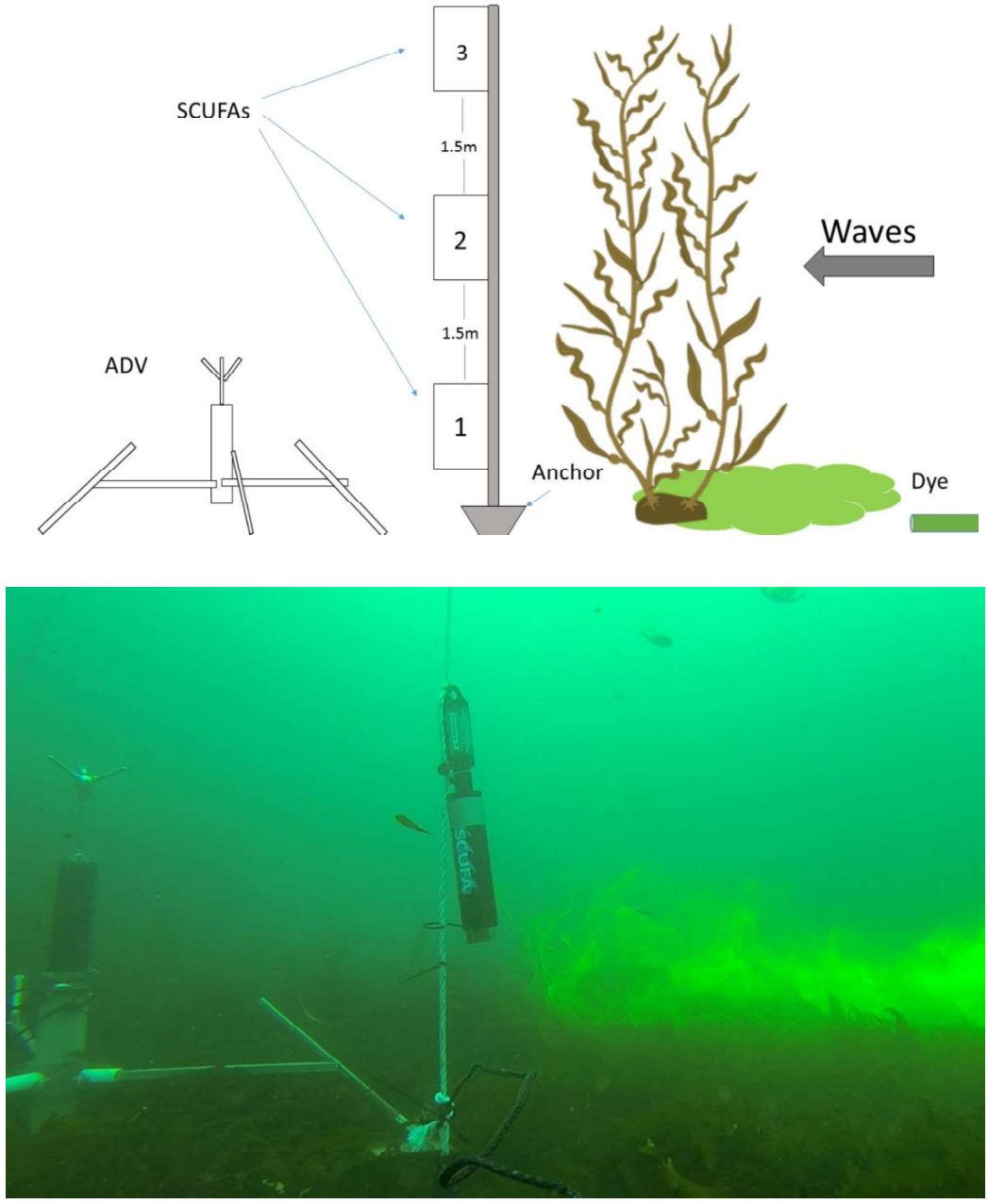

Figure 5: SCUFA (self-contained underwater fluorescence analyzer) array suspended through the water column. Three SCUFAs were placed at 1.5m intervals from the bottom and attached by line with an 8 lb. mushroom anchor and a surface float. The ADV (acoustic doppler velocimeter) was placed just downstream of the SCUFA array to not interfere with dye flow. The photo below shows the array set up outside of a kelp.

Figure 6: Stillwater Cove and Carmel State Beach, CA. Circles represent locations for dye release and wave velocity. Experimental sites within Stillwater Cove were considered sheltered from waves. All dye release experiments were preformed July- September 2017.

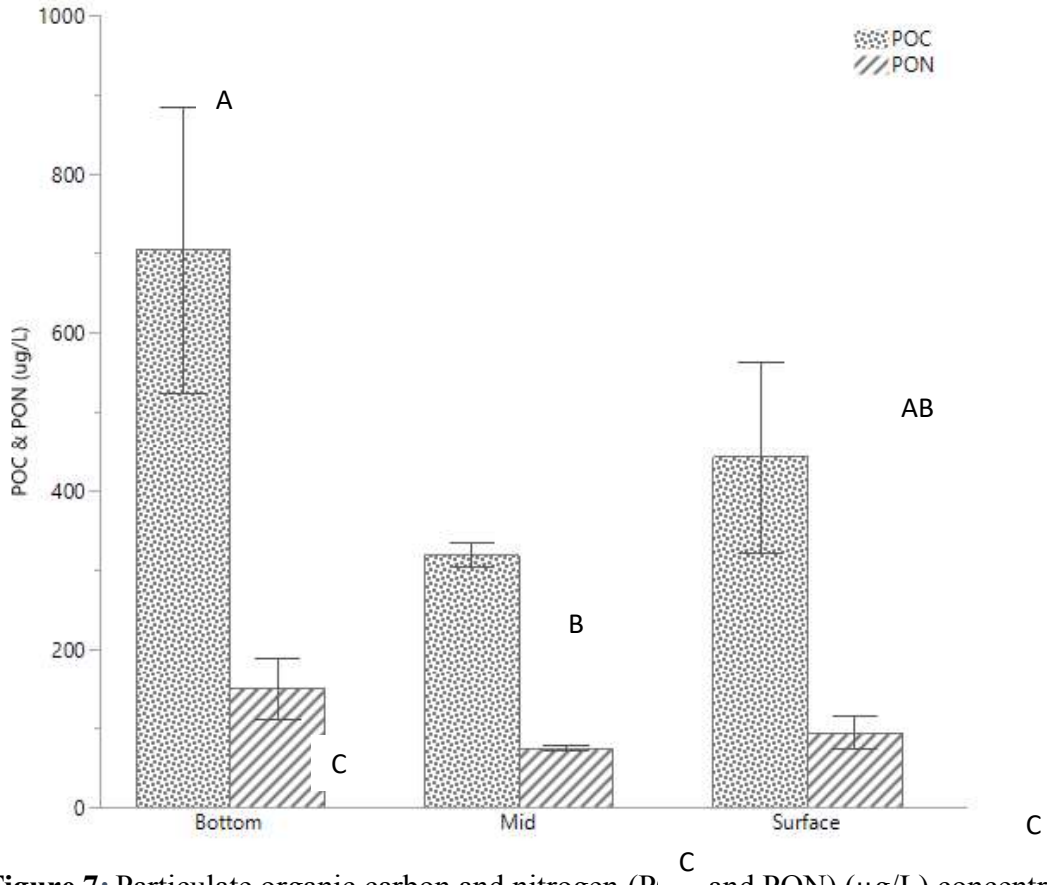

Figure 7: Particulate organic carbon and nitrogen (POC and PON) (µg/L) concentrations among depths: surface water (0m), midwater (2.5m), sea bottom (~6m) within all plots before treatment. Letters above bars indicate significant differences ($p < 0.05$, Tukey HSD). Error bars are ±SE

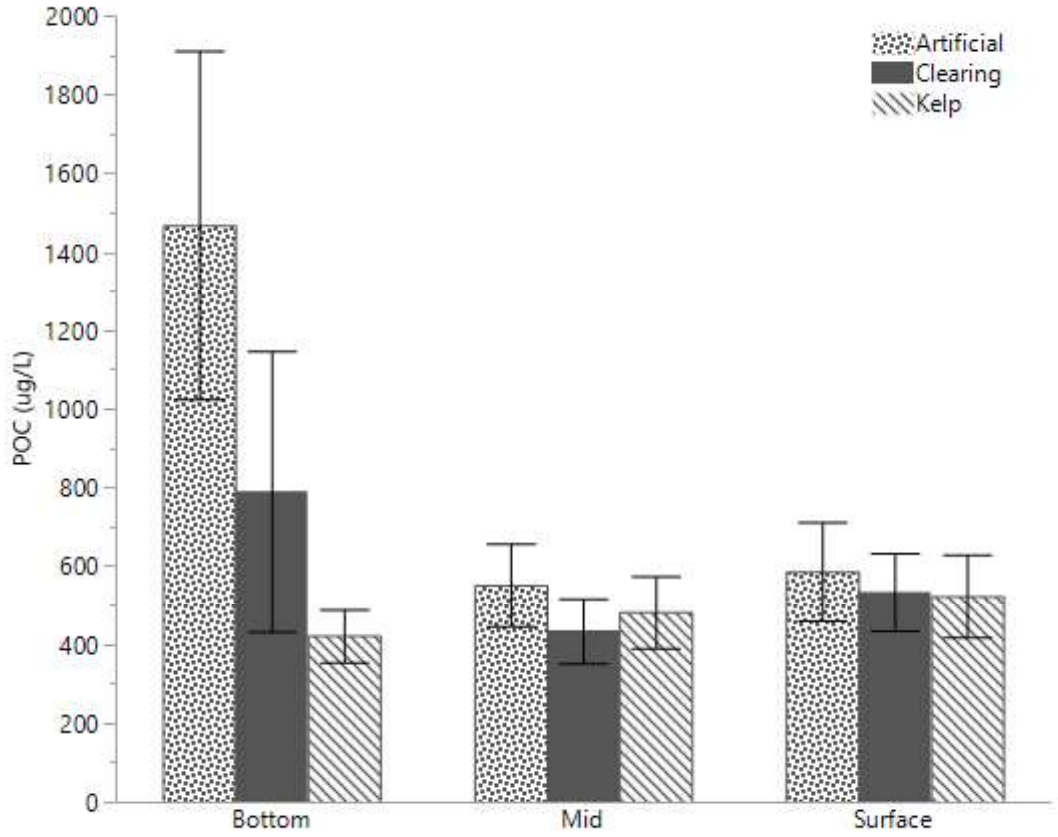

Figure 8: Particulate organic carbon (POC) concentration (µg/L) among depth: surface water (0m), midwater (2.5m), sea bottom (~6m) and treatments: (kelp, cleared kelp, artificial kelp). Error bars are ±SE.

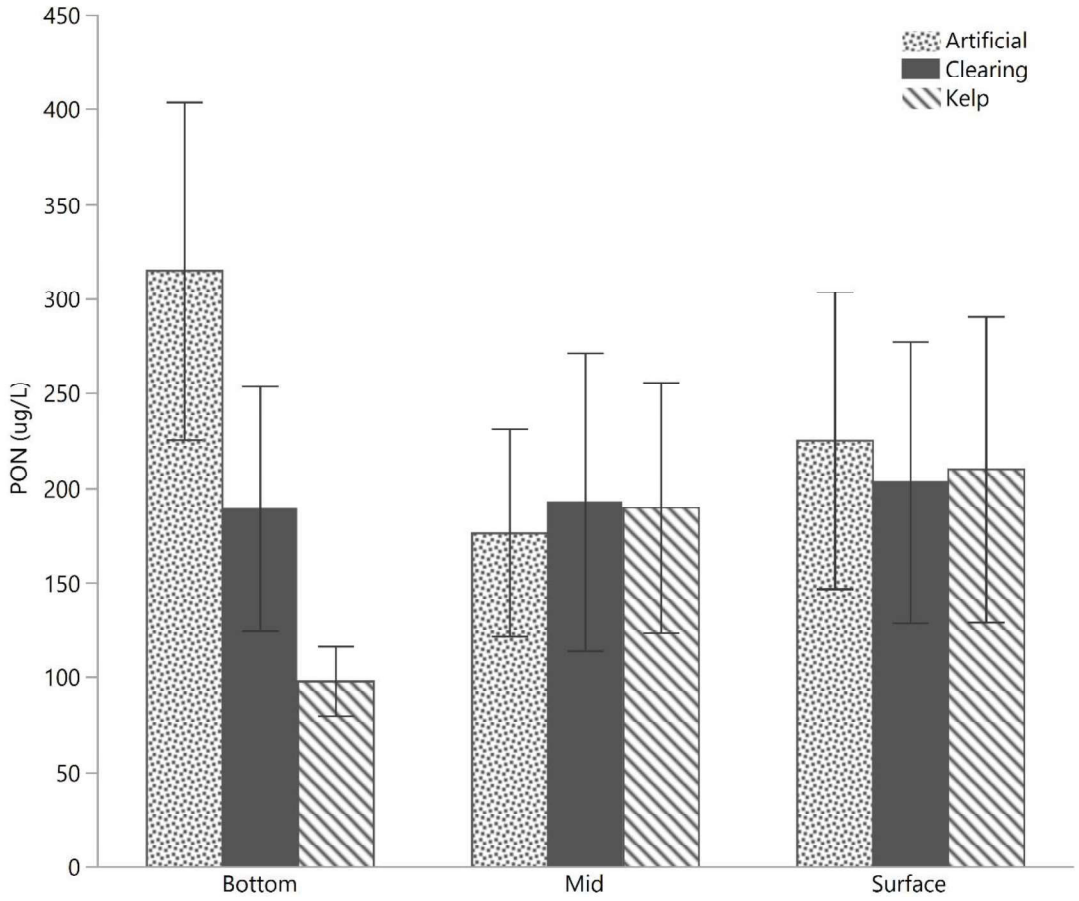

Figure 9: Particulate organic nitrogen (PON) concentration (µg/L) among depth: surface water (0m), midwater (2.5m), sea bottom (~6m) and treatments (kelp, cleared kelp, artificial kelp). Error bars are ±SE.

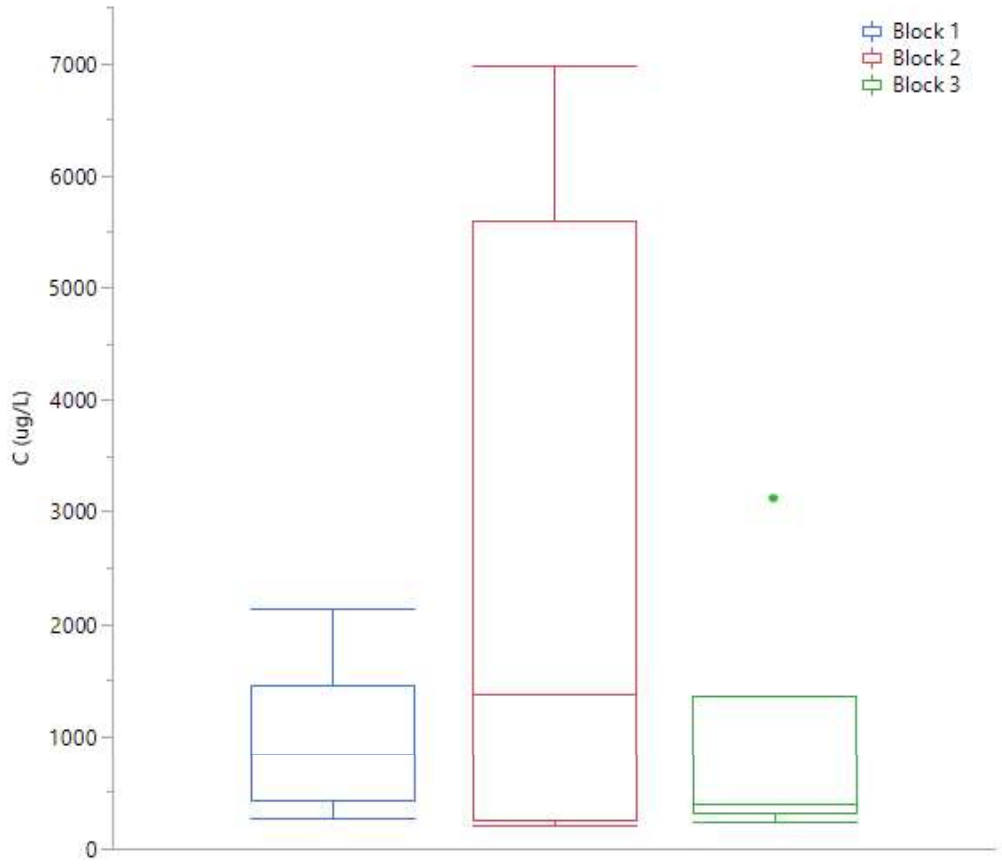

Figure 10: Organic carbon (µg/L) on the seafloor within artificial kelp plots only. Showing block 2 with highest variance.

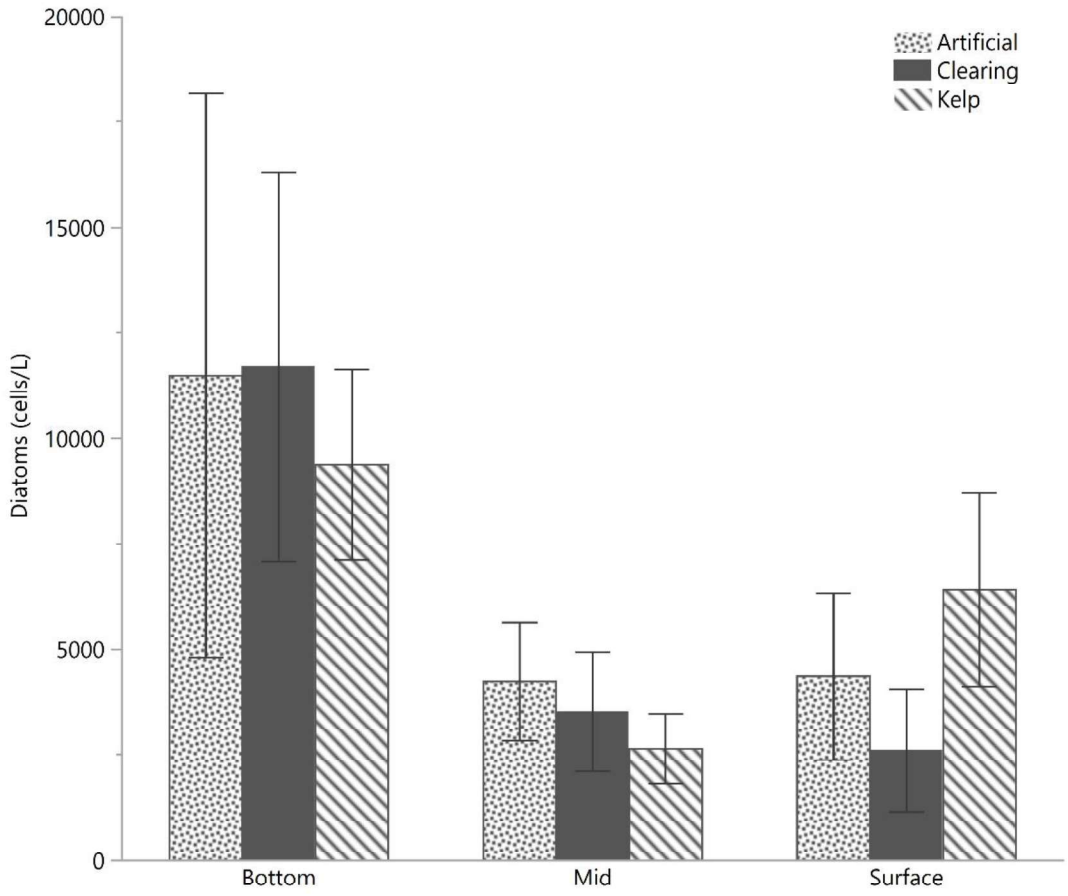

Figure 11: Diatom concentrations (cells/L) among depth: surface water (0m), midwater (2.5m), sea bottom (~6m) midwater (2.5m), and sea surface (0m), and treatment (artificial kelp plots, kelp cleared plots, and natural kelp plots). Error bars are ±SE.

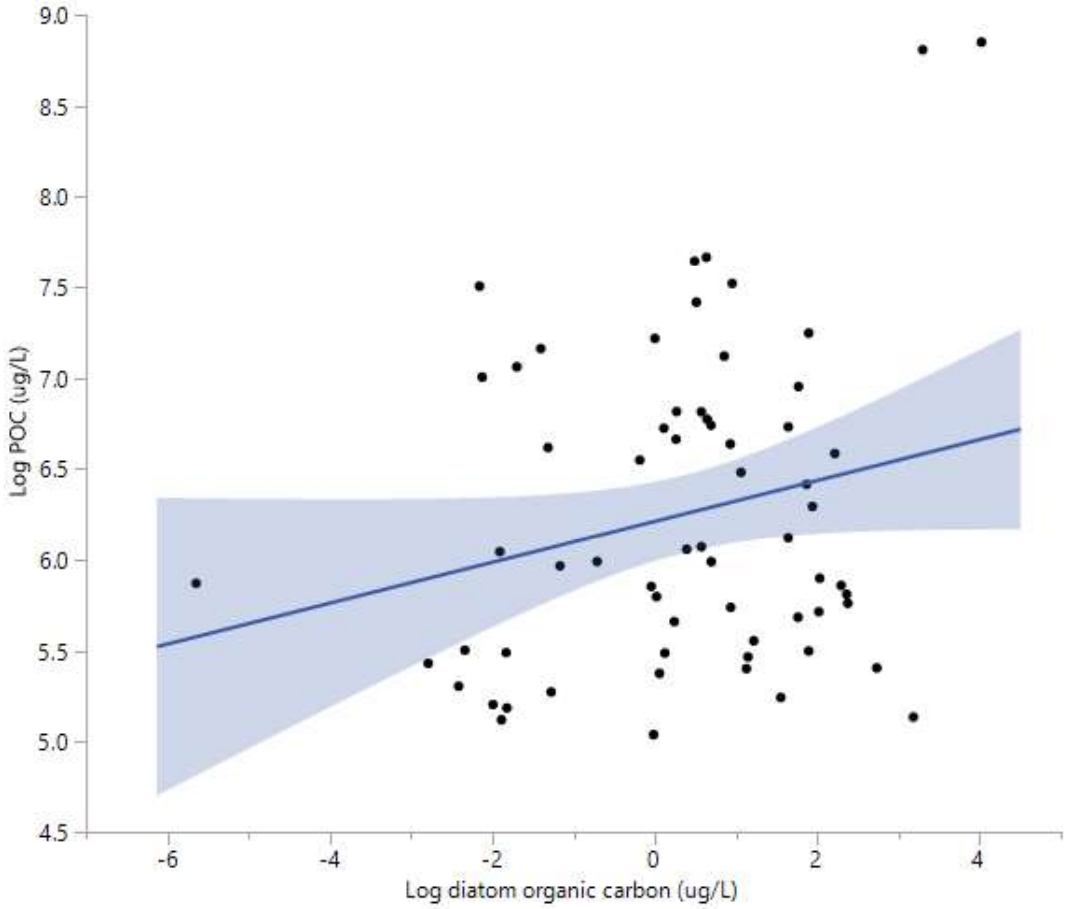

Figure 12: Regression of diatom-derived carbon (µg/L) against total POC (µg/L) when diatoms were present (y = 6.21 + 0.112*x). Shaded region is 95% confidence interval.

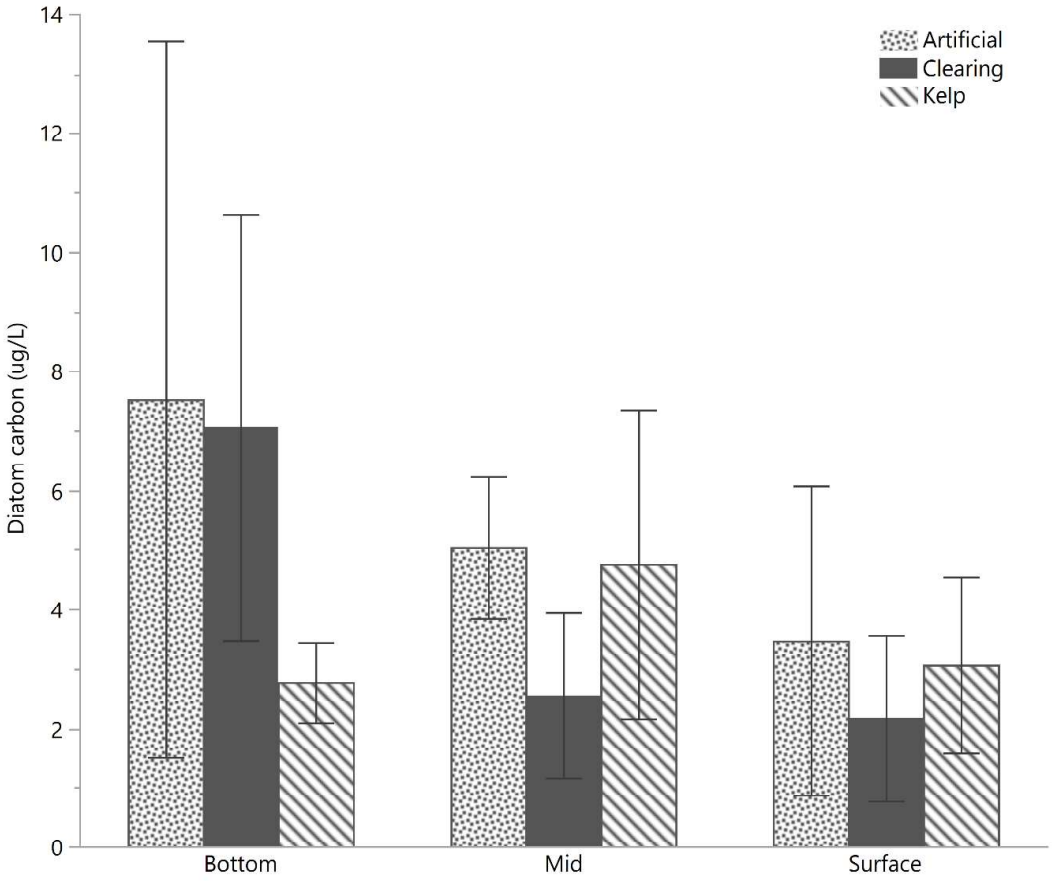

Figure 13: Diatom-derived organic carbon (µg/L) among depths: surface water (0m), midwater (2.5m), sea bottom (~6m), and treatment (artificial kelp plots, kelp cleared plots, and natural kelp plots). Error bars are ±SE.

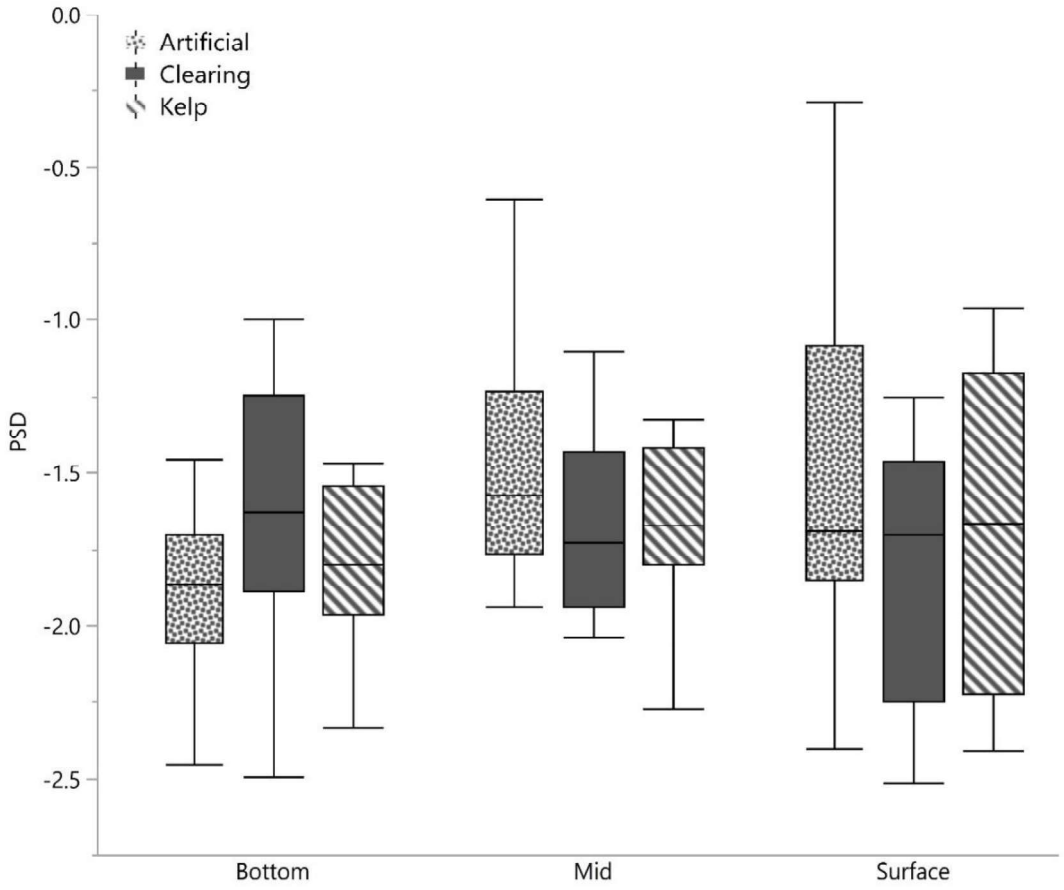

Figure 14: Slope of particle size distribution (PSD) among depths: surface water (0m), midwater (2.5m), sea bottom (~6m), and treatment (artificial kelp plots, kelp cleared plots, and natural kelp plots). Larger negative values indicate a higher proportion of smaller particles.

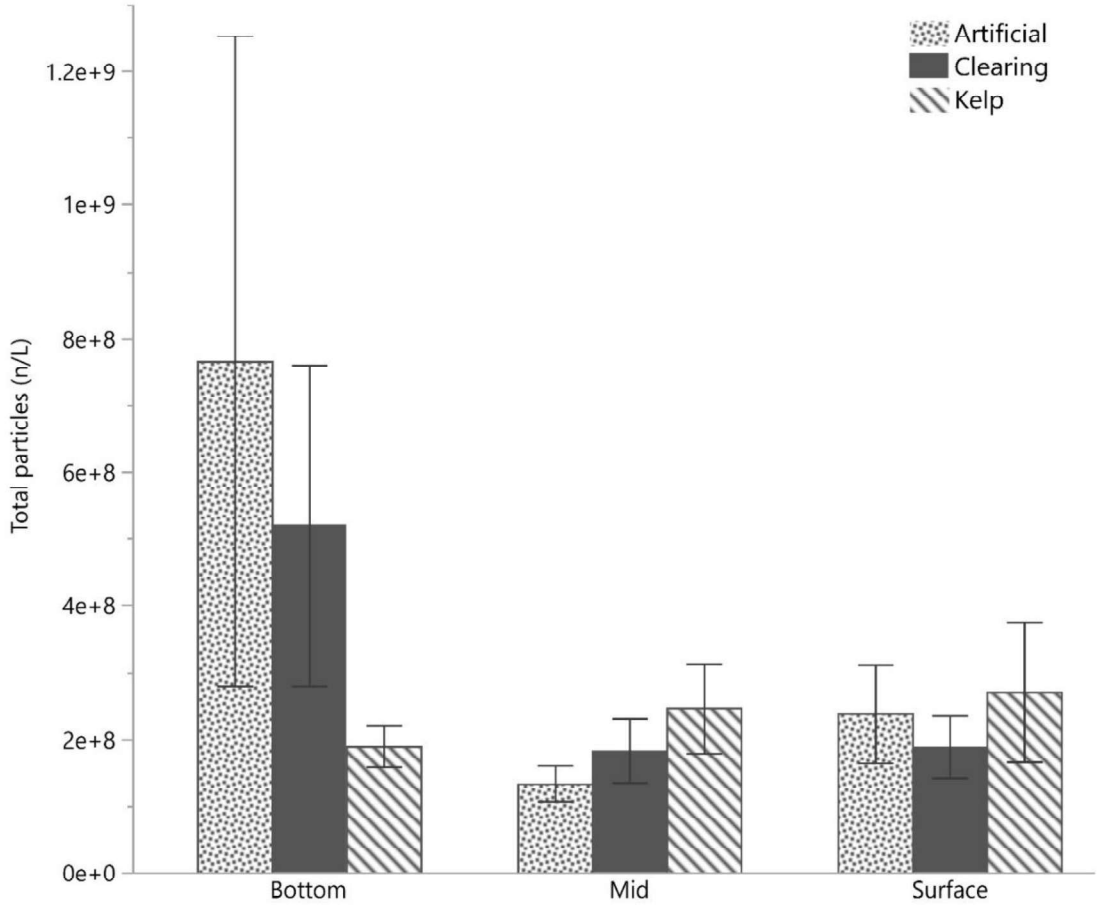

Figure 15: Total particles (n/L) among depths: surface water (0m), midwater (2.5m), sea bottom (~6m), and treatment (artificial kelp plots, kelp cleared plots, and natural kelp plots). Error bars are ±SE.

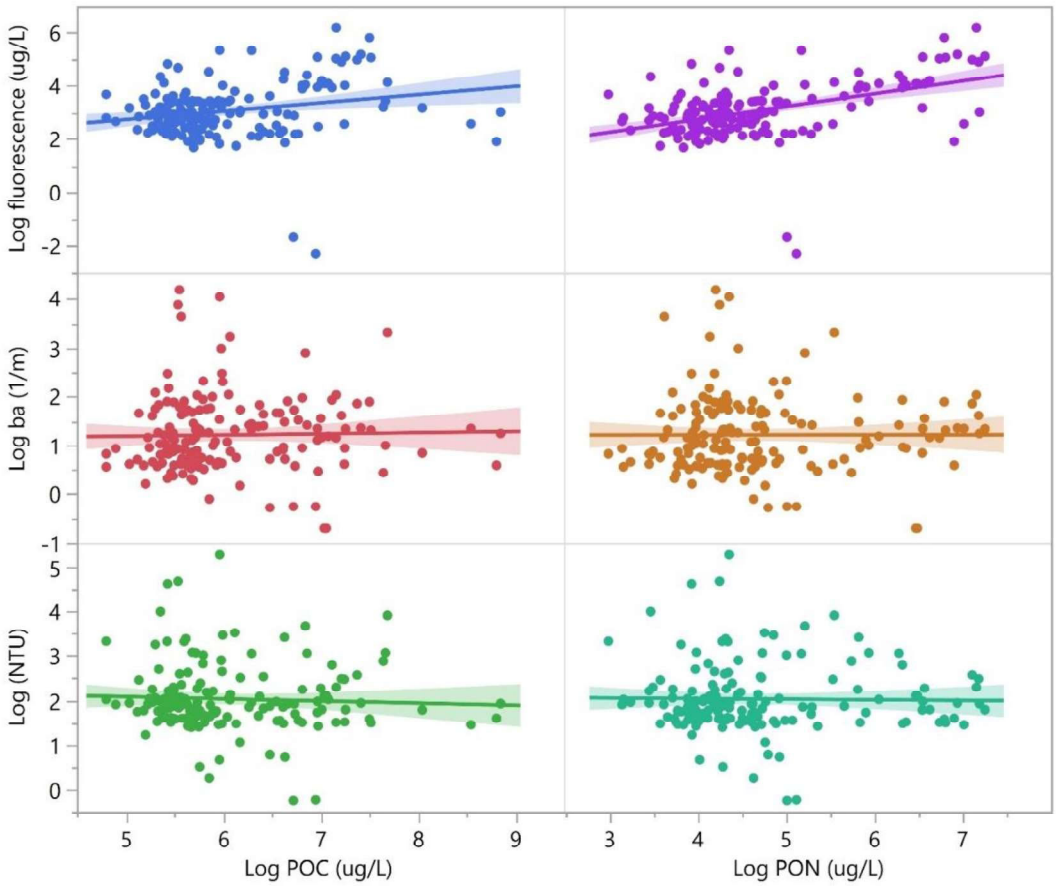

Figure 16: Relationships strength between POC and PON by SCUFA fluorescence (ug/L), beam attenuation (1/m), and turbidity (TNU) by regression analysis. Shaded region is 95% confidence interval.

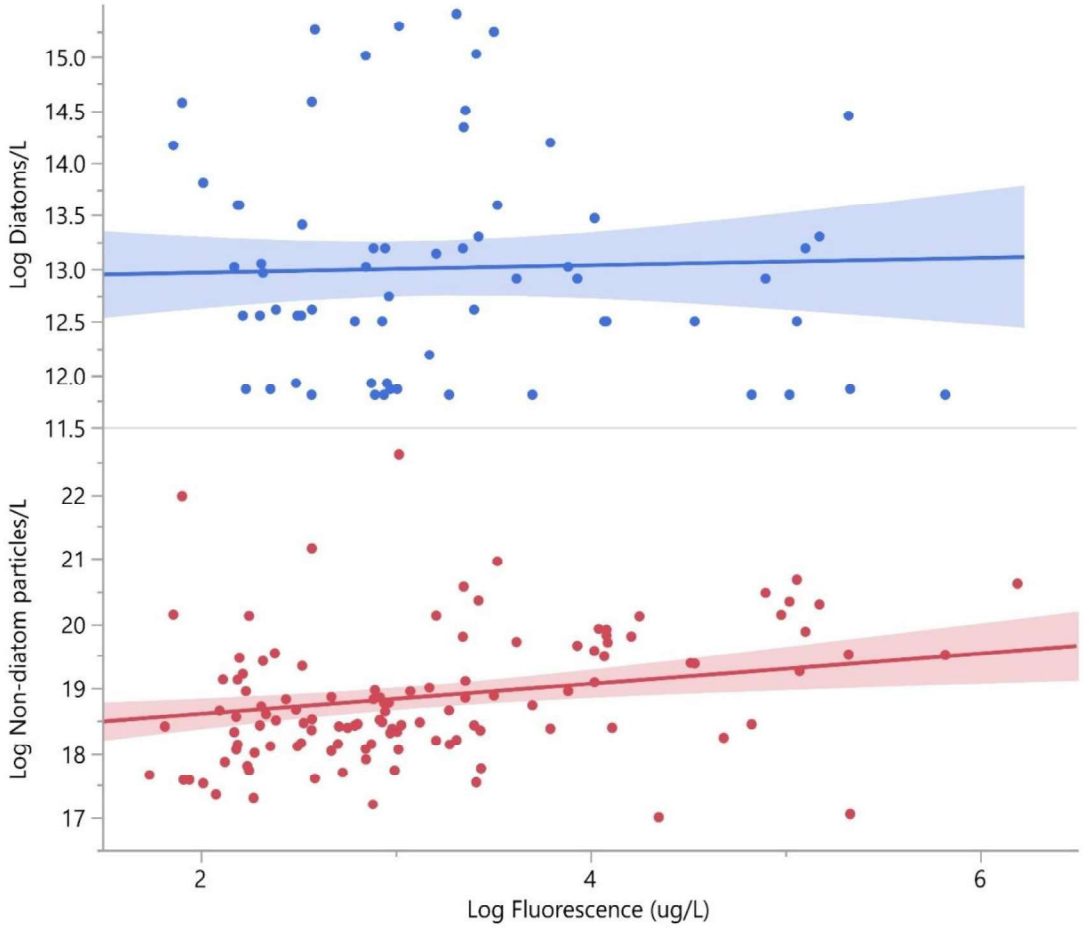

Figure 17: Regression analysis of diatom and non-diatom particle concentrations (n/L) by SCUFA fluorescence (ug/L). Shaded region is 95% confidence interval.

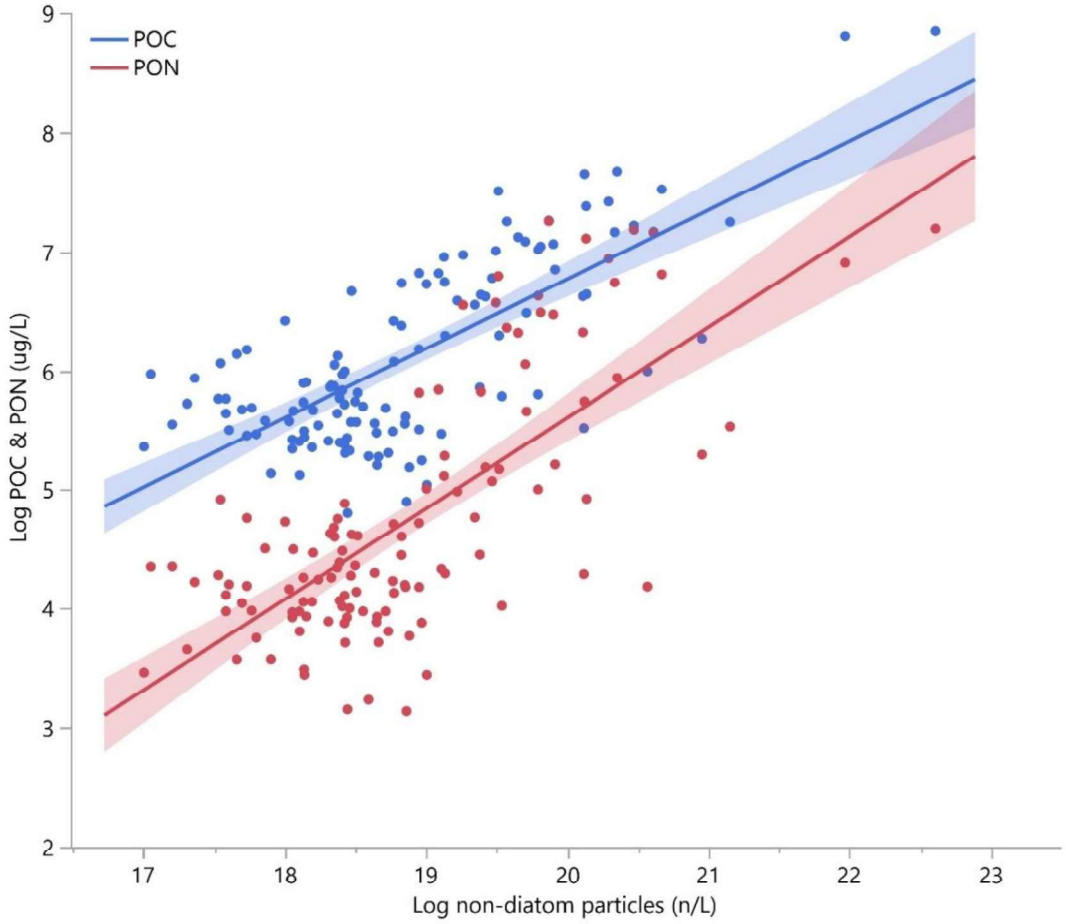

Figure 18: Relationship between particulate organic carbon and nitrogen (POC & PON) (µg/L) and non-diatom particulate concentration (n/L) (POC: y = -4.867 + 0.5816*x, PON: y = -9.642 + 0.762*x). Shaded region is 95% confidence interval.

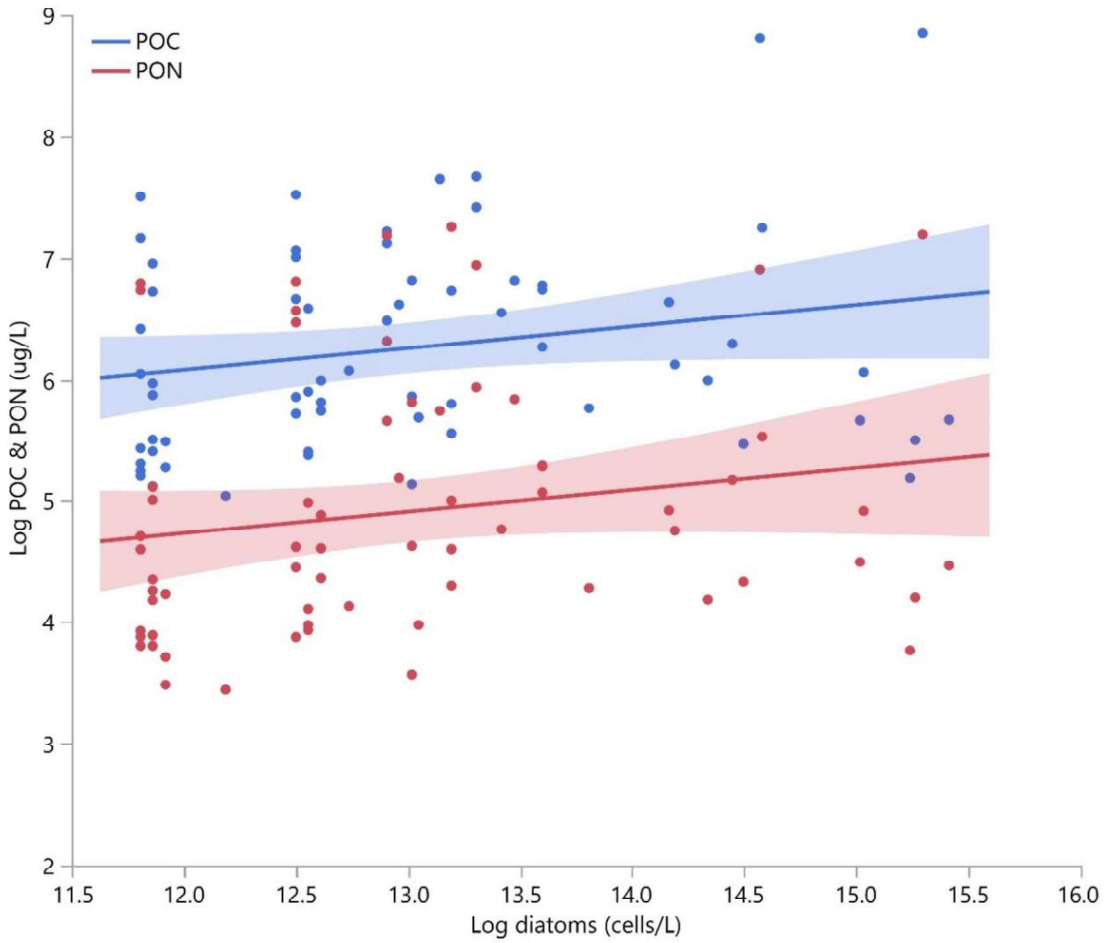

Figure 19: Relationships between particulate organic carbon and nitrogen (POC & PON) and total diatom concentration (cells/L) (POC: y = 3.932 + 0.1788*x, PON: y = 2.5837 + 0.1791*x). Shaded region is 95% confidence interval.

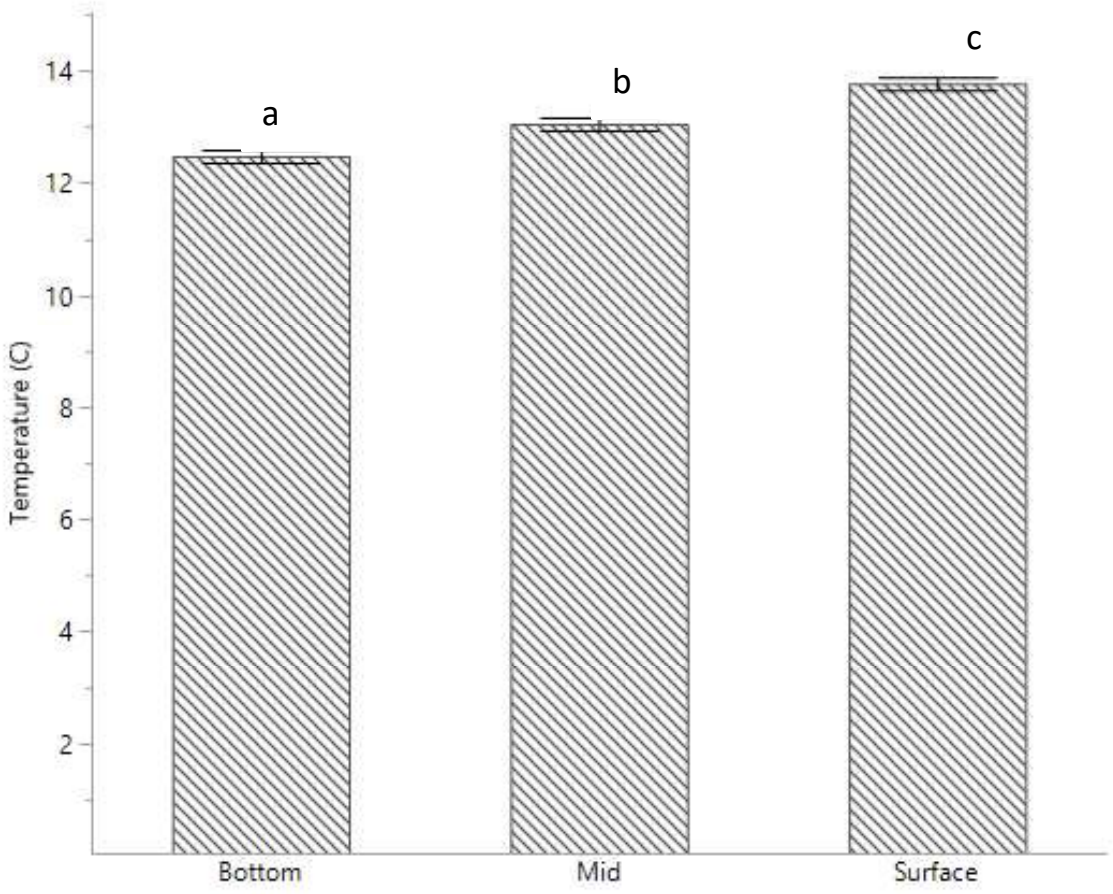

Figure 20: Temperature (ºC) among depth: surface water (0m), midwater (2.5m), bottom (~6m). Letters above bars represent significant differences ($p<0.01$, Tukey HSD). Error bars are ±SE.

A)

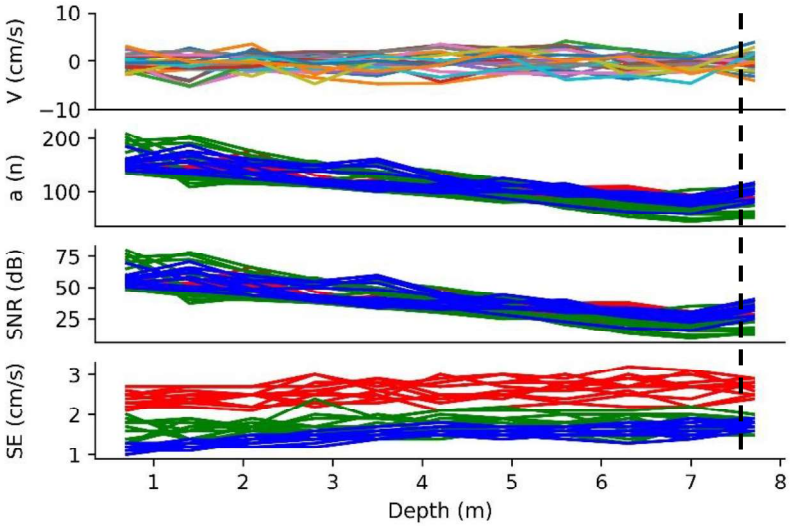

B)

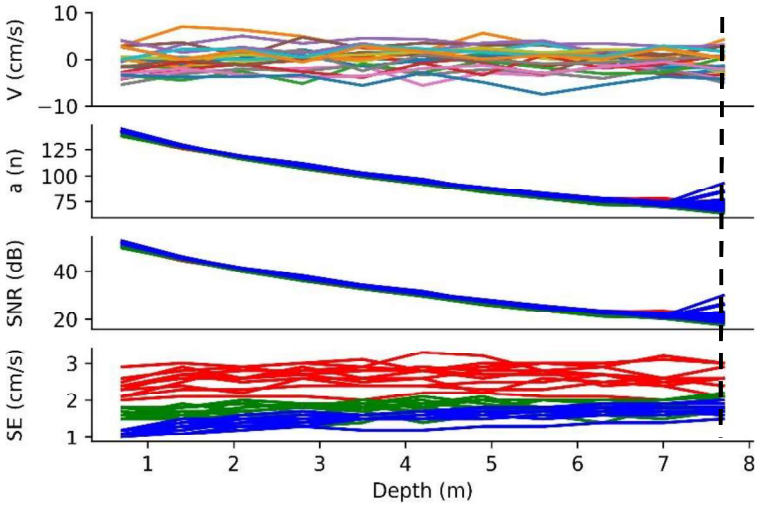

Figure 21: Velocity profiles from acoustic doppler profiler (ADP). Each series is an averaged one-minute profile. The ADP used three sound beams, denoted by red, green, and blue. Each line represents a 1-minute profile. The seafloor was determined by the inflection point of the signal amplitude indicated by the dashed line. The quality of the ADP velocity (V) data is indicated by the standard error (SE), while the signal to noise ratio (SNR) shows the strength of the signal and mirrored the signal amplitude. A) shows a profile within a natural kelp plot with physical obstructions present, where B) shows a profile within a kelp removal site with no obstruction. The consistency of the SE indicated that kelp interference did not distort the velocity data.

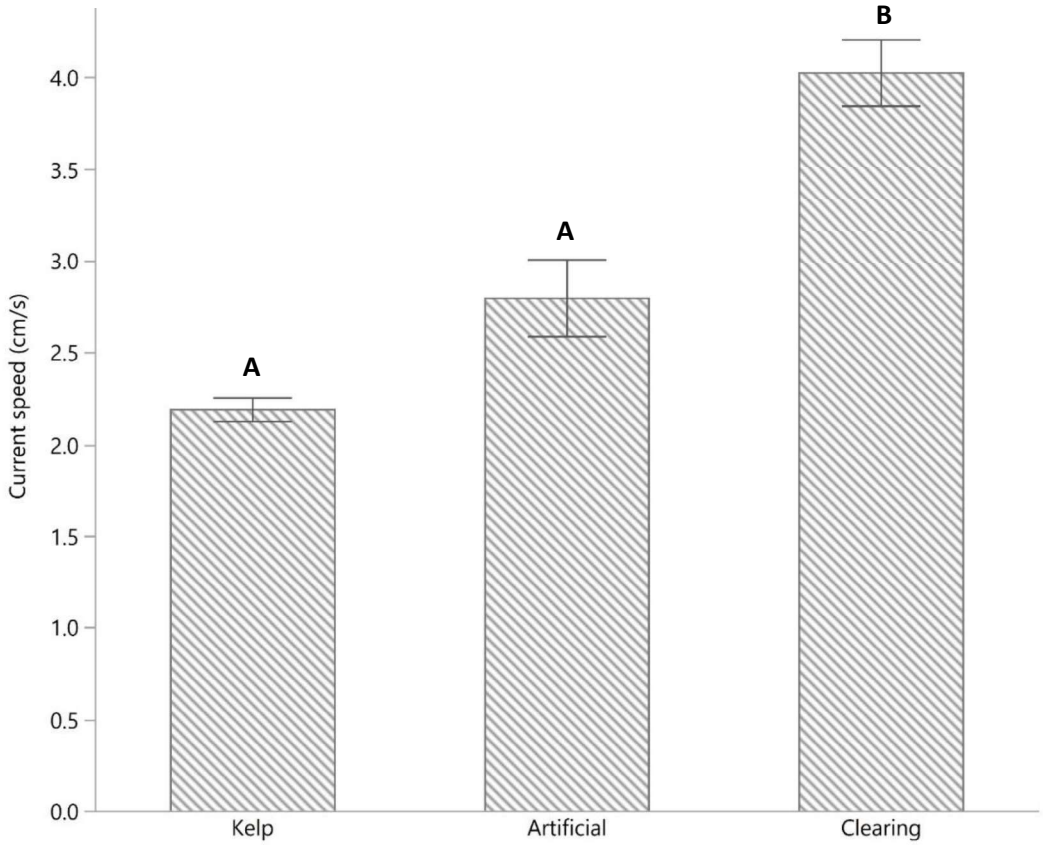

Figure 22: Differences in mean current speed (cm/s) among treatments (natural kelp, artificial kelp, kelp removed) at depths 0m (surface), 2.5m (Mid), and ~6m (bottom). Letters above bars indicate significant differences ($p < 0.01$, Tukey HSD). Error bars are ±SE.

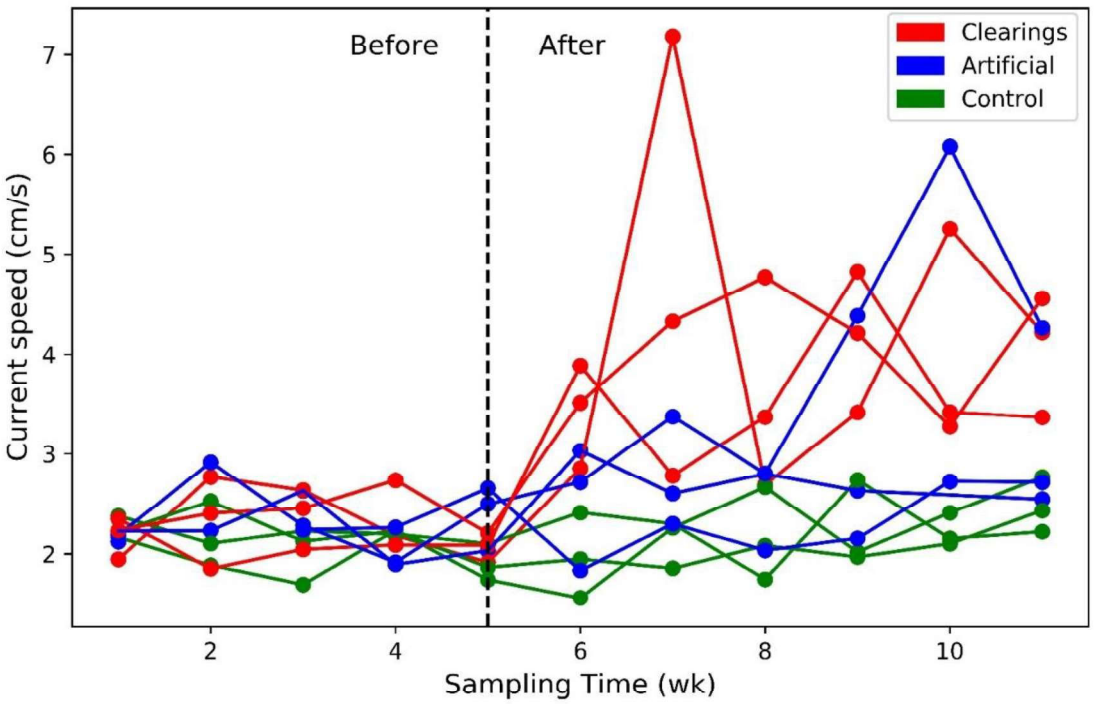

Figure 23: Current speeds (cm/s) within plots through time. The dashed line marks when plots were manipulated from natural kelp plots to artificial kelp (blue), kelp removed (red), and control (green) plots.

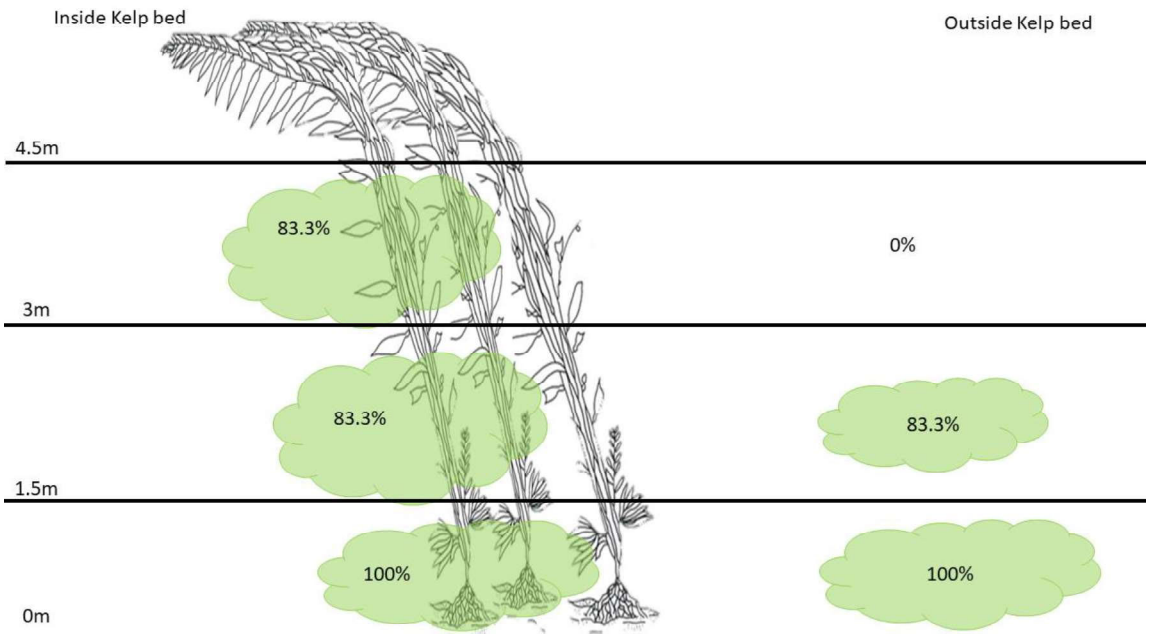

Figure 24: An illustration of frequency of occurrence of dye detection (y/n) by SCUFA inside and outside of kelp beds. SCUFAs were suspended through the water column by line (Fig. 5), where internode distance was 1.5m. Three grams of fluorescein dye (Uranine powder 40%) was pumped to the sea bottom from boat and allowed to flow for 20 minutes. The values in the green dye cloud indicate the percent chance of dye detection at each depth.

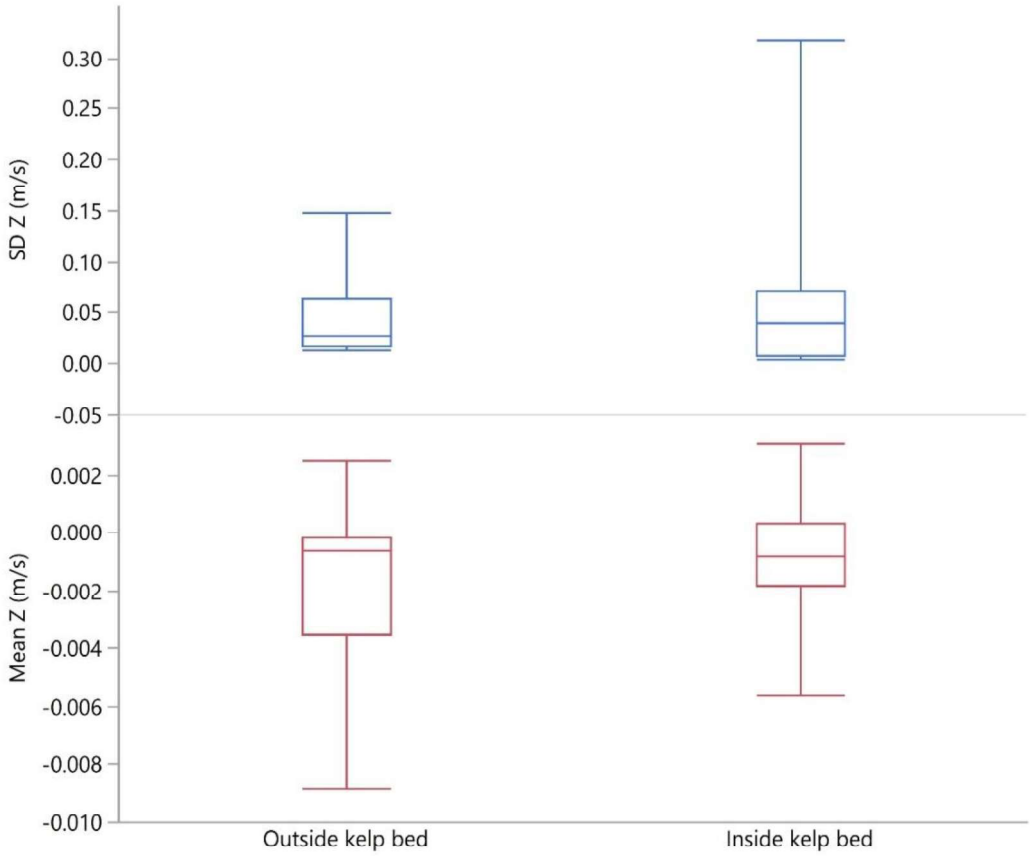

Figure 25: Boxplot of the SD and mean of the vertical component *Z* of water velocity (m/s) inside and outside of kelp beds.

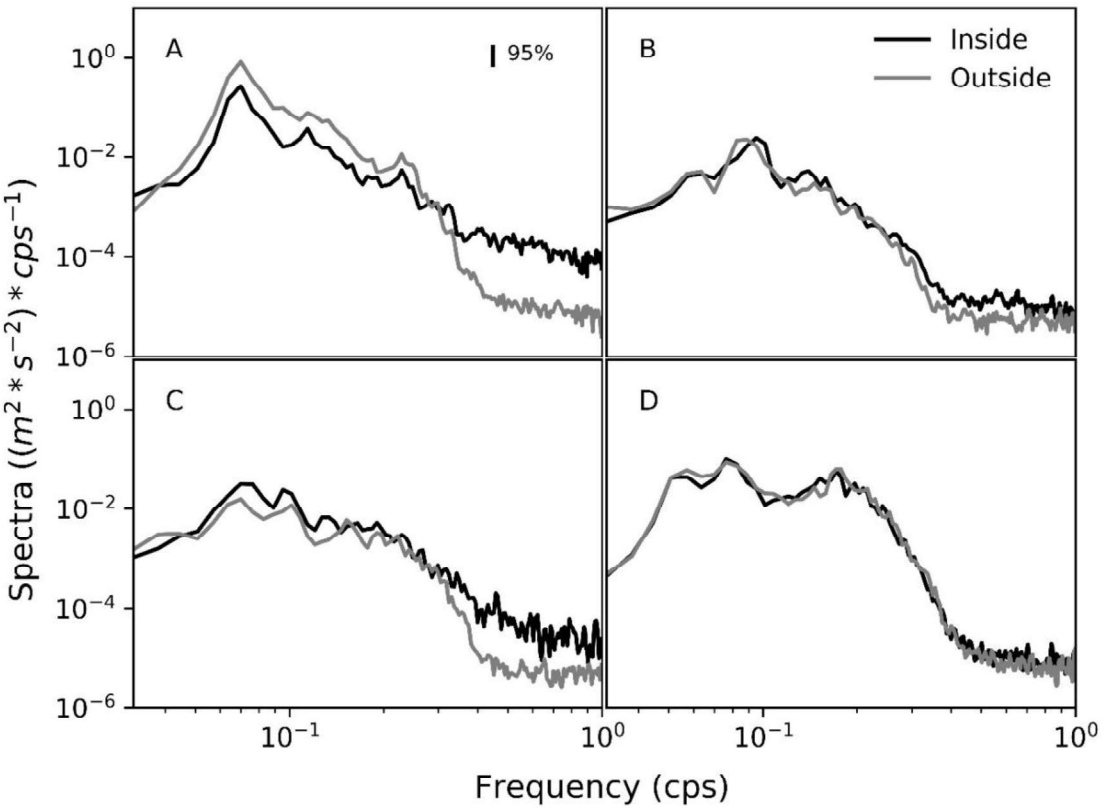

Figure 26: Spectra of wave orbit speed oscillations along the principal horizontal axis. Gray lines represent data inside kelp beds while black lines are outside the bed. Recorded by a Nortek acoustic doppler velocimeter (ADV -300 m) 1m above the seafloor along Carmel Beach CA. Sample rate = 2Cps, Δt = 20 minutes, N= 2,400. Each time-series has been smoothed with a Hanning window, df = 42.6. The 95% confidence interval is noted in frame A. Each frame (A, B, C, D) are separate coupled measurements, with inside and outside a kelp bed within 1 hour.

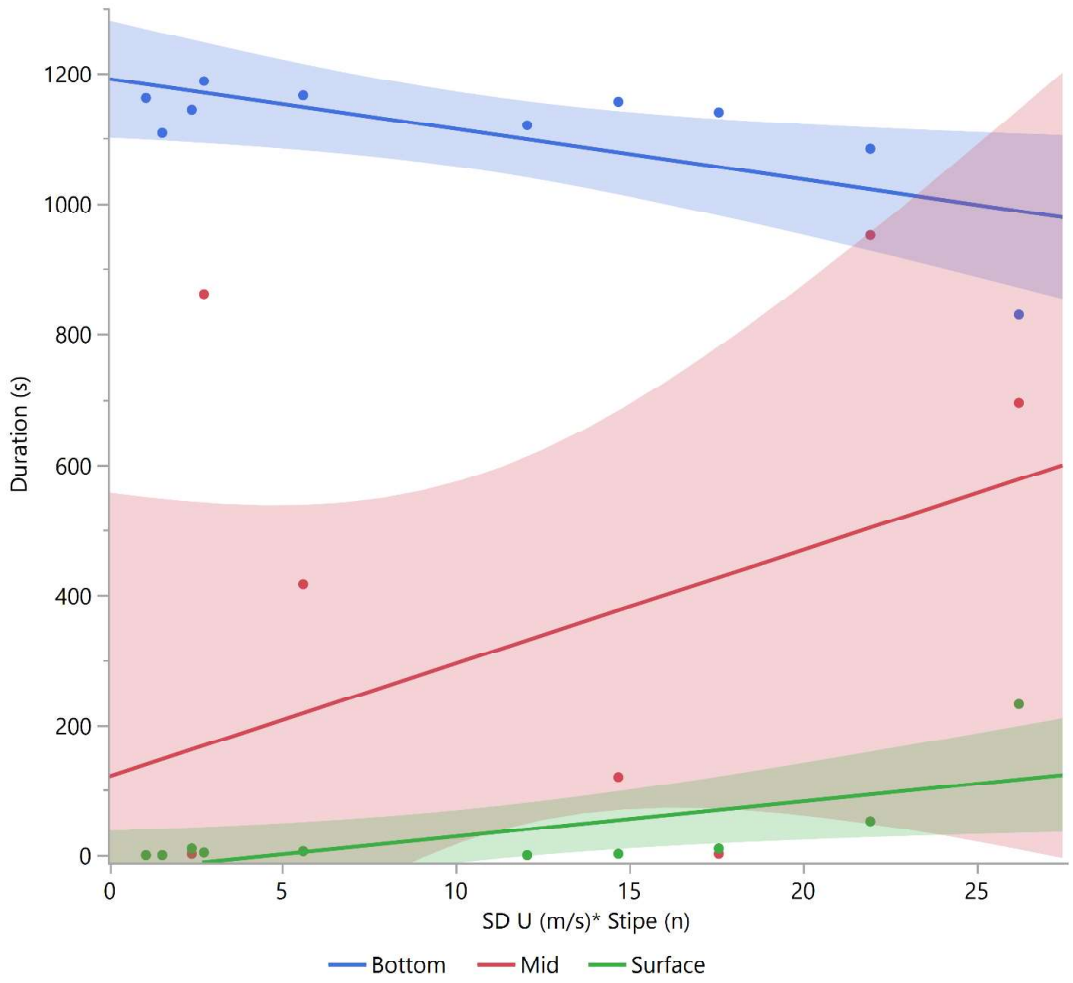

Figure 27: Relationships of dye duration (s) with the interaction of stipe number (n) and the SD of Northeast water speed (m/s). Dye duration was detected by three SCUFA sensors in the water column: bottom water (1.5 m from seafloor), mid water (3 m from seafloor), and upper water (4.5 m from sea floor). The sensor array was placed on the downstream side of enumerated kelp stipe bundles while the dye was released ~2m upstream of the kelp stipes. Dye duration in the bottom water had a negative relationship with stipes*water speed ($R^2 = 0.34$, $p = 0.0475$, $y = 33.89-0.84x$) while the upper water duration was positively correlated with stipes*U ($R^2 = 0.3$, $p = 0.0477$, $y = 1.82+2.261x$). There was no significant relationship with dye duration and water speed*stipes ($R^2 = 0.03$). Shaded area is 95% confidence fit.

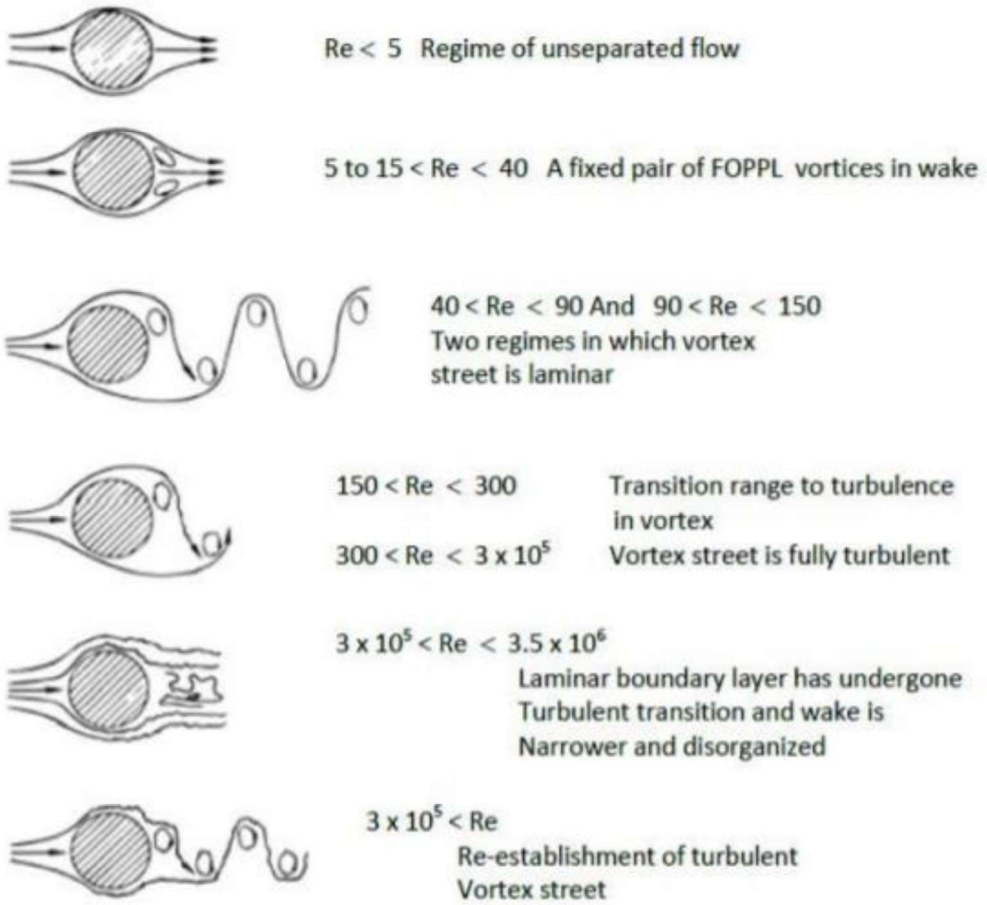

Figure 28: Regimes of fluid flow across a smooth tube. From Blevins, R. D. (1990), Flow Induced Vibration, 2nd edition.

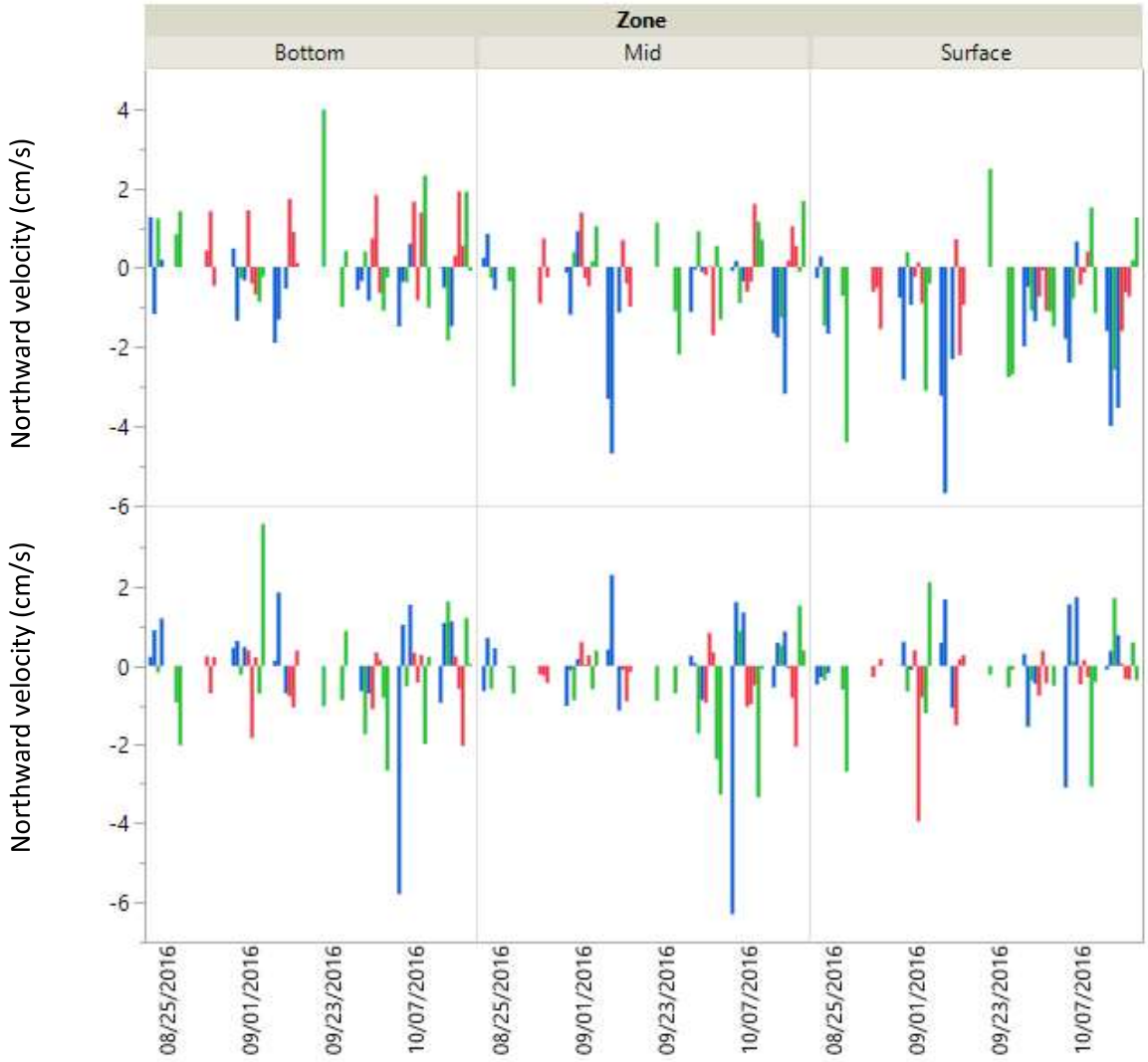

Figure 29: Mean Eastward and Northward current velocities (cm/s) within study plots through time by water depth. Negative values indicate current in the opposite direction. Colored bars represent plots by block: red = block 1, blue = block 2, green = block 3). Samples taken with SonTek acoustic doppler profiler (ADP) (Aug. 25- Oct. 16, 2016).

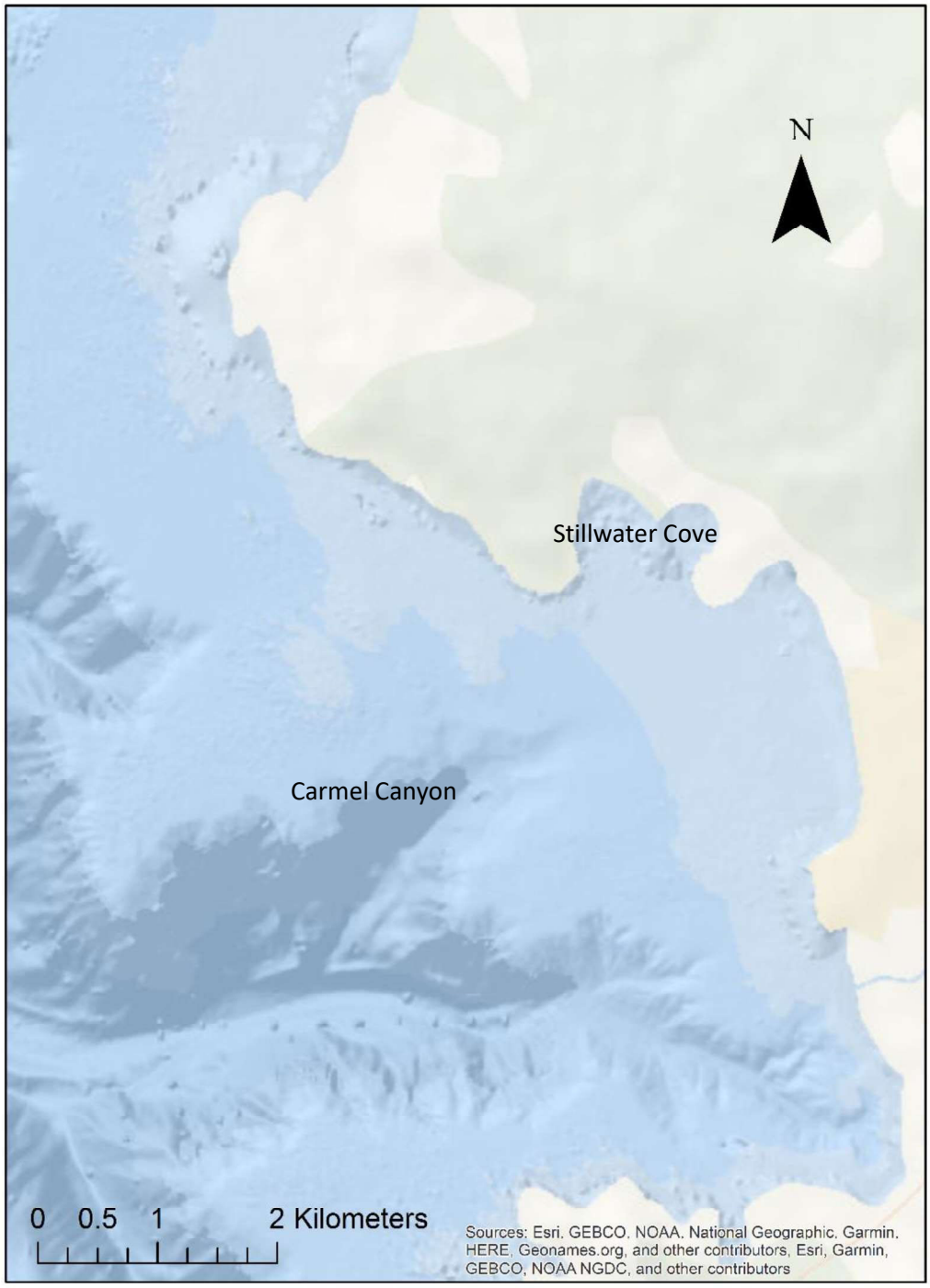

Figure 30: Map showing distance from the Carmel Canyon to study area of Stillwater Cove, CA.

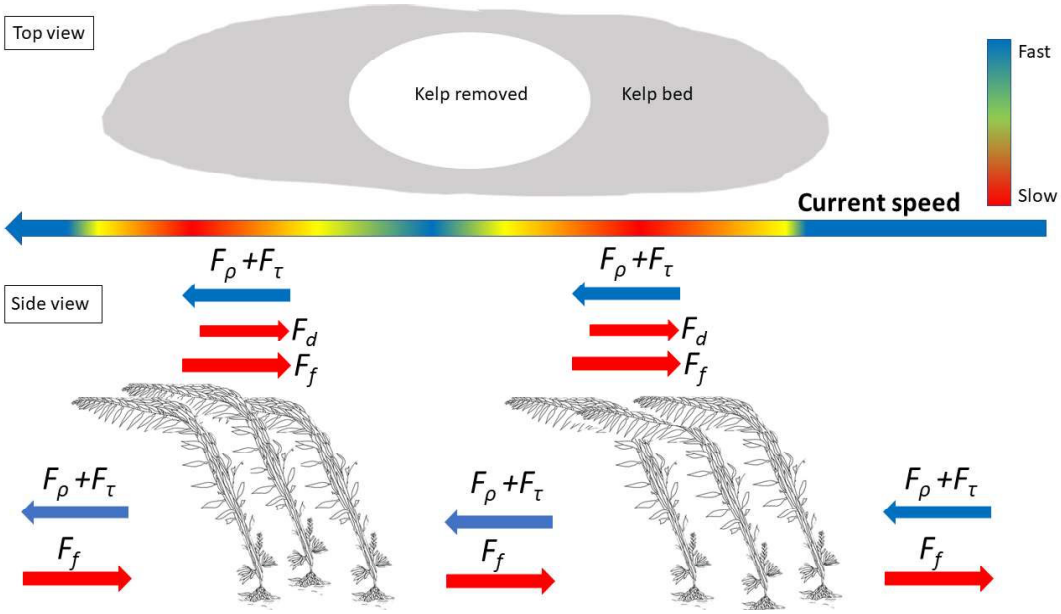

Figure 31: Conceptual current flow dynamics though a kelp bed with a kelp removal located within the bed's center. The forces moving the body of water are denoted as F_ρ = density gradient forcing, F_τ = wind forcing, F_D = drag, and F_f = bottom friction. Blue indicates faster, unimpeded flow, while red represents slowed currents by kelp drag or bottom friction.

TABLES

Table 1: Blocked one-way Analysis of Variance (ANOVA) tests comparing Particulate Organic Carbon and Nitrogen (POC, PON) (µg/L) among depths, Surface water (0 m), Midwater (2.5 m), and bottom water (~6 m) within kelp beds.

a) POC

Source	DF	SS	F Ratio	P-value
Block	2	4.600	7.051	0.001*
Depth	2	2.376	3.643	0.028*
Error	127	41.30		

b) PON

Source	DF	SS	F Ratio	P- value
Block	2	3.774	6.319	0.002*
Depth	2	1.116	1.869	0.158
Error	127	37.99		

Table 2: Blocked two-way Analysis of Variance (ANOVA) comparing particulate organic carbon and nitrogen (POC, PON) (µg/L) among blocked treatments (kelp, cleared kelp, and artificial kelp), depths (Surface water 0m, Midwater 2.5m, and bottom ~6m), and treatment*depth.

POC

Source	DF	SS	F Ratio	P-value
Depth	2	1.041	0.915	0.402
Treatment	2	7.547	6.629	0.001*
Treatment*Depth	4	4.141	1.8188	0.128
Block	2	1.727	1.517	0.222
Error	152	86.03		

PON

Source	DF	SS	F Ratio	P-value
Depth	2	0.077	0.030	0.96
Treatment	2	6.793	3.489	0.225
Treatment*Depth	4	4.042	1.038	0.961
Block	2	1.908	0.980	0.377
Error	151	146.99		

Table 3: A comparison of mean particulate organic carbon and nitrogen (POC and PON) concentration (µg/L) within plots before and after treatments: kelp control (K), artificial kelp (A), and kelp clearings (C). POC and PON values were log-transformed to correct left-skewed distribution. Tests preformed were Student's t-test (S) or Welch's F-test (W).

	Before			After						
Treatment	$\bar{X}_1$	**SE**	**n**	$\bar{X}_2$	**SE**	**n**	$\bar{X}_2 - \bar{X}_1$	**Test**	**df**	**p**
POC										
K 1	-0.57633	0.18965	15	-0.607	0.24162	18	-0.03137	S	31	0.129
K 2	-0.01866	0.25917	15	-0.619	0.25917	18	-0.60054	S	31	0.785
K 3	0.248429	0.21701	15	-0.21	0.21701	15	-0.46543	S	28	0.645
A 1	-0.07621	0.31701	15	-0.089	0.31445	18	-0.01369	S	31	0.155
A 2	0.45324	0.26854	15	0.142	0.2061	18	-0.31124	S	31	0.717
A 3	-0.53975	0.29912	14	-0.3	0.2444	18	0.23975	S	30	0.06
C 1	-0.16391	0.15941	15	-0.898	0.33235	18	-0.73459	W	31	0.928
C 2	0.325123	0.17726	15	-0.136	0.2134	18	-0.46142	S	31	0.968
C 3	-0.24367	0.1481	15	-0.712	0.25307	18	-0.46873	W	31	0.825
PON										
K 1	-0.44196	0.13989	15	-0.550	0.27259	18	-0.10854	S	31	0.143
K 2	-0.14929	0.26682	15	-0.872	0.29321	18	-0.72331	S	31	0.793
K 3	0.185748	0.15848	15	0.209	0.15159	18	0.023552	S	31	0.127
A 1	-0.05472	0.27472	15	-0.212	0.33342	18	-0.15748	S	31	0.215
A 2	0.21587	0.2444	18	-0.166	0.24866	15	-0.38247	S	31	0.426
A 3	-0.45238	0.24811	14	-0.442	0.26155	18	0.00968	S	30	0.129
C 1	-0.22476	0.16762	15	-0.897	0.36644	18	-0.67264	W	31	0.805
C 2	0.292058	0.11368	15	-0.181	0.22687	18	-0.47386	S	31	0.985
C 3	-0.22086	0.14101	15	-0.699	0.27677	18	-0.47884	W	31	0.738

Table 4: X^2 test of presence and absence of diatoms among treatments and depth (A), and a blocked two-way ANOVA testing the difference in diatom abundance (cells/L) when present (B) among depth (0m, 2.5m, and ~6m), treatment (kelp, cleared kelp, and artificial kelp), and depth* treatment.

A) Diatom Presence / Absence

Source	DF	R^2	X^2	Prob > X^2
Depth	2	0.01	1.72	0.42
Treatment	2	0.005	0.83	0.65
Block	2	0.011	1.83	0.40

B) Diatom abundance when present

Source	DF	SS	F Ratio	Prob > F
Depth	2	10.626	10.619	< 0.001*
Treatment	2	1.348	1.347	0.267
Treatment*Depth	4	1.230	0.614	0.653
Block	2	5.782	5.778	0.005*
Error	57	28.51		

Table 5: Blocked two-way ANOVA test of difference in diatom-derived organic carbon (µg/L) among depth (0m, 2.5m, and ~6m), treatment (kelp, cleared kelp, and artificial kelp), and depth* treatment.

Source	DF	SS	F Ratio	Prob > F
Depth	2	7.719	1.310	0.278
Treatment	2	2.191	0.372	0.691
Treatment*Depth	4	8.479	0.719	0.582
Block	2	23.588	4.003	0.024*
Error	53	156.140		

Table 6: Two-way Analysis of Variance (ANOVA) tests comparing a) the difference in particle concentration (n/L), b) the difference in total particle equivalent spherical diameter (ESD), and c) the particle size distribution slope (PSD) among depth (0m, 2.5m, and ~6m) and treatment (control, artificial kelp, and kelp removal plots).

	Source	DF	SS	F Ratio	Prob > F
Particles (n/L)	Treatment	2	0.088	0.0466	0.954
	Depth	2	5.451	2.8634	0.061
	Depth*Treatment	4	4.546	1.1942	0.317
	Error	66	52.99		
Particle PSD	Treatment	2	0.392	1.0527	0.392
	Depth	2	1.227	3.2905	0.044
	Depth*Treatment	4	0.286	0.3847	0.818
	Error	66	10.44		

Table 7: Regression analysis of UDAS data, beam attenuation (1/m), SCUFA turbidity (NTU), and SCUFA fluorescence in relationship to POC and PON.

	df	SS	R^2	F	p
POC					
Beam attenuation	1	0.05	0.0005	0.8	0.76
error	160	96.6			
Turbidity	1	0.21	0.0022	0.36	0.54
error	160	96.46			
Fluorescence	1	5.01	0.05	8.74	0.003
error	160	91.6			
PON					
Beam attenuation	1	0.0005	0.000003	0.0006	0.98
error	160	155.95			
Turbidity	1	0.042	0.0002	0.043	0.83
error	160	155.9			
Fluorescence	1	31.33	0.2	40.23	< 0.001
error	160	124.6			

Table 8: Blocked two-way Analyses of Variance (ANOVA) tests comparing the difference in temperature (ºC) among depth, treatment (natural kelp, kelp removed, and artificial kelp), and depth* treatment.

Source	DF	SS	F Ratio	Prob > F
Depth	2	23.370	26.695	<.0001*
Treatment	2	0.435	0.497	0.609
Block	2	0.069	0.078	0.924
Treatment*Depth	4	0.096	0.055	0.994
Error	151	363.95		

Table 9: Blocked two-way Analyses of Variance (ANOVA) tests comparing the difference in salinity (PSU) among depth, treatment (natural kelp, kelp removed, and artificial kelp), and depth* treatment.

Source	DF	SS	F Ratio	Prob > F
Depth	2	0.0017	0.556	0.574
Treatment	2	0.0029	0.935	0.394
Block	2	0.0052	1.684	0.189
Treatment*Depth	4	0.0013	0.210	0.932
Error	151	0.234		

Table 10: Results of two-way analysis of variance (ANOVA) tests comparing the differences in horizontal current speed between water depth and treatment (natural kelp, kelp removed, and artificial kelp).

Source	DF	SS	F Ratio	Prob > F
Block	2	11.627	5.727	0.004*
Treatment	2	26.878	13.239	0.0001*
Depth	2	0.580	0.285	0.751
Depth*Treatment	4	0.514	0.126	0.972
Error	151	153.27		

Table 11: Results of two-way analysis of variance (ANOVA) tests comparing the differences in vertical current speed, between water depth and treatment (natural kelp, kelp removed, and artificial kelp).

Source	DF	SS	F Ratio	Prob > F
Block	2	0.2617	3.6972	0.0271*
Treatment	2	0.2005	2.8332	0.062
Depth	2	0.0746	1.0541	0.351
Depth*Treatment	4	0.0750	0.5300	0.713
Error	151	5.344		

Table 12: Comparison of mean horizontal (Northeast) current speed (SD, cm/s) within each plot before and after (B/A) before and after treatments; kelp control (K), artificial kelp (A), and kelp clearings (C). Means were compared by Student's t-test, or Welch's F-test.

	Before			After						
Treatment	$\bar{X}_1$	**SE**	**n**	$\bar{X}_2$	**SE**	**n**	$\bar{X}_2 - \bar{X}_1$	**Test**	**df**	**p**
K 1	2.20559	0. 07989	20	2.07229	0.06612	24	-0.1333	W	42	0.206
K 2	2.14229	0.08822	20	2.15890	0.09669	23	0.01661	S	41	0.89
K 3	1.97716	0.07248	20	2.28214	0.12190	18	0.30498	S	36	0.056
A 1	2.25596	0.10188	20	2.26913	0. 25834	18	0.01317	W	36	0.962
A 2	2.27488	0.08981	16	2.29568	0.10448	18	0.0208	S	32	0.88
A 3	2.25601	0.12473	20	3.89786	0.29045	19	1.64185	S	37	< 0.001*
C 1	2.25399	0.10141	20	4.34586	0. 36371	22	2.09187	S	40	< 0.001*
C 2	2.09879	0.06890	20	3.60976	0.19733	18	1.51097	S	36	< 0.001*
C 3	2.38068	0.10926	20	4.13924	0.13127	24	1.75856	W	42	< 0.001*

Table 13: Results of two-way analysis of variance (ANOVA) tests with effect summary comparing the duration of detectable dye (s), in relation to the number of kelp stipes and horizontal wave orbit speed (U), by SCUFA (1 = seafloor, 2 = midwater, 3 = upper water). SCUFA internode distance = 1.5 m.

SCUFA 1 (1.5 from Sea floor)

Source	DF	Sum of Squares	F Ratio	Prob > F
Stipes	1	5.5758	4.4942	0.0783
SD_U(m/s)	1	0.0015	0.0013	0.9728
SD_U(m/s)*Stipes	1	7.6633	6.1768	0.0475*
Error	6	28468		

SCUFA 2 (3m from seafloor)

Source	DF	Sum of Squares	F Ratio	Prob > F
Stipes	1	1.045	0.0066	0.938
SD_U(m/s)	1	402.423	2.5326	0.166
SD_U(m/s)*Stipes	1	5.107	0.0321	0.863
Error	6	937265		

SCUFA 3 (4.5m from seafloor)

Source	DF	Sum of Squares	F Ratio	Prob > F
Stipes	1	26.557	3.8275	0.0982
SD_U(m/s)	1	13.314	1.9189	0.2153
SD_U(m/s)*Stipes	1	42.733	6.1590	0.0477*
Error	6	14821		

Table 14: Reynolds number calculations using the SD of water velocity *U* (m/s) and kelp stipe bundle diameter (cm). In reference to the upper water dye detector (4.5m from bottom), detection is noted as yes or no (y/n) and the amount of time the dye was detected.

Stipes	D (cm)	SD_U (m/s)	Detection (y/n)	Duration (s)	R
128	10.6	0.124	Y	206	20811
131	12.59	0.167	Y	52	17213
90	8.95	0.120	Y	8	16634
88	8.8	0.085	Y	2	14051
78	8.3	0.092	Y	6	5688
34	5.5	0.073	Y	4	4213
70	7.89	0.034	Y	10	2559
45	6.3	0.027	N	0	2052
30	6.02	0.035	N	0	1746

APPENDIX- A: Artificial kelp construction

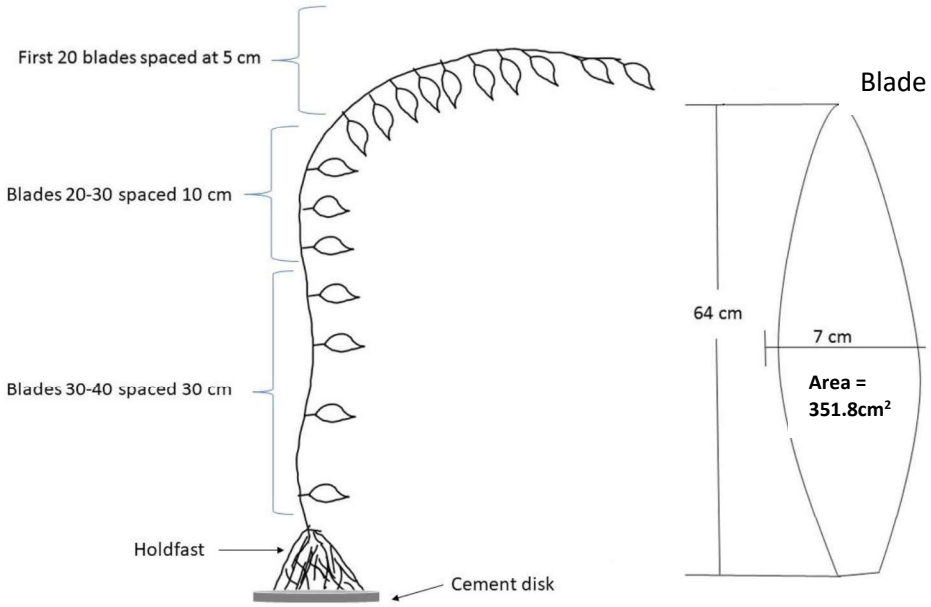

Fig A1: Artificial kelp schematic. Blades were 64cm long and 7cm at their widest point for an elliptical area of 351.85cm^2. Each stipe has 40 blades attached at different internode distances. All ropes were fed through plastic dishes then the dish was filled with cement to keep the thallus upright and keep the rope fronds together.

Fig. A2: Mapping of kelp distribution through two kelp beds in SWC, CA June - Aug. 2015. The kelp bed in green was outlined by a boat and GPS tracking and each yellow pin is a kelp species. For every kelp encountered the species, depth, and stipe number were recorded.

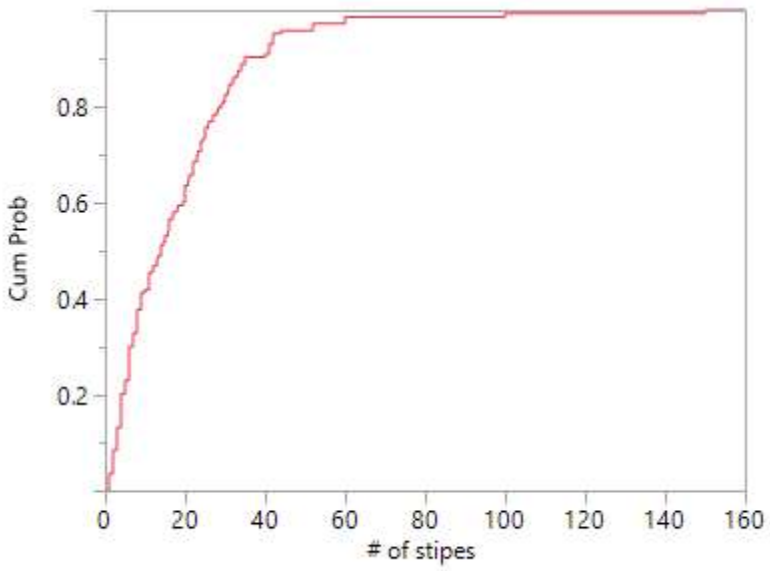

Fig. A3: CDF (cumulative distribution function) plot showing accumulative probability of individual *M. pyrifera* stipe bundle size at depths < 7.62 m at study site from June - Aug. 2015. This distribution was used to determine the number of kelp individuals at varying stipe counts.

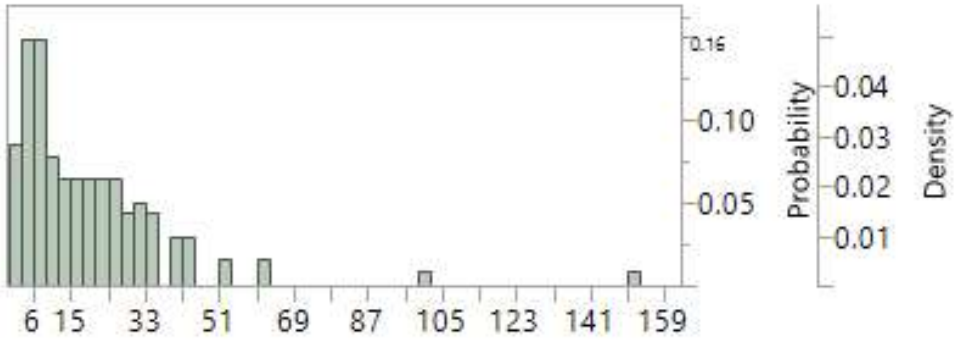

Fig. A4: Histogram of stipe bundles at study sites where the depth < 7.62 m at study site from June - Aug. 2015. This distribution was used to determine the number of kelp individuals at varying stipe counts.

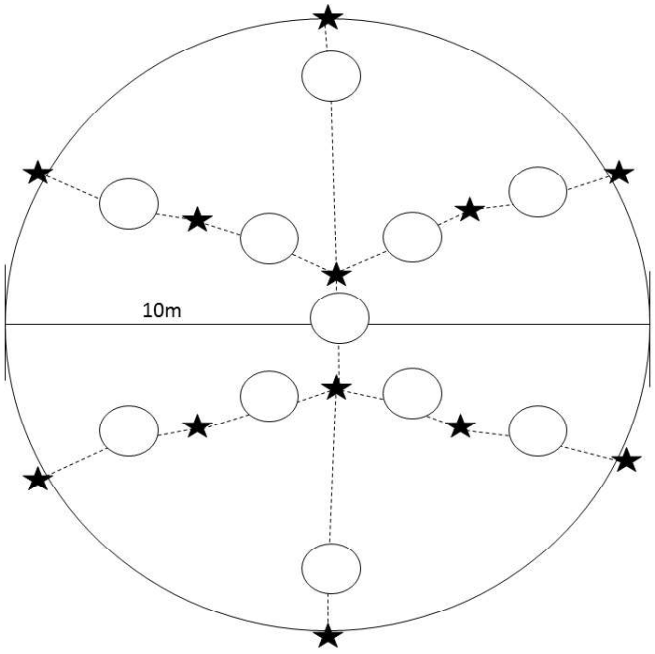

Figure A5: Artificial kelp plot lay out. Each circle represents a randomly placed artificial kelp thallus of either 3, 6, 8, 13, and 28 stipes. Dark starts indicate where a 3/8 x 6" stainless steel eye bolt was placed in the substrate with a led lag shield and z-spar. Dashed lines are where ropes attached from the eye bolts to the bottom of the stipes. Each thallus had at least 2 points of connection.

A6: Artificial kelp mid construction.

A7: Artificial kelp canopy with young of year rockfish (YOY)

A8: Artificial kelp with kelp rockfish and snails present.

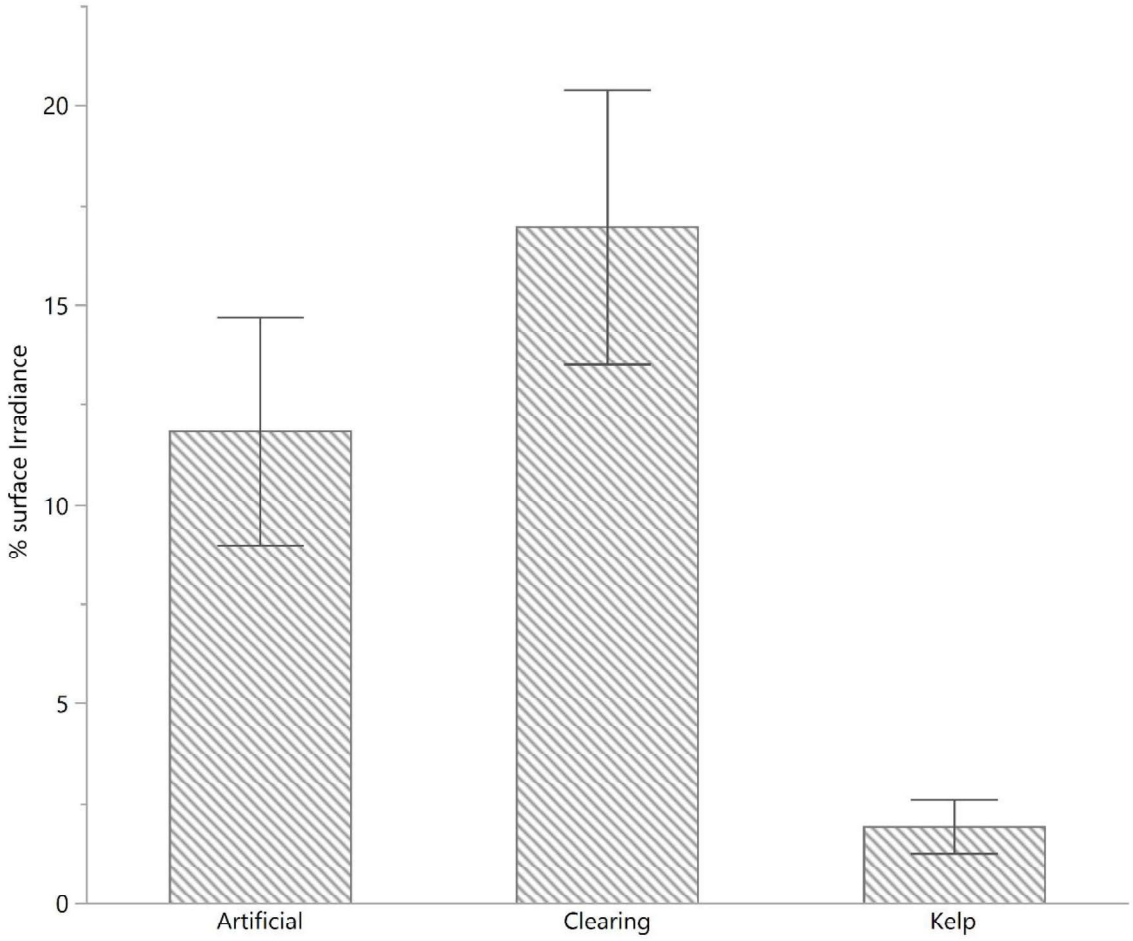

Figure A9: Percent surface irradiance at depths 0, 2.5, 5, and 7.5 meters within natural kelp beds, kelp cleared and artificial kelp treatments.

APPENDIX- B: ImageJ particle analysis script

```
dir = getDirectory("Choose a Directory ");
n=substring(dir,60,63);
input = dir;
output = dir;
function action(input,output, filename) {
        open(input + filename);
        run("Set Scale...", "distance=98 known=100 pixel=1 unit=um");
        run("8-bit");
        run("Subtract Background...", "rolling=200 light");
        //run("Brightness/Contrast...");
        getMinAndMax(min,max);
        if (min != 0 && max != 255) run("Apply LUT");
        setMinAndMax(0, 255);
        setAutoThreshold("Intermodes dark");
        //run("Threshold...");
        //setThreshold(129, 255);
        run("Convert to Mask");
        run("Variance...", "radius=2");
        run("Fill Holes");
        run("Dilate");
        run("Fill Holes");
        run("Options...", "iterations=1 count=3 pad");
        run("Erode");
        run("Erode");
        run("Erode");
        run("Analyze Particles...", "  show=Outlines display clear include summarize");
```

```
        path = dir+n+"-"+substring(getTitle(),16,19)+".xls";
        path2 = dir+"image"+".jpg";
    saveAs("results", path);
        saveAs("Jpeg",path);
    close();
}
list = getFileList(input);
for (i = 0; i < list.length-1; i++)
    action(input, output, list[i]);
```

APPENDIX- C: Python particle size distribution (PSD) code

```
import pandas as pd
import numpy as np
import glob
import matplotlib.pyplot as plt
from scipy import stats
import scipy
import csv


#Define your path to directory with raw particle data
path = "017"

# for loop that combines all .xls files within path directory. Creates
new variable "all_data" as .csv
# and saves within path directory as "total_particles"
all_data = pd.DataFrame()
for f in glob.glob(path+'\*.xls'): #you may need to change \ -> / if on
mac
    df = pd.read_csv(f,sep='\s+') #you may need to change \ -> / if on
mac
    df['fileName'] = f[4:11]
    df['ParticleNumber'] = range(len(df)+1)[1:] # add particle number
for matching up plankton

    all_data = all_data.append(df,ignore_index=True)


all_data.to_csv(path+'/total_particles.csv')

# Read new total_particle.csv and define variable "area"
file= path+'/total_particles.csv'
df = pd.read_csv(file,header=0)
area=df['Area']
TP = len(area)
print(TP)

# transform surface area to equivalent spherical diameter (ESD)
ESD = (2*(area/np.pi)**.5)
41
# define bins (how many, width, and center). Code in this cell modified
from Colleen Durkin.
```

```
bins = []
for x in np.arange(2,10,.5):  #This was 1.5,10,.5
    bin = 2**x
    bins.append(bin)

bin_mids = []
for y in np.arange(0,len(bins)-1):
    mid = bins[y] + (bins[y+1]-bins[y])/2
    bin_mids.append(mid)

bin_width = []
for z in np.arange(0,len(bins)-1):
    width = (bins[z+1]-bins[z])
    bin_width.append(width)

# Use numpy histgram to sort particle counts into size class bins. This
sorted data is then normalized by bin width.

histogram=np.histogram(ESD,bins=bins,range=None, normed=False,
weights=None, density=None)
n=((histogram[0]*30.376)/bin_width)*10 #normalized multiplied counts by
(30.376) to represent particles/1mL

# get rid of bins with no data

bin_mids_array=np.asarray(bin_mids) # change bin_mids from tuple to
array so can be indexed
ii=np.where(n>0) # index to remove zero data
bin_mids_nonzero=bin_mids_array[ii] # only bins with data
n_nozero=n[ii] # no zero values

# PSD function will be used in max.min to calculate differences in
estimated power equation from real data

def PSD (var, bin_mid, normalized): #var is in format of [#,#],
normilized = my n
    normalized_n = normalized#[normalized>0]
    bin_center = bin_mids_nonzero # figure this line out
    Y = (10**var[0])*bin_mids_nonzero**var[1]
    difference = np.sum((np.log(Y)- np.log(n_nozero))**2)
    return difference

# optimize the power equation fit using PSD function. Output is
variables A and B in equation y = A(x)^B
```

```
maxmin=scipy.optimize.minimize(PSD, [1, -3], args= (bin_mids, n)) #
then use these to plot y= over hist with estimates of [1,-3]
intercept = np.round(maxmin['x'][0],2)
slope = np.round(maxmin['x'][1],2)
```

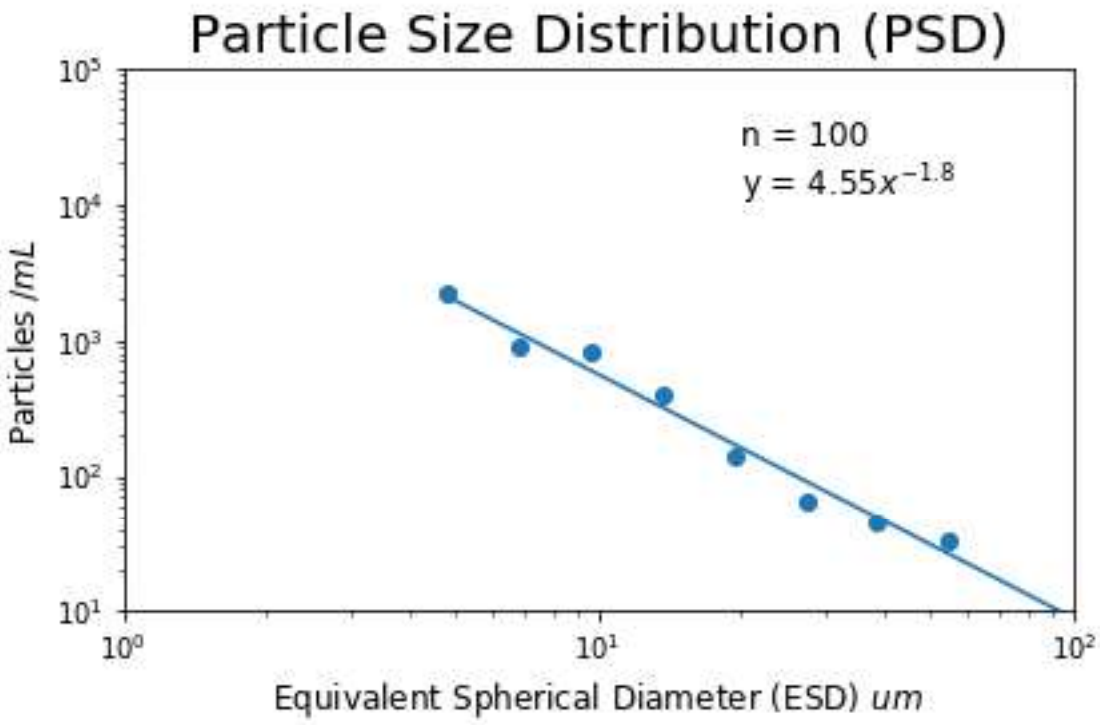

C1: PSD calculation of a single water sample. Twenty microscope images were processed via ImageJ particle analysis (Appendix B), then the slope was fit to the data using the code in Appendix C.

APPENDIX- D: Python script for ADV spectra

```
%matplotlib notebook
import numpy as np
import matplotlib.pyplot as plt
import pandas as pd
import os
import matplotlib.patches as mpatches
from physoce import tseries as ts
from scipy.signal import welch
from scipy.stats import chi2
from scipy import stats

#load combined file from ADV processing
os.chdir("path/")
filename ="combined.8.03.17.csv"
df = pd.read_csv(filename)

#Define start and end time of each experiment from the dataset
start_time1, end_time1 = (1401, 1421) #select start and end time of in
kelp run
start_time2, end_time2 = (1446, 1506)#select start and end time of out
of bed run
df['Time']= (df['Hour']*100)+ (df['Minute']) #make new time column for
indexing in military time
runindex_in = (df['Time']>start_time1-1) & (df['Time']<end_time1+1) #
index by start and end time for in bed run
runindex_out = (df['Time']>start_time2-1) & (df['Time']<end_time2+1) #
index

#use PCA to rotate axis to make variable with most variation U
theta, major, minor=ts.princax(df['Velocity_East(m/s)'],
df['Velocity_North(m/s)']) #theta = angle, major = SD major axis, SD
minor axis
U, V= ts.rot(df['Velocity_East(m/s)'], df['Velocity_North(m/s)'], -
theta)
df['U'] = U
df['V']= V

#make variables you want to play with
U_in = df['U'][runindex_in]
```

```
U_out = df['U'][runindex_out]
N1 = (len(U_in))
N2 = (len(U_out))

#Fast Fourier Transform alogorithm
U_fft_in = np.fft.fft(U_in)
U_fft_out = np.fft.fft(U_out)

#calculate spectra and frequency, where delta t is sample rate
deltat1 = .5
deltat2 = .5
f_in = np.fft.fftfreq(N1,deltat1)
S_in = (2/N1)*deltat1*np.abs(U_fft_in)**2

f_out = np.fft.fftfreq(N2, deltat2)
S_out = (2/N2)*deltat2*np.abs(U_fft_out)**2

#smoothing the spectra with Hanning window
f4_in_f4,S4_in_f4 =
welch(U_in_f4,fs=2,nperseg=N1_f4/8,window='hanning',detrend='linear')
f4_out_f4,S4_out_f4 =
welch(U_out_f4,fs=2,nperseg=N2_f4/8,window='hanning',detrend='linear')

#calculate confidance intervals
a = ((1 - .95)/2) + .95
b = 1 - a
DF = 8*2*(8/3) #this df comes from the window and using a hanning (8/3)
(Emery & Thomson 1998)
upper=chi2_upper = stats.chi2.ppf(a,DF)
lower=chi2_lower = stats.chi2.ppf(b,DF)
```

APPENDIX- E: NOAA station 46042 mean wave period

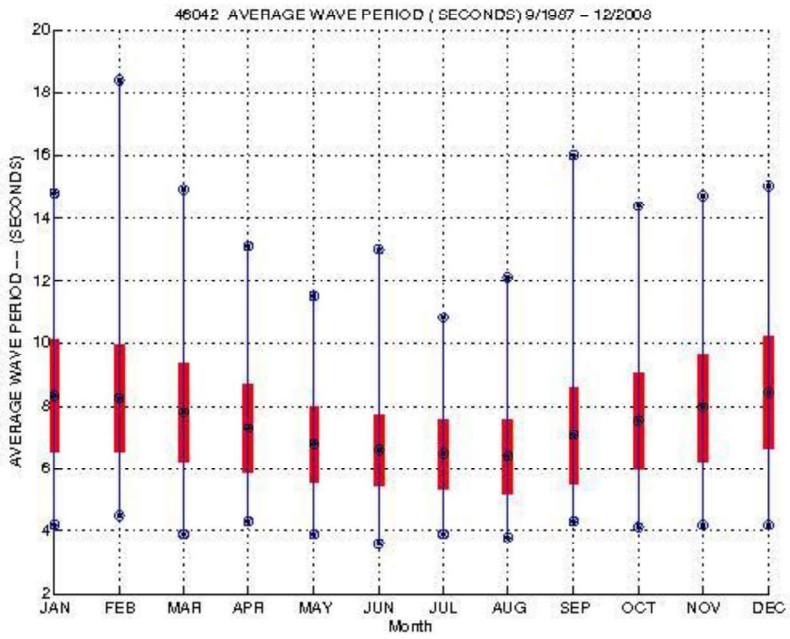

Fig. E1: NOAA station 46042average wave period (s) by month. Data from (9/1987 – 12/2008).

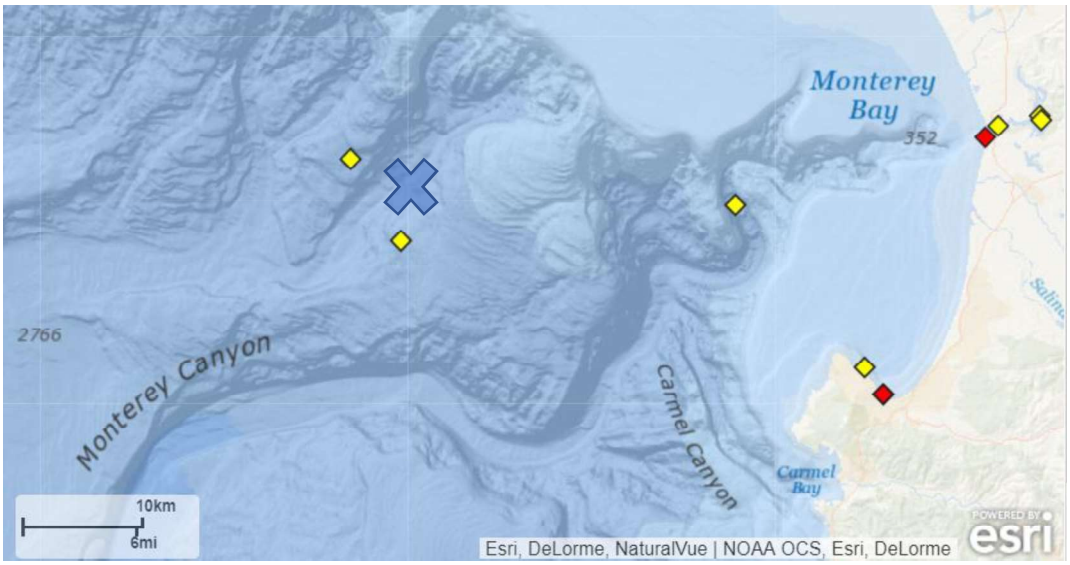

Fig. E2: Location of NOAA station 46042 indicated by yellow triangle with blue "X".